Controlled coating of nanoparticles with peptides and

lanthanide complexes: a photophysical evaluation

By

Alison Clare Savage

A thesis submitted to the University of Birmingham for the degree of

DOCTOR OF PHILOSOPHY

UNIVERSITY OF BIRMINGHAM

University of Birmingham Research Archive

e-theses repository

Abstract

There is great potential to use gold nanoparticles as a method of assembling multiple probes into one targeted imaging agent. This thesis describes the co-coating of gold nanoparticles with different combinations of lanthanide complexes and peptides, and the effect of this co-coating on the photophysical properties of the lanthanide complexes has been examined. A photophysical study of europium (III) ions binding to two surface active peptides in solution is presented and the ability of these peptides to bind the europium ions whilst tethered to gold nanoparticles is discussed. The peptides selected for this study contain two thiols for stronger binding to the gold nanoparticle surface. Lanthanide complexes with a diethylenetriaminepentaacetic acid (DTPA) binding motif were prepared and attached to gold nanoparticles with different nuclear localisation signal peptides to investigate their photophysical properties and their potential as a cellular imaging agent has been demonstrated. The effects on the photophysical properties of the lanthanide complexes in the presence of different peptides on gold nanoparticles have also been compared.

The co-coating of gold nanoparticles with europium and gadolinium complexes is also introduced, with the combinations on gold nanoparticles giving rise to an interesting energy transfer effect between the two different lanthanide complexes. These nanoparticles have the potential to be used as a multi-modal imaging agent for luminescent and magnetic resonance imaging.

The synthesis of an azo-dye has been undertaken and its ability to bind and sensitise the near-infrared lanthanides neodymium (III) and ytterbium (III) has been demonstrated. It was found to form complexes with these lanthanides, and the high molar absorption coefficients in the visible region allows for excitation at wavelengths up to 500 nm.

Table of Contents

Chapter 4:

Dual lanthanide coated gold nanoparticles: preparation and photophysical characterisation.

Chapter 6:

List of figures

Chapter 3:

Chapter 4:

Chapter 5:

List of tables

Introduction

1   The lanthanide elements

The lanthanides are the group of 15 elements in the periodic table from lanthanum to lutetium with the atomic numbers 57-71. They are distinguished by their electronic configuration [Xe] $4f^n$, n = 0-14, with the occupation of the $4f$ orbitals. The chemical properties, particularly oxidation states of the lanthanides are similar across the series as the lanthanides typically exist as trivalent Ln^{3+} in aqueous solution.[1]

The atomic radii of the lanthanides decrease across the series, due to the directional and dispersed nature of the $4f$ orbitals, which means that the addition of electrons to the orbital does not counteract the effect of the increased nuclear charge. This is often referred to as the lanthanide contraction. The large ionic radii of lanthanides allow for coordination numbers greater than 6, with the lanthanides typically exhibiting coordination numbers around 8 and 9.

Luminescence from lanthanide(III) ions is caused by the electronic rearrangements within the 4f subshells. Relaxation of an *f*-electron from the excited state to the ground state causes a release of energy in the form of a photon of light. Lanthanide ions have very weak absorption coefficients due to the parity-forbidden *f-f* transitions. This is as stated by the Laporté selection rule, which prohibits the redistribution of elections within the $4f$ subshells. Their weak absorption coefficients can also be attributed to the shielding of the 4f orbitals by the filled $5p^6 6s^2$ sub-shells, which results in little interaction with the surrounding chemical environment. They exhibit characteristic narrow line-like emission due to their well-defined transitions with

lifetimes within the region of 0.1 - 1.0 ms due to the forbidden nature of the transitions.[2]
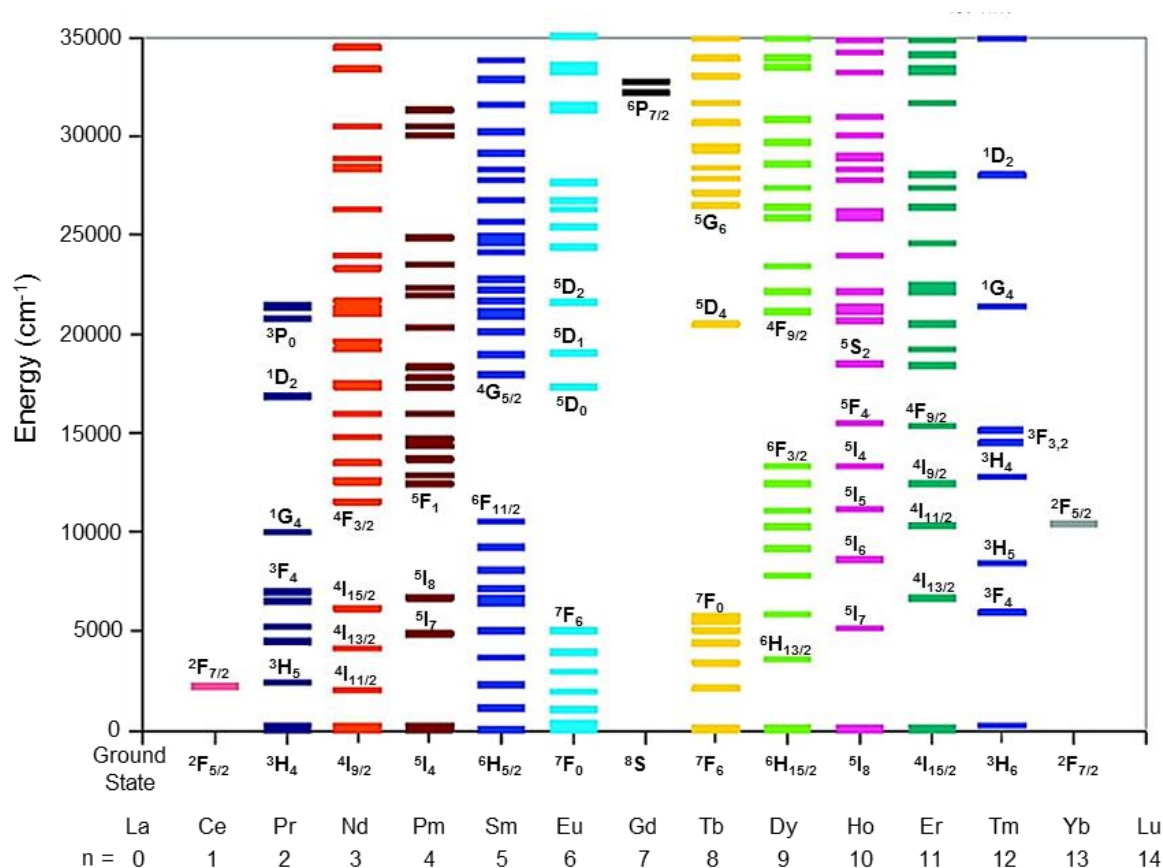
Figure 1.1: Electronic excited-state energy level diagram for the lanthanides. n is the f-orbital electron configuration across the series. Diagram reproduced from reference [3]

Lanthanide luminescence is caused by the radiative relaxation of an excited-state *f*-electron to the ground state. The wavelengths at which this emission is observed is dependent upon the energy gap between the excited state and the ground state and is characteristic for each lanthanide. Emission of lanthanides can be observed in the visible and near-infrared regions depending on the lanthanide.[4] The luminescence of

europium, terbium, samarium and dysprosium(III) is observed in the visible region, whilst neodymium, ytterbium and erbium(III) all exhibit luminescence in the near-infrared region. Gadolinium(III) emits in the UV region and is more difficult to excite than the other lanthanides because it has a higher energy excited state which requires non-conventional excitation (i.e. excitation at low temperature).

Lanthanides(III) ions exhibit long luminescence lifetimes and characteristic narrow emission bands. The weak absorption coefficients for direct excitation as a result of the parity-forbidden *f-f* absorption transitions can be overcome by the complexation of lanthanides within close proximity to an antenna which is able to absorb energy and transfer it to the lanthanide ion. This is shown by the absorption, energy transfer, emission (AETE) mechanism, shown in figure 1.2.[5]
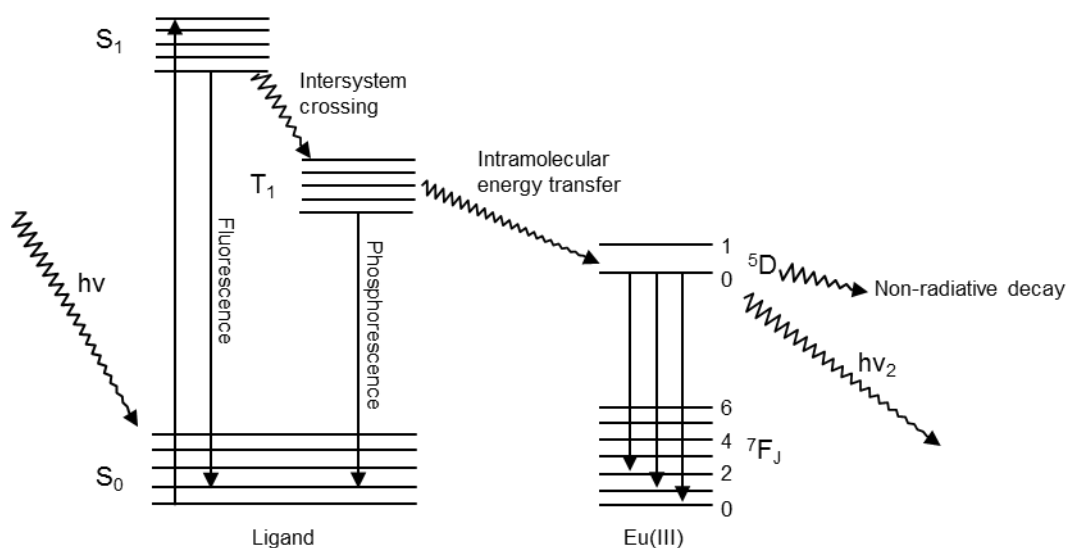
Figure 1.2: Schematic representation of the AETE mechanism for the indirect population of lanthanide luminescent states

The energy transfer mechanism for the sensitisation of lanthanides involves the intramolecular energy transfer from the triplet state of the organic chromophore to the excited state of the lanthanide ion.

A great deal of research has focussed on the development of highly stable lanthanide complexes designed with efficient chromophores for indirect lanthanide excitation.

2   Lanthanide ion coordination

Many binding motifs have been investigated for the binding of lanthanide ions, and have been reviewed extensively within the literature.[1, 6-10] Ln^{3+} are classified as hard acids by the Pearson scheme,[11] and coordinate hard donors such as oxygen and nitrogen atoms. Lanthanides ions exist in a hydrated form, which means these hard donors are required to displace molecules of water from the inner coordination sphere. Coordination of lanthanide ions can be achieved by coordination with polydentate chelating ligands[7, 12] and macrocycles[6, 8, 13-16] or alternatively encapsulation within cryptands.[5, 17] Designing a chelating ligand for lanthanide ions should be based on several key features, such as the inclusion of a chromophore with an excited energy state suitably close to the lanthanide acceptor state to allow intramolecular energy transfer to occur but not too close that back energy transfer occurs.[17] The chelating ligand should also be stable and chemically inert, particularly for biological applications in which the release of the lanthanide ion from the chelating ligand or an exchange with biological cations such as Ca^{2+} could raise issues with toxicity via transmetallation. Exclusion of water molecules from the inner coordination sphere by means of a polydentate chelator can limit the exposure of the

lanthanides to specific bond oscillators (e.g. O-H bonds), which can cause quenching by non-radiative decay.

This effect has been exploited to calculate the number of inner-sphere water molecules (q) using the equation:

$$q = A(k_H - k_D)$$

Where A is a proportionality constant specific to each individual lanthanide and k_H and k_D are the rates of luminescence decay (reciprocal observed luminescence lifetime) measured in protonated and deuterated solvents respectively.[18]

Chelating ligands based on diethylenetriaminepentaacetic acid (DTPA) are widely studied for their ease of modification for various applications (figure 1.3). They are known to bind strongly to lanthanide ions, and can be modified with varying degrees of functionality to give either mono-amide or bis-amide complexes. Preparation of these mono and bis-amide complexes can be achieved by a condensation reaction of DTPA-bisanhydride with the desired amine molecules to form the amide arm(s).
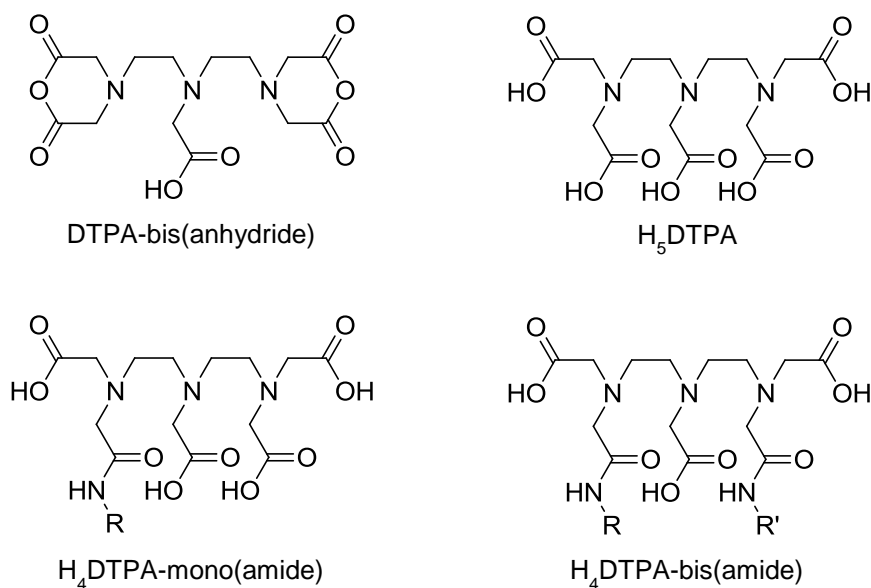
Figure 1.3: Structures of basic DTPA derivatives

The ability of these complexes to chelate lanthanide ions, and the simple procedure for modification of these chelates with chromophores and other functionalising groups make them desirable for use as bifunctional lanthanide chelating ligands.

3   Luminescent lanthanide complexes for cellular imaging

The unique photophysical properties of lanthanides have been exploited for the use as cellular probes. Emission from lanthanide(III) ions elicited by the antenna effect generally have large Stokes shift as the energy transfer is mediated by a number of energy states. This allows the emission to be easily distinguished from the excitation source.

The long luminescent lifetimes of lanthanide complexes can be utilised for cellular imaging, by carrying out delay time-gate experiments (figure 1.4). Any fluorescence

observed from organic molecules within the cells usually has only very short-lived lifetimes which are in the nanosecond range. Thus the emission can be monitored with a time delay after excitation to allow for detection of the lanthanide without observing autofluorescence.
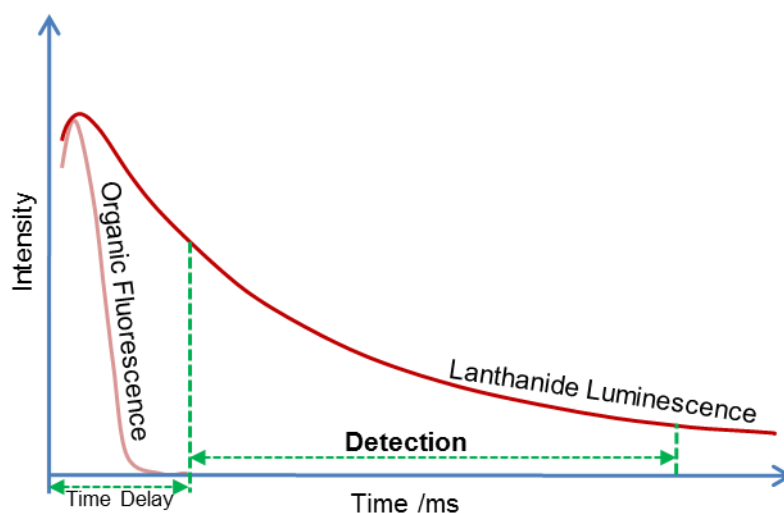
Figure 1.4: Principle of time-gated spectroscopy

There have been many examples of lanthanide cellular probes in the literature,[4, 9, 10, 15, 19-25] using different lanthanides to produce complexes that emit either in the the visible or near infrared regions for detection by luminescence microscopy. Lanthanide complexes are also heavily employed as contrast agents for magnetic resonance imaging (MRI),[12] with some gadolinium complexes being commercially available for clinical use as contrast agents such as the gadolinium(III) complex Omniscan® which is a bis amidomethyl DTPA derivative.

3.1   Visible emitting lanthanide complexes

Europium and terbium(III) complexes are commonly studied for use as cellular imaging probes due to them possessing longer luminescence lifetimes than their near-infrared counterparts. The cellular uptake of some macrocyclic lanthanide complexes has been thoroughly investigated by Parker *et al.*[15, 20, 25] The structure of the complexes was found to contribute to their sub-cellular localisation. Different complexes containing tetraazatriaphenylene and azaxanthone chromophores were found to localise in four distinct sub-cellular regions: lysosomes, mitochondria, nucleoli and mitochondria + lysosomes.

Mitochondria and Lysosomes

Nucleolus

Mitochondria

Lysosomes
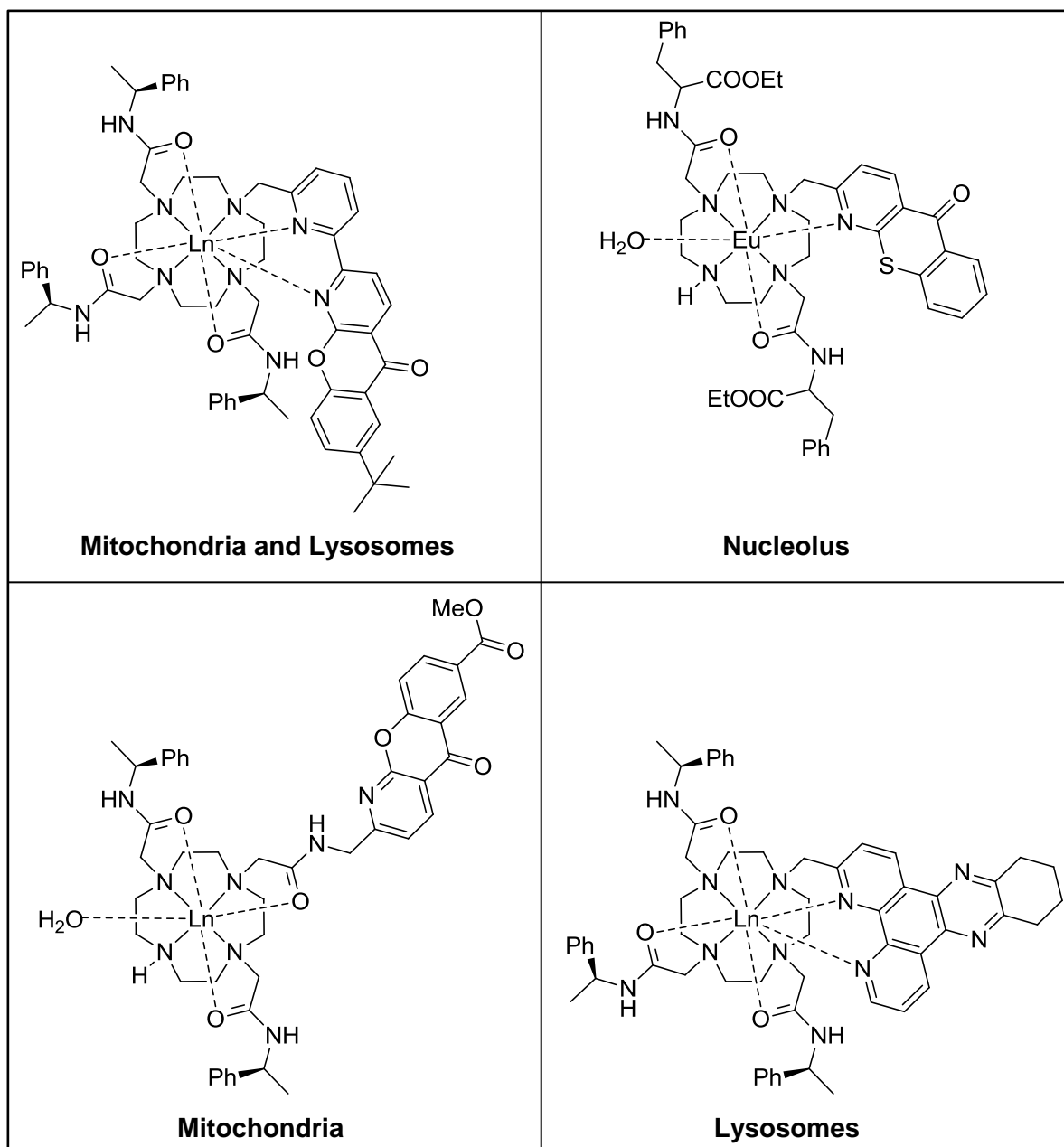
Figure 1.5: Examples of lanthanide complexes and their cellular localisation. Ln = Eu or Tb.[20]

Bünzli *et al.* reported the use of lanthanide bimetallic triple-stranded helicates as imaging probes.[24, 26, 27] The water soluble europium helicates were found to be taken up by human cervical adenocarcinoma cell line (HeLa) and were visible in the

cytoplasm of the cells when examined by confocal microscopy. These helicates have a reported quantum yield of 18 ± 2 %.[24]
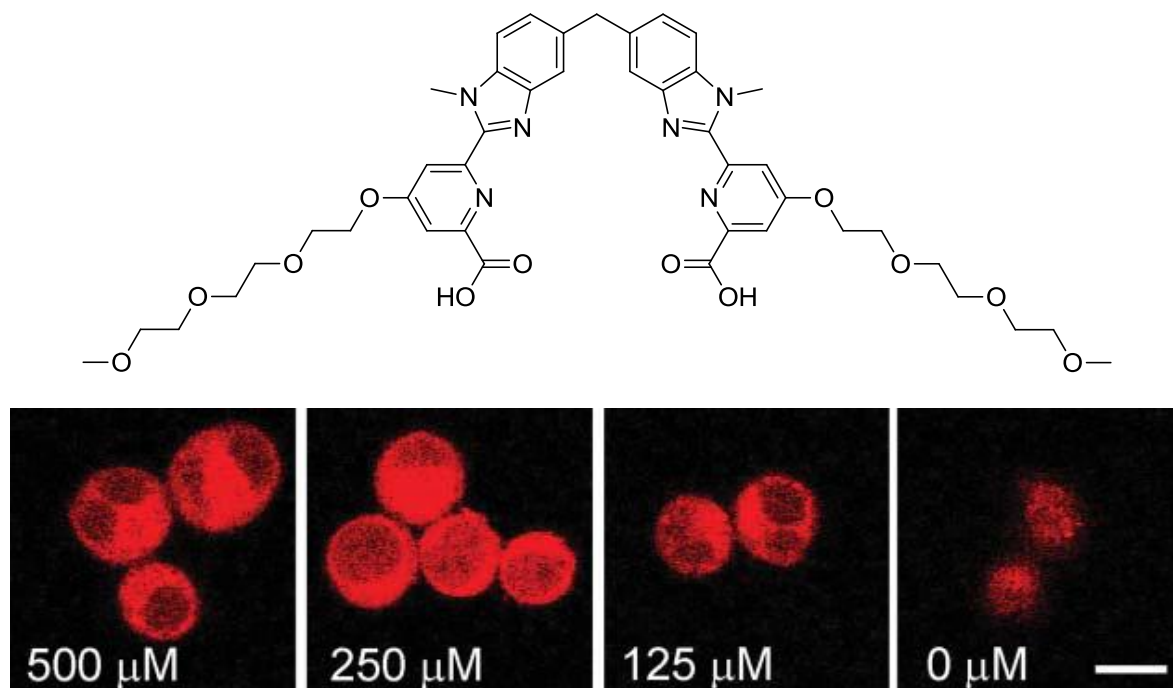
Figure 1.6: Structure of ligand which forms helicates with lanthanide ions at a ratio of 2 lanthanides to 3 ligands. Confocal microscopy images of RPMI-1640 incubated with various concentrations of helicates. λ_{exc} = 405 nm, scale bar 17 µM. Confocal images reproduced from reference [24].

One of the drawbacks to lanthanide complexes that emit in the visible region is that the human body contains biological molecules that can absorb in the visible region, such as haemoglobin which can affect the probes' ability as an imaging agent. Furthermore due to the higher energy excited state of the visible lanthanides, the energy required to populate the lanthanide excited state is much higher which limits the excitation wavelengths required to wavelengths in the UV region. Such excitation wavelengths are undesirable for the similar reasons as the excitation light can be

absorbed by biological molecules, which limits the effectiveness of the lanthanide complex. Near-infrared lanthanides have excited states which are lower in energy, making it possible for the use of wavelengths in the visible region.[28] Therefore work has been carried out to develop probes that emit in the near-infrared to prevent this problem.

3.2   Near-infrared emitting lanthanide complexes

Lanthanide complexes that emit in the near-infrared are desirable for use as cellular probes, as near-infrared light is able to penetrate skin and other tissue.[29] Biological molecules absorb in the UV region, thus limiting the depth at which shorter wavelengths of light can penetrate.[30] Emission in the near-infrared allows for the use of a chromophore which can be excited at higher wavelengths within the visible region. Tissue has minimal absorption at wavelengths greater than 600 nm, therefore the signal to noise ratio is greatly improved with the use of near-infrared probes.[30] There have been different strategies for the sensitisation of near-infrared lanthanides, with the use of chelating ligands with attached organic chromophores[16, 31-34] or transition metal complexes.[35-39]

1

2

3

4
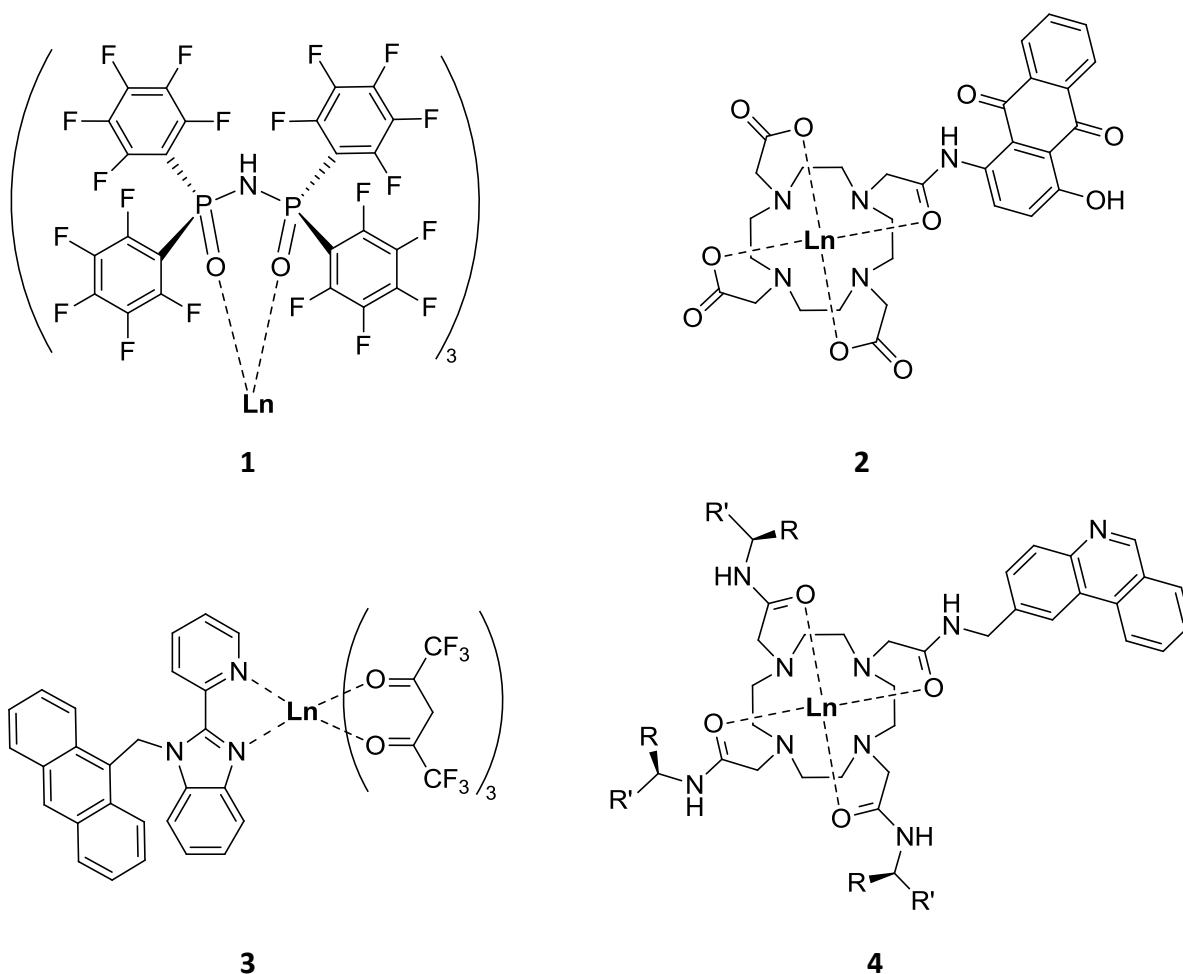
Figure 1.7: Structures of some reported near-infrared emitting complexes. **1:** Fluorinated imidodiphosphinate ligand for sensitisation of Ln = Nd, Sm, Eu, Gd, Tb, Dy, Er, Yb.[31] **2:** Anthraquinone chromophore attached to a tetraaza macrocyclic ligand for Ln = Nd, Gd, Er, Yb.[33] **3:** 2-(2-pyridyl)benzimidazole unit with an anthracene group for Ln = Nd, Gd, Er, Yb.[16] **4:** Phenanthridine sensitised complex for ytterbium. R = Me, R' = Ph.[34]

The near-infrared lanthanide complexes typically exhibit shorter luminescence lifetimes than the visible lanthanides such as terbium and europium. A fluorinated imidodiphosphinate ligand was reported to give long luminescence lifetimes for the near-infrared lanthanides neodymium, ytterbium and erbium of 44 μs, 741 μs and

1111 µs respectively (figure 1.7, structure 1).[31] The design of this compound was based on the need for a hydrophobic shell around the lanthanide, to minimise the coordination of solvent molecules to the lanthanide ion which can cause quenching.[40] Near-infrared complexes have also been developed with chromophores that can be excited in the visible region, such as anthraquinone, anthracene and phenanthridine complexes (figure 1.7, structures 2,3 and 4).[16, 33, 34]

3.3   Lanthanide complexes as MRI contrast agents

The paramagnetic properties of gadolinium(III) have been exploited for use as contrast agent for magnetic resonance imaging. Magnetic resonance imaging (MRI) is a powerful diagnostic technique for imaging anatomical structures of the body, and is useful for detecting diseased soft tissue such as tumours.[41] The technique relies on the enhancement of relaxation of water protons in a magnetic field by use of a contrast agent.[42] Gadolinium is known to enhance T_1 relaxivity, the longitudinal relaxation time of surrounding water molecules.[43] Gadolinium(III) ions are toxic and therefore cannot be administered directly, therefore the design of gadolinium contrast agents have to incorporate a strong chelating ligand to bind the ions. The structure of the chelating ligand should also allow for a free coordination site for the coordination at least one water molecule for exchange with surrounding water molecules. Some examples of commercially available gadolinium contrast agents are shown in figure 1.8.
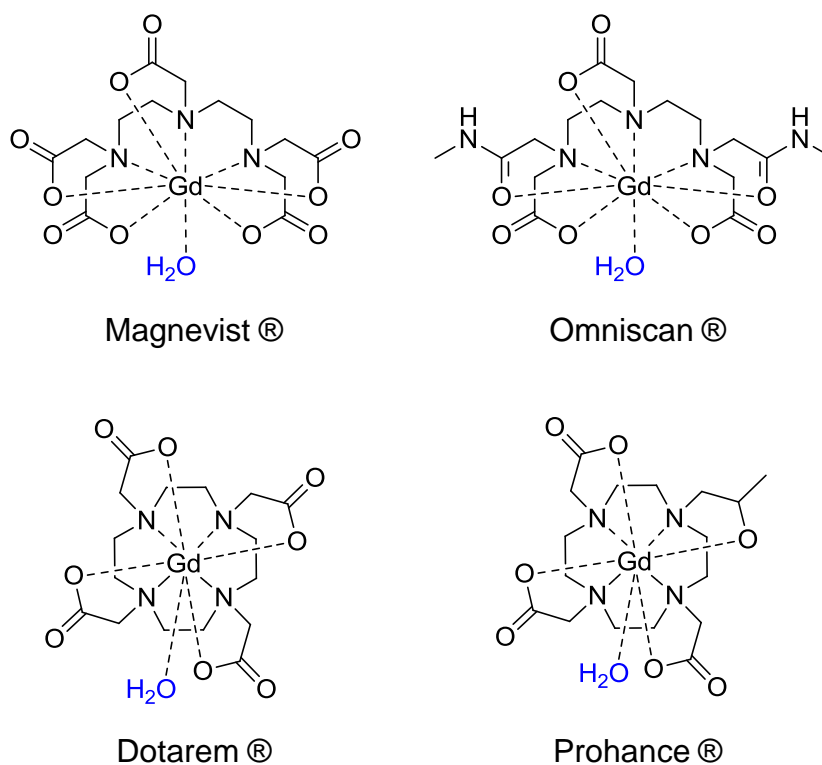
Figure 1.8: Structures of some commercially available contrast agents based on DTPA or macrocyclic complexes.[41]

Each of the commercially available gadolinium chelates shown in figure 1.8 have similar relaxivity r_1 at 37°C of 3.5-3.8 mM^{-1}s^{-1} (20 MHz).[41] These chelating ligands are highly stable (K = 10^{15}),[44] which means that when used as contrast agents they are safely excreted intact via the renal pathway.

4   Gold nanoparticles

Gold nanoparticles' unique optical properties, large surface area and biocompatibility make them highly desirable in the development of cellular probes. Gold nanoparticles of different sizes can be prepared easily by the reduction of a gold salt with a reducing agent such as citrate.[45, 46] The reduction of $HAuCl_4$ in water with citrate leads to the formation of gold nanoparticles stabilised by a weakly bound shell of anionic citrate, which remain mono-dispersed in solution due to electrostatic repulsion between the particles.[47] The citrate ions on these gold nanoparticles can be readily exchanged with thiol-containing ligands that form stronger bonds to the gold surface, to form sterically stabilised gold nanoparticles.[48] Citrate reduction of gold typically produces stable monodisperse gold nanoparticles, and different size nanoparticles between 10-150 nm can be prepared by adjusting the concentrations of starting reagents.[45, 46] Small particles of 1-3 nm can be prepared by the two phase transfer method reported by Brust *et al.*[49] Briefly, gold salt is transferred from aqueous phase to organic phase with tetraoctylammonium bromide and is then reduced by sodium borohydride in the presence of an alkanethiol. This leads to gold nanoparticles stabilised in the organic phase with alkanethiols.

Gold nanoparticles adhere to Mie theory,[50] where an electromagnetic frequency induces a resonant coherent oscillation of free electrons at the nanoparticle surface.[51] This is called the surface plasmon resonance (SPR). The absorption of gold nanoparticles is within the visible range, with 13 nm citrate-stabilised particles characteristically exhibiting a SPR band at approximately 520 nm. The optical properties of gold nanoparticles can vary depending on the size, shape and surrounding chemical environment.[52] The surface of gold nanoparticles can be easily

modified with fluorophores,[53, 54] peptides,[55-60] antibodies and other biologically relevant molecules[61] through the formation of gold-sulphur bonds. Gold nanoparticles provide a large surface area for the assembly of multiple probes and functionalising moieties. The functionalisation of gold nanoparticles can be monitored by changes in the SPR band observed by UV-Vis spectroscopy.

Gold nanoparticles have excellent light scattering abilities, and can used in imaging by a number of different techniques. Transmission electron microscopy (TEM) is the most commonly used technique for imaging which exploits the high atomic weight of gold.[51] The scattering properties can be imaged by dark-field microscopy, fluorescence microscopy and X-ray tomography.[62] Gold nanoparticles are also ideal for intracellular imaging using surface-enhanced Raman scattering (SERS) as they provide huge enhancement of SERS signal.[63]

5   Gold nanoparticles functionalised with lanthanides

Gold nanoparticles have been widely developed as scaffolds for the delivery of multiple probes into cells. Gold nanoparticles are chemically inert within the body and provide a large surface area for the assembly of many functionalising moieties.[64] Therefore attaching lanthanide complexes to gold nanoparticles is desirable to aid the delivery of a larger concentration of the imaging probe into cells. Lanthanide coated gold nanoparticles have received increasing attention in recent publications.[65-72] Initial reports on the functionalisation of gold nanoparticles with lanthanide complexes took advantage of simple gold-sulphur chemistry to tether complexes to

the gold nanoparticle. Lanthanide coated gold nanoparticles have been developed for different applications, such as sensors for metal ions,[65] pH,[72] anions and small molecules.[69, 71] Gunnlaugsson *et al.* developed an assay utilising lanthanide complexes (1.Eu; figure 1.9A) on gold nanoparticles for the detection of biologically significant phosphate anions such as Flavin monophosphate.[71] The assay works by the displacement of a sensitising antenna from the lanthanide complex by the phosphate leading to quenching of the lanthanide emission.
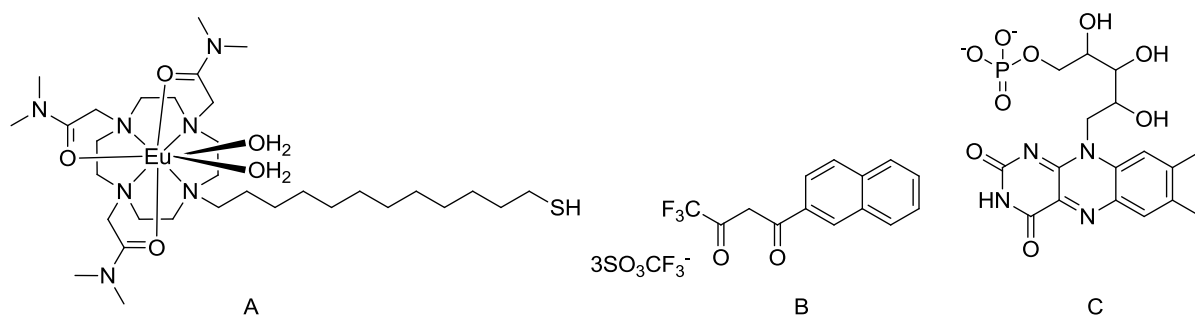
Figure 1.9: (A) 1.Eu ligand; (B) β-diketone antennae; which upon excitation causes the 1.Eu ligand to become highly luminescent (C) Flavin monophosphate displaces the antennae from the 1.Eu ligand.

Lanthanide nanoparticles have also been developed as cellular imaging probes.[66-68, 71] Europium diethylene triamine pentaacetic acid (DTPA) complexes (figure 1.10A) have been tethered to gold nanoparticles and were found to exhibit the characteristic red luminescence of Eu(III).[67] Further investigations with these europium coated gold nanoparticles found that they could be successfully imaged and their intracellular distribution monitored by high-resolution synchrotron x-ray fluorescence microscopy.[66] Coating gold nanoparticles with a different europium DTPA complex

(figure 1.10B) and a pH low insertion peptide (pHLIP) was found to promote the uptake of gold nanoparticles into platelets at pH 6.5.[68]
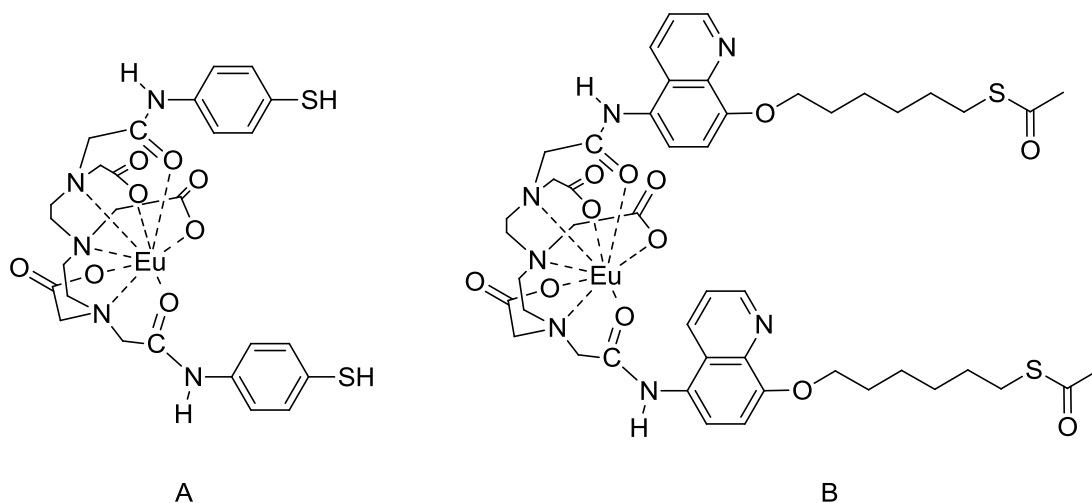
Figure 1.10: Europium DTPA complexes for attachment to gold nanoparticles from literature. Complex A,[66, 67] Complex B[68]

6   Peptide coated gold nanoparticles

Peptides are small chains of amino acids, which are often studied for biological applications. Typically they are used for targeting specific biomarkers or receptors in cells,[73] as well as delivering molecules and imaging agents into the cell.[74-76] Peptides have been modified with lanthanides for various biological applications to take advantage of their biocompatibility in the delivery of luminescent lanthanide probes.[76-78] More recent work has seen peptides being utilised for stabilising gold nanoparticles. The rational design of the small peptide CALNN reported by Fernig *et al* lead to the preparation of CALNN coated gold nanoparticles that were found to be

highly stable and water soluble. [79] Further research into peptides has seen a rise in their use for the delivery of nanoparticles into cells.[55, 56, 68, 80]

6.1   Cell Penetrating Peptides

Cell penetrating peptides (CPP) are of particular interest due to their ability to deliver nanoparticles and other payloads into cells.[60, 81] These peptides are short sequences of amino acids that are believed to be internalised via receptor- and endocytosis-independent mechanisms,[82] although the mechanisms are not fully understood and cause a lot of debate within literature.[83] Various different CPPs have been reported in recent years such as TAT[60, 84, 85] and sweet arrow peptide.[56] The peptide TAT is a particularly well reported peptide, which has been used to modify many different types of nanoparticles for cellular delivery such as gold nanoparticles, magnetic nanoparticles (e.g. iron oxide) and quantum dots.[60] Further examples are given in table 1.1.

Peptide	Sequence	Reference
Tat	GRKKRRQRRR	60, 84, 85
Penetratin	RQIKIWFQNRRMKWKK	85, 86
Transportan	GWTLNSAGYLLGKINLKALAALAKKIL	87
Sweet arrow peptide	(VRLPPP)$_3$	56

Table 1.1: Sequences of commonly used cell penetrating peptides.

6.2   Nuclear localisation signals

One particular class of cell penetrating peptides are nuclear localisation signals (NLS), which are of interest as they are able to cross the nuclear membrane and enter the cell nucleus. The delivery of targeted molecules into the nucleus is desirable for cellular imaging[58, 59] and the delivery of drugs and biologically active molecules.[55] They are particularly useful for targeting DNA and gene silencing, which requires access to the nucleus. They have also been tethered to gold nanoparticles to allow them to pass through the nuclear membrane into the nucleus of cells.[59] A study into the cellular trajectories of peptides on gold nanoparticles has revealed that two nuclear localisation signals are able to enter the nucleus of some cell lines.[59] The peptide CGGFSTSLRARKA tethered to gold nanoparticles were found to localise in the nucleus of HeLa cells, but not 3T3/NIH or HepG2 cells. The peptide CKKKKKKGGRGDMFG however was found to enter HepG2 cells and target the nucleus. The ability of these peptides to deliver gold nanoparticles into the nucleus allows for great potential to exploit the large surface area of nanoparticles for delivery of multiple probes and therapeutics.

6.3   CALNN coated gold nanoparticles

Gold nanoparticles can be translocated into cells via the attachment of peptides to the nanoparticle surface. Small peptides have been designed for the preparation of highly stable water-soluble gold nanoparticles.[88] The peptide CALNN consists of a cysteine which provides sulphur for attachment to gold nanoparticles. The alanine and leucine amino acids closest to the gold nanoparticle surface are hydrophobic and

promote the self-assembly of the peptide. The two asparagine amino acids are hydrophilic, which aids in the solubility of the nanoparticles. The peptide CALNN and longer derivatives of the peptide have been used in the delivery of gold nanoparticles into cells.[57, 85, 89] Wang *et al.* reported the cellular uptake of gold nanoparticles coated in the pentapeptide CALNN and an arginine-rich derivative CALNNR$_8$.[57] It was found that coating gold nanoparticles with just CALNNR$_8$ localised in the endoplasmic reticulum, whilst co-coating gold nanoparticles with CALNN and CALNNR$_8$ were able to target the nucleus. Brust *et al.* investigated the effect of the cell penetrating peptides TAT (AGRKKRRQRRR) and Pntn (GRQIKIWFQNRRMKWKK) and the nuclear localisation signal (GGFSTSLRARKA) appended to CALNN peptide on gold nanoparticles.[89] The predominant finding with the gold nanoparticles coated with the cell penetrating peptides TAT and Pntn was that the uptake into cells was mediated by endocytosis. Upon incubation of cells with gold nanoparticles coated with TAT, Pntn and NLS, it was observed that the nanoparticles were present in the cytosol, endosomes and in the nucleus. Further groups of nanoparticles were found near damaged endosomes, which suggests that the particles coated in this combination of peptides are capable of disrupting endosomal morphology. From these studies,the mechanism of uptake of peptide coated gold nanoparticles is not fully understood.

CALNN stabilised gold nanoparticles have also been investigated as colorimetric sensors of various biologically relevant molecules such as Heparin,[90] Abscisic acid[91] and lysozyme,[92] as well as detecting Al^{3+} cations on living cellular surfaces.[93]

7 Multi-modal nanoparticles for imaging

The development of agents able to serve multiple functions is desirable to allow the use of two or more imaging techniques or theragnosis for both imaging and therapy.[94] Gold nanoparticles are particularly useful for multi-modal imaging due to their unique optical properties. However with further surface modification, gold nanoparticles can be altered to provide different properties for imaging and therapeutics. Gold nanoparticles have been modified with various anti-cancer drugs for treatment[95] and siRNA for gene silencing.[96] The quenching properties of gold nanoparticles have also been widely investigated, with fluorescent molecules being quenched in close proximity to the gold surface. The release of these molecules from the nanoparticle surface, which can be triggered by the presence of certain proteins[97] or light activation,[98] causes a fluorescence enhancement.

Gold nanoparticles have been modified with gadolinium complexes for potential use as a MRI contrast agent.[99-102] A gadolinium complex consisting of DTPA conjugated to 4-aminothiophenol has been reported on gold nanoparticles as a MRI contrast agent. The structure of this complex is similar to the europium complex shown in figure 1.10A. The complex alone and on the gold nanoparticles exhibit higher r1 relaxivity than that of the commercially available contrast agent Omniscan®. The r1 value of the gadolinium complex on gold nanoparticles per [Gd] was reported as 10.0 mM^{-1}s^{-1}, whilst the free gadolinium complex was lower at 6.3 mM^{-1}s^{-1} and the Omniscan® was lower still at 3.3 mM^{-1}s^{-1}. The gadolinium coated gold nanoparticles have also been presented as potential computed tomography (CT) contrast agents. Other DTPA gadolinium complexes have been reported on gold nanoparticles as multimodal MRI and CT contrast agents,[103] as well as blood pool contrast agents.[101]

Gold nanoparticles have shown great promise in therapeutic applications using hyperthermic treatment. Upon exposure to laser irradiation, gold nanoparticles and nanorods begin to heat up which damages the cells in the vicinity. El Sayed *et al.* have reported selective photo-thermal therapy using gold nanoparticles with conjugated antibodies.[104] By conjugating anti-epithelial growth factor receptor (Anti-EGFR) to gold nanoparticles, the nanoparticles can be used as a selective targeting and therapeutic agent. The nanoparticles were incubated with three epithelial cell lines, two malignant and one benign, then treated with a continuous visible argon ion laser at 514 nm. The malignant cells required less energy to kill the cells than the benign cells after incubation with the anti-EGFR gold nanoparticles, suggesting that these particles selectively target the malignant cells and offer opportunity for targeted photothermal therapy.

8   Thesis outline

The large surface area of gold nanoparticles makes them ideal scaffolds for the assembly of multiple probes for a variety of applications. Lanthanide complexes with their unique photophysical properties, such as long luminescent lifetimes and large Stokes shifts from the excitation source make them suitable as cellular imaging probes. This thesis describes the co-coating of gold nanoparticles with lanthanide complexes and targeting peptides for the development of targeting luminescent imaging probes. A photophysical study of europium (III) binding to two different peptides in solution, and the ability of these peptides to bind europium (III) ions whilst tethered to gold nanoparticles is presented in chapter 2. Lanthanide complexes with

a DTPA binding motif were prepared and attached to gold nanoparticles with different nuclear localisation signal peptides to investigate their photophysical properties and their potential as a cellular imaging agent in chapter 3. Whilst DTPA complexes have been used previously to coat gold nanoparticles, [66-68, 100, 101] the lanthanide complexes selected for this study have not previously been studied with peptides on gold nanoparticles. The comparison of the photophysical effects of the same peptide sequences with different thiol-containing terminal group has also been presented.

Chapter 4 introduces the co-coating of gold nanoparticles with europium and gadolinium complexes, with the combinations on gold nanoparticles giving rise to an interesting energy transfer effect between the two different lanthanide complexes. These co-coated gold nanoparticles were designed as a potential multi-modal luminescent and magnetic resonance imaging agents, utilising the photophysical and paramagnetic properties of the europium (III) and gadolinium (III) complexes.

The near-infrared lanthanides have recently attracted attention as cellular probes as near-infrared light can readily penetrate skin and tissue. The development of an azo-dye for sensitisation of the near-infrared lanthanides ytterbium (III) and neodymium (III) is discussed in chapter 5. The azo-dye was chosen for its high molar absorption coefficient in the visible region due to its extensive conjugation, which allows for excitation at wavelengths up to 500 nm. The azo-dye was found to form a complex with the lanthanide ions in a ratio of 3:1, exhibiting the characteristic emission of both ytterbium (III) and neodymium (III).

References

1 J. C. G. Bunzli and C. Piguet, *Chem. Soc. Rev.,* 2005, **34**, 1048-1077.

2 G. R. Choppin and D. R. Peterman, *Coord. Chem. Rev.,* 1998, **174**, 283-299.

3 E. G. Moore, A. P. S. Samuel and K. N. Raymond, *Acc. Chem. Res.,* 2009, **42**, 542-552.

4 A. Thibon and V. C. Pierre, *Anal. Bioanal. Chem.,* 2009, **394**, 107-120.

5 B. Alpha, R. Ballardini, V. Balzani, J. Lehn, S. Perathoner and N. Sabbatini, *Photochem. Photobiol.,* 1990, **52**, 299-306.

6 V. Alexander, *Chem. Rev.,* 1995, **95**, 273-342.

7 D. Parker, R. S. Dickins, H. Puschmann, C. Crossland and J. A. K. Howard, *Chem. Rev.,* 2002, **102**, 1977-2010.

8 D. Parker, *Chem. Soc. Rev.,* 2004, **33**, 156-165.

9 S. V. Eliseeva and J. C. G. Bunzli, *Chem. Soc. Rev.,* 2010, **39**, 189-227.

10 J. C. G. Bunzli, *Chem. Rev.,* 2010, **110**, 2729-2755.

11 R. G. Pearson, *J. Am. Chem. Soc.,* 1963, **85**, 3533-3539.

12 P. Caravan, J. J. Ellison, T. J. McMurry and R. B. Lauffer, *Chem. Rev.,* 1999, **99**, 2293-2352.

13 E. J. New, D. Parker and R. D. Peacock, *Dalton Trans.,* 2009, **4**, 672-679.

14 B. S. Murray, E. J. New, R. Pal and D. Parker, *Org. Biomol. Chem.,* 2008, **6**, 2085-2094.

15 E. J. New, D. Parker, D. G. Smith and J. W. Walton, *Curr. Opin. Chem. Biol.,* 2010, **14**, 238-246.

16 T. Lazarides, M. A. H. Alamiry, H. Adams, S. J. A. Pope, S. Faulkner, J. A. Weinstein and M. D. Ward, *Dalton Trans.,* 2007, , 1484-1491.

17 B. Alpha, J. Lehn and G. Mathis, *Angew. Chem. Int. Ed.,* 1987, **26**, 266-267.

18 W. D. Horrocks and D. R. Sudnick, *J. Am. Chem. Soc.,* 1979, **101**, 334-340.

19 C. M. Andolina, P. J. Klemm, W. C. Floyd, J. M. J. Frechet and K. N. Raymond, *Macromolecules,* 2012, **45**, 8982-8990.

20 E. J. New, A. Congreve and D. Parker, *Chem. Sci.,* 2010, **1**, 111-118.

21 J. G. Bünzli, A. Chauvin, C. D. B. Vandevyver, S. Bo and S. Comby, *Ann. N. Y. Acad. Sci.,* 2008, **1130**, 97-105.

22 E. Debroye, S. V. Eliseeva, S. Laurent, L. Vander Elst, S. Petoud, R. N. Muller and T. N. Parac-Vogt, *Eur. J. Inorg. Chem.,* 2013, **14**, 2629-2639.

23 E. Deiters, B. Song, A. Chauvin, C. D. B. Vandevyver, F. Gumy and J. G. Bünzli, *Chem- Eur J.,* 2009, **15**, 885-900.

24 C. D. B. Vandevyver, A. S. Chauvin, S. Comby and J. C. G. Bunzli, *Chem. Commun.,* 2007, , 1716-1718.

25 E. J. New and D. Parker, *Org. Biomol. Chem.,* 2009, **7**, 851-855.

26 E. Deiters, B. Song, A. Chauvin, C. D. B. Vandevyver and J. C. G. Bunzli, *New J. Chem.,* 2008, **32**, 1140-1152.

27 E. Deiters, B. Song, A. S. Chauvin, C. D. B. Vandevyver, F. Gumy and J. C. G. Bunzli, *Chem- Eur J.,* 2009, **15**, 885-900.

28 S. I. Klink, L. Grave, D. N. Reinhoudt, F. C. J. M. van Veggel, M. H. V. Werts, F. A. J. Geurts and J. W. Hofstraat, *J Phys Chem A,* 2000, **104**, 5457-5468.

29 S. Faulkner, A. Beeby, R. Dickins, D. Parker and J. A. G. Williams, *J. Fluoresc.,* 1999, **9**, 45-49.

30 S. A. Hilderbrand and R. Weissleder, *Curr. Opin. Chem. Biol.,* 2010, **14**, 71-79.

31 P. B. Glover, A. P. Bassett, P. Nockemann, B. M. Kariuki, R. Van Deun and Z. Pikramenou, *Chem- Eur J.,* 2007, **13**, 6308-6320.

32 D. J. Lewis, F. Moretta, A. T. Holloway and Z. Pikramenou, *Dalton Trans.,* 2012, **41**, 13138-13146.

33 J. E. Jones and S. J. A. Pope, *Dalton Trans.,* 2009, **39**, 8421-8425.

34 A. Beeby, S. Faulkner and J. A. G. Williams, *J. Chem. Soc. , Dalton Trans.,* 2002, **9**, 1918-1922.

35 S. I. Klink, H. Keizer and F. C. J. M. van Veggel, *Angew. Chem. Int. Ed.,* 2000, **39**, 4319-4321.

36 M. D. Ward, *Coord. Chem. Rev.,* 2007, **251**, 1663-1677.

37 S. Singaravadivel, E. Babu, M. Velayudham, K. Lu and S. Rajagopal, *Polyhedron,* 2013, **60**, 54-58.

38 T. Lazarides, N. M. Tart, D. Sykes, S. Faulkner, A. Barbieri and M. D. Ward, *Dalton Trans.,* 2009, , 3971-3979.

39 N. M. Shavaleev, L. P. Moorcraft, S. J. A. Pope, Z. R. Bell, S. Faulkner and M. D. Ward, *Chem- Eur J.,* 2003, **9**, 5283-5291.

40 S. W. Magennis, S. Parsons and Z. Pikramenou, *Chem- Eur J.,* 2002, **8**, 5761-5771.

41 Z. Zhou and Z. Lu, *Wiley Interdisciplinary Reviews: Nanomedicine and Nanobiotechnology,* 2013, **5**, 1-18.

42 M. Bottrill, L. Kwok and N. J. Long, *Chem. Soc. Rev.,* 2006, **35**, 557-571.

43 P. Caravan, C. T. Farrar, L. Frullano and R. Uppal, *Contrast Media & Molecular Imaging,* 2009, **4**, 89-100.

44 C. Paul-Roth and K. N. Raymond, *Inorg. Chem.,* 1995, **34**, 1408-1412.

45 J. Turkevich, P. C. Stevenson and J. Hillier, *Discuss. Faraday Soc.,* 1951, **11**, 55-75.

46 G. Frens, *Nature Phys Sci,* 1973, **241**, 20-22.

47 L. Srisombat, A. C. Jamison and T. R. Lee, *Colloids Surf. Physicochem. Eng. Aspects,* 2011, **390**, 1-19.

48 D. Roy and J. Fendler, *Adv Mater,* 2004, **16**, 479-508.

49 M. Brust, M. Walker, D. Bethell, D. J. Schiffrin and R. Whyman, *J. Chem. Soc. , Chem. Commun.,* 1994, **7**, 801-802.

50 G. Mie, *Ann. Phy-Berlin,* 1908, **330**, 377-445.

51 E. Boisselier and D. Astruc, *Chem. Soc. Rev.,* 2009, **38**, 1759-1782.

52 K. Saha, S. S. Agasti, C. Kim, X. Li and V. M. Rotello, *Chem. Rev.,* 2012, **112**, 2739-2779.

53 J. Wang, J. Moore, S. Lauhle, M. Nantz, S. Achilefu and K. A. Kang, *Nanotechnology,* 2012, **23**, 095501.

54 T. Biver, N. Eltugral, A. Pucci, G. Ruggeri, A. Schena, F. Secco and M. Venturini, *Dalton Trans.,* 2011, **40**, 4190-4199.

55 A. Kumar, H. Ma, X. Zhang, K. Huang, S. Jin, J. Liu, T. Wei, W. Cao, G. Zou and X. Liang, *Biomaterials,* 2012, **33**, 1180-1189.

56 S. Pujals, N. G. Bastus, E. Pereiro, C. Lopez-Iglesias, V. F. Punte, M. J. Kogan and E. Giralt, *Chembiochem,* 2009, **10**, 1025-1031.

57 L. L. Sun, D. J. Liu and Z. X. Wang, *Langmuir,* 2008, **24**, 10293-10297.

58 A. G. Tkachenko, H. Xie, D. Coleman, W. Glomm, J. Ryan, M. F. Anderson, S. Franzen and D. L. Feldheim, *J. Am. Chem. Soc.,* 2003, **125**, 4700-4701.

59 A. G. Tkachenko, H. Xie, Y. Liu, D. Coleman, J. Ryan, W. R. Glomm, M. K. Shipton, S. Franzen and D. L. Feldheim, *Bioconjug. Chem.,* 2004, **15**, 482-490.

60 C. C. Berry, *Nanomedicine,* 2008, **3**, 357-365.

61 N. Erathodiyil and J. Y. Ying, *Acc. Chem. Res.,* 2011, **44**, 925-935.

62 R. A. Sperling, P. Rivera Gil, F. Zhang, M. Zanella and W. J. Parak, *Chem. Soc. Rev.,* 2008, **37**, 1896-1908.

63 E. A. Vitol, Z. Orynbayeva, G. Friedman and Y. Gogotsi, *J. Raman Spectrosc.,* 2012, **43**, 817-827.

64 C. Kim, P. Ghosh and V. M. Rotello, *Nanoscale,* 2009, **1**, 61-67.

65 B. I. Ipe, K. Yoosaf and K. G. Thomas, *J. Am. Chem. Soc.,* 2006, **128**, 1907-1913.

66 D. J. Lewis, C. Bruce, S. Bohic, P. Cloetens, S. P. Hammond, D. Arbon, S. Blair-Reid, Z. Pikramenou and B. Kysela, *Nanomedicine,* 2010, **5**, 1547-1557.

67 D. J. Lewis, T. M. Day, J. V. MacPherson and Z. Pikramenou, *Chem. Commun.,* 2006, **13**, 1433-1435.

68 A. Davies, D. J. Lewis, S. P. Watson, S. G. Thomas and Z. Pikramenou, *PNAS,* 2012, **109**, 1862-1867.

69 C. S. Bonnet, J. Massue, S. J. Quinn and T. Gunnlaugsson, *Org. Biomol. Chem.,* 2009, **7**, 3074-3078.

70 S. Comby and T. Gunnlaugsson, *ACS Nano,* 2011, **5**, 7184-7197.

71 J. Massue, S. J. Quinn and T. Gunnlaugsson, *J. Am. Chem. Soc.,* 2008, **130**, 6900-6901.

72 L. K. Truman, S. Comby and T. Gunnlaugsson, *Angew. Chem. Int. Ed.,* 2012, **51**, 9624-9627.

73 L. Zheng, X. Lin, N. Wu, M. Liu, Y. Zheng, J. Sheng, X. Ji and M. Sun, *BBA - Rev. Cancer.,* 2013, **1836**, 42-48.

74 P. Laverman, J. K. Sosabowski, O. C. Boerman, W. J. Oyen and G., *Eur. J. Nucl. Med. Mol. I.,* 2012, **39**, 78-92.

75 P. Järver and Ü Langel, *BBA - Biomembranes,* 2006, **1758**, 260-263.

76 E. Pazos, O. Vazquez, J. L. Mascarenas and M. Eugenio Vazquez, *Chem. Soc. Rev.,* 2009, **38**, 3348-3359.

77 K. N. Allen and B. Imperiali, *Curr. Opin. Chem. Biol.,* 2010, **14**, 247-254.

78 A. Marguerre and R. Krämer, *Bioorg. Med. Chem. Lett.,* 2009, **19**, 5757-5759.

79 R. Levy, N. T. K. Thanh, R. C. Doty, I. Hussain, R. J. Nichols, D. J. Schiffrin, M. Brust and D. G. Fernig, *J. Am. Chem. Soc.,* 2004, **126**, 10076-10084.

80 R. Levy, *Chembiochem,* 2006, **7**, 1141-1145.

81 M. J. Kogan, I. Olmedo, L. Hosta, R Guerrero Ariel, L. J. Cruz and F. Albericio, *Nanomedicine,* 2007, **2**, 287-306.

82 S. Pujals, J. Fernández-Carneado, C. López-Iglesias, M. J. Kogan and E. Giralt, *BBA - Biomembranes,* 2006, **1758**, 264-279.

83 R. Lévy, U. Shaheen, Y. Cesbron and V. Sée, *Nano Reviews,* 2010, **1**, 4889.

84 J. M. de la Fuente and C. C. Berry, *Bioconjug. Chem.,* 2005, **16**, 1176-1180.

85 Z. Krpetic, S. Saleemi, I. A. Prior, V. See, R. Qureshi and M. Brust, *ACS Nano,* 2011, **5**, 5195-5201.

86 D. Derossi, G. Chassaing and A. Prochiantz, *Trends Cell Biol.,* 1998, **8**, 84-87.

87 M. Pooga, M. Hällbrink, M. Zorko, U. Langel and Io, *The FASEB Journal,* 1998, **12**, 67-77.

88 R. Lévy, N. T. K. Thanh, R. C. Doty, I. Hussain, R. J. Nichols, D. J. Schiffrin, M. Brust and D. G. Fernig, *J. Am. Chem. Soc.,* 2004, **126**, 10076-10084.

89 P. Nativo, I. A. Prior and M. Brust, *ACS Nano,* 2008, **2**, 1639-1644.

90 K. J. Jeong, K. Butterfield and A. Panitch, *Langmuir,* 2008, **24**, 8794-8800.

91 G. Zhou, Y. Liu, M. Luo, Q. Xu, X. Ji and Z. He, *ACS Appl. Mater. Interfaces,* 2012, **4**, 5010-5015.

92 H. Huang, Q. Zhang, J. Luo and Y. Zhao, *Anal. Methods,* 2012, **4**, 3874-3878.

93 X. Li, J. Wang, L. Sun and Z. Wang, *Chem. Commun.,* 2010, **46**, 988-990.

94 D. Lee, H. Koo, I. Sun, J. H. Ryu, K. Kim and I. C. Kwon, *Chem. Soc. Rev.,* 2012, **41**, 2656-2672.

95 E. C. Dreaden, M. A. Mackey, X. Huang, B. Kang and M. El-Sayed, *Chem. Soc. Rev.,* 2011, **40**, 3391-3404.

96 G. B. Braun, A. Pallaoro, G. Wu, D. Missirlis, J. A. Zasadzinski, M. Tirrell and N. O. Reich, *ACS Nano,* 2009, **3**, 2007-2015.

97 X. Wang, Y. Xia, Y. Liu, W. Qi, Q. Sun, Q. Zhao and B. Tang, *Chem- Eur J.,* 2012, **18**, 7189-7195.

98 W. F. Zandberg, A. B. S. Bakhtiari, Z. Erno, D. Hsiao, B. D. Gates, T. Claydon and N. R. Branda, *Nanomed. - Nanotechnol.,* 2012, **8**, 908-915.

99 N. S. Md, H. K. Kim, J. A. Park, Y. Chang and T. J. Kim, *Bull. Korean. Chem. Soc.,* 2010, **31**, 1177-1181.

100 J. Park, H. Kim, J. Kim, S. Jeong, J. Jung, G. Lee, J. Lee, Y. Chang and T. Kim, *Bioorg. Med. Chem. Lett.,* 2010, **20**, 2287-2291.

101 H. Kim, H. Jung, J. Park, M. Huh, J. Jung, Y. Chang and T. Kim, *J. Mater. Chem.,* 2010, **20**, 5411-5417.

102 P. -. Debouttière, S. Roux, F. Vocanson, C. Billotey, O. Beuf, A. Favre-Réguillon, Y. Lin, S. Pellet-Rostaing, R. Lamartine, P. Perriat and O. Tillement, *Adv. Funct. Mater.,* 2006, **16**, 2330-2339.

103 C. Alric, J. Taleb, G. Duc, C. Mandon, C. Billotey, A. Meur-Herland, T. Brochard, F. Vocanson, M. Janier, P. Perriat, S. Roux and O. Tillement, *J. Am. Chem. Soc.,* 2008, **130**, 5908-5915.

104 I. H. El-Sayed, X. Huang and M. A. El-Sayed, *Cancer Lett.,* 2006, **239**, 129-135.

Lanthanide binding peptides and peptide coated gold nanoparticles

1   Introduction

Peptides have been utilised as vehicles for the delivery of luminescent probes into cells for targeting and monitoring specific protein-peptide interactions. Peptides that are able to bind lanthanides are particularly well studied due to their desirable photophysical properties, such as large Stokes shift, emission signal in the visible or near-infrared and luminescence lifetimes in microsecond to millisecond range.[1, 2] The design of these lanthanide binding peptides are strongly dependant on two key features, firstly a ligating site to bind the lanthanide ion and a chromophore in close proximity to the ligating site to allow for the excitation of the lanthanide. The ligating sites can be designed based on the structural organisation of the peptide using the naturally occurring amino acids,[3, 4] or modification of the peptide to incorporate a podand or macrocyclic structure (figure 2.1).[5-8] Figure 2.1 shows two strategies of lanthanide for peptide labelling with lanthanide binding tags.[3] The first strategy involves the chemical modification of the peptide by targeting certain amino acids with groups that can be easily modified such as cysteine which contains sulphurs. The second strategy is the encoding of the lanthanide binding tag at DNA level, leading to the expression of proteins with the lanthanide binding tag located on the N-terminus or C-terminus or alternatively located in a loop within the protein structure.[3] The similar reactivity of the lanthanides allows for the use of non-luminescent lanthanides for MRI imaging,[9] NMR analysis of structural information[10] or X-ray structural elucidation.[11] For this reason, lanthanide binding peptides are widely studied and have been investigated for many different functions.
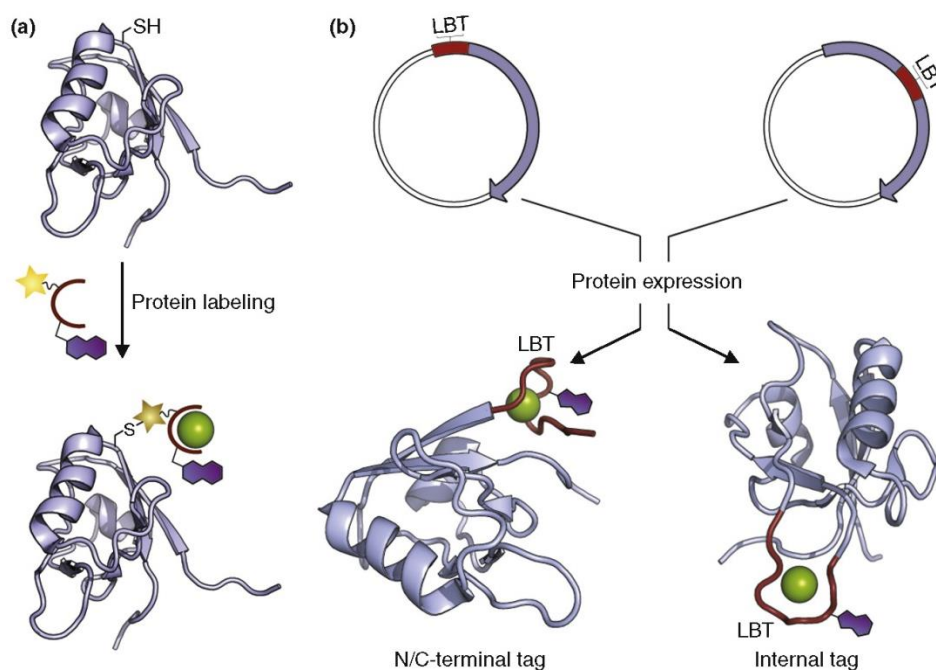
Figure 2.1: Strategies for labelling peptides with lanthanides. (a) Modification of peptide with a synthetic lanthanide chelator. Chemical modification can occur between a reactive group (star) and cysteines (shown here) or other amino acids. LBT peptides may also be linked to the target protein by chemical modification of target cysteines. (b) Peptide-based lanthanide-binding ion tags (red) are encoded at the DNA level and fused to either the N-terminus or C-terminus of the target protein or into a loop.Figure reproduced from reference 3

Gold nanoparticles are widely researched for their biomedical applications, as they provide a suitable platform for the delivery of multiple probes into cells. Due to the large surface area of gold nanoparticles, the surface can be functionalised with many different functional molecules. Peptide coated nanoparticles in particular are of interest in their potential applications in cellular binding and delivery.[12-14] Certain peptide sequences have been found to translocate cell membranes and deliver functionalising moieties into cells.[15] Combining lanthanides and peptides onto gold nanoparticles is desirable for the targeted delivery of multiple luminescent probes into cells.

Work within our group has previously utilised lanthanide complexes on gold nanoparticles as cellular probes.[16] The combination of a europium complex and a pH low insertion peptide (pHLIP) has been found to deliver the luminescent gold nanoparticles into platelets in a pH dependant manner.[17] At pH above 7 the pHLIP peptide exhibits an unstructured formation and loosely associates with the cell membrane. At low pH, the peptide forms an alpha-helix across the lipid bilayer and inserts across the cell membrane (figure 2.2).

pHLIP peptide: AAEQNPIYWARYADWLFTTPLLLLDLALLVDADEGTCG

In solution peptide is unstructured

pH > 7 unstructured peptide loosely associates with membrane

pH < 7 trans-membrane α-helix formation and insertion across the cell membrane

Lipid bilayer
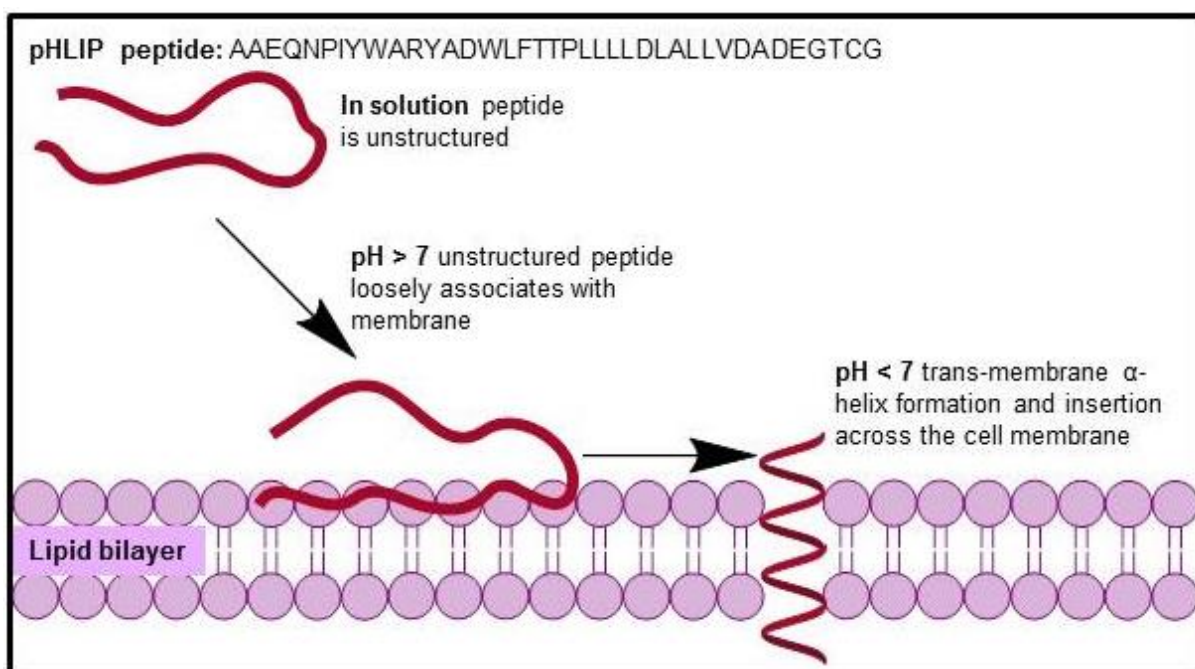
Figure 2.2: Mechanism of pH controlled uptake of pHLIP peptide.[17]

In this chapter, a peptide has been designed and synthesised based on the peptide CALNN which is known to stabilise gold nanoparticles in aqueous solutions.[18] The peptide ThioALNN has been found to bind lanthanide ions both in solution and also whilst bound to gold nanoparticles.[19] Other peptides have also been investigated for

their ability to bind lanthanides in solution and on nanoparticles. The peptides discussed in this chapter are shown in figure 2.3.
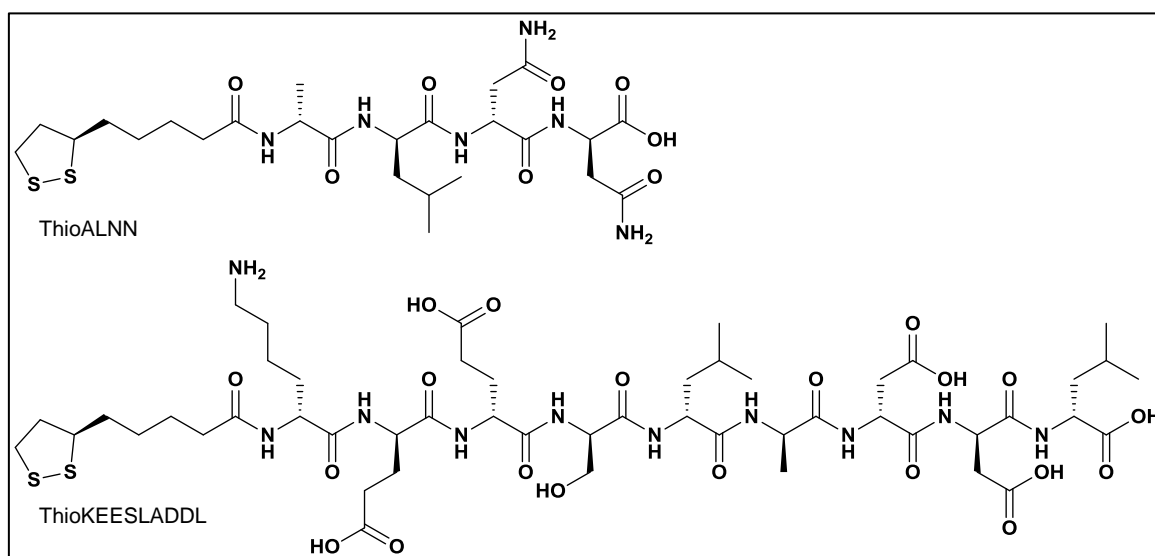
Figure 2.3: Structure of peptides ThioALNN and ThioKEESLADDL

2   Results and Discussion

2.1   Synthesis and characterisation of ThioALNN peptide and *Citrate.Au*

ThioALNN peptide was designed based on the peptide CALNN, which has been found to stabilise gold nanoparticles in aqueous solutions.[18] The addition of a thioctic acid on the end of the peptide provides two sulphurs for stronger binding to gold nanoparticles. The peptide was prepared using FMOC-based solid-phase peptide synthesis, and purified by HPLC. The peptide was characterised by MALDI-TOF mass spectrometry, which showed a peak at 641 corresponding to the sodium adduct of the final peptide. A peak was also present at 643, suggesting that the peptide was also present in the reduced form. ThioALNN peptide was characterised by UV-Vis spectroscopy, which showed a single peak with a λ_{max} at 203 nm.

The gold nanoparticles prepared for this study were citrate stabilised gold nanoparticles (*Citrate.Au*). They were chosen as the preparation is a simple one-step synthesis to give stable and monodisperse nanoparticles of uniform size and shape in aqueous solution. *Citrate.Au* were prepared by the well-established citrate reduction of $HAuCl_4$ giving monodisperse gold nanoparticles approximately 13 nm in diameter (figure 2.4A). The deep red colloid gives the expected profile by UV-Vis spectroscopy with a λ_{max} at 521 nm (figure 2.4B), characteristic of the surface plasmon resonance band (SPR) of nanoparticles of this size.

The surface modification of *Citrate.Au* can be easily achieved by the formation of gold/sulphur bonds on the surface of the nanoparticles. The addition of peptides or any other moieties containing sulphur groups into *Citrate.Au* can be monitored by UV-Vis spectroscopy, as any changes to the surface of the citrate stabilised gold

nanoparticles gives rise to changes in the SPR band, which is sensitive to changes in the surface chemistry of the gold nanoparticles.
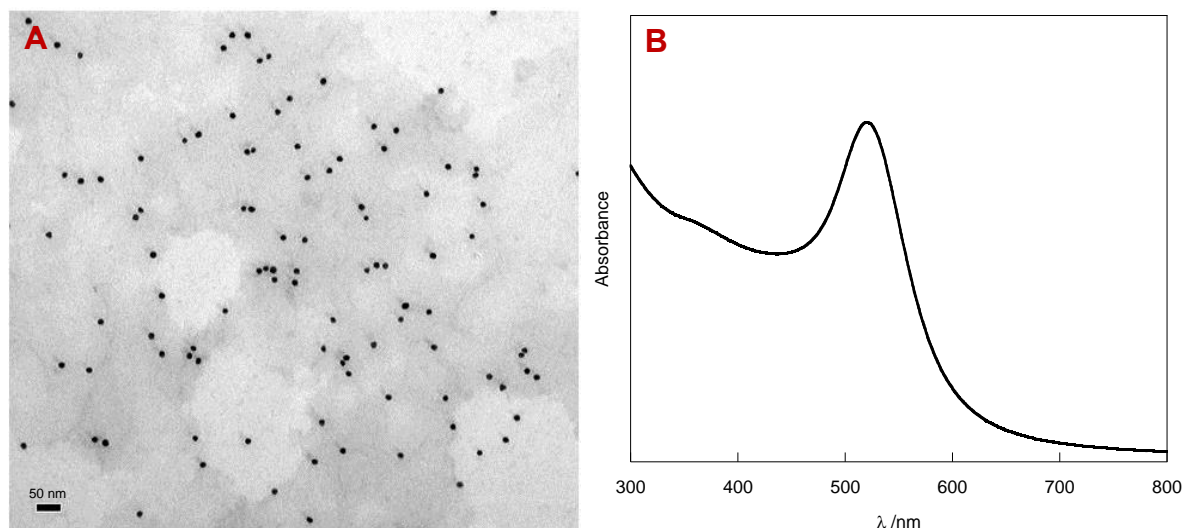
Figure 2.4: Characterisation of **Citrate.Au**. **A**: TEM of citrate stabilised gold nanoparticles, **Citrate.Au.** Scale bar = 50 nm. **B**: UV-Vis spectrum of **Citrate.Au**. [**Citrate.Au**] = 4.5 nM.

2.2   Europium (III) binding studies to peptides

As peptides are useful vehicles in cellular delivery, it is interesting to investigate whether peptides are able to bind lanthanide ions for the development of luminescent peptide probes. The binding of lanthanide ions to ThioALNN peptide was investigated by luminescence spectroscopy. Upon titration of a stock solution of europium (III) into a solution of ThioALNN in water, an increase in europium emission is observed. Further additions of europium (III) resulted in a plateau indicative of the saturation of the peptide binding sites with europium (III). Since the ThioALNN peptide contains no chromophoric units for sensitisation of europium ion emission, any increase in

emission intensity can be attributed to exclusion of water from the lanthanide coordination sphere due to a binding event. The luminescence spectra of the titration of a solution of europium (III) into a 0.18 mM solution of ThioALNN peptide shows an increase in europium emission upon addition of stock solution of europium (III) in water (figure 2.5). The europium (III) binding event to ThioALNN is shown by the saturation of europium emission at a europium (III) concentration of 60 µM. This suggests that the ratio of binding is three peptides to one lanthanide ion.
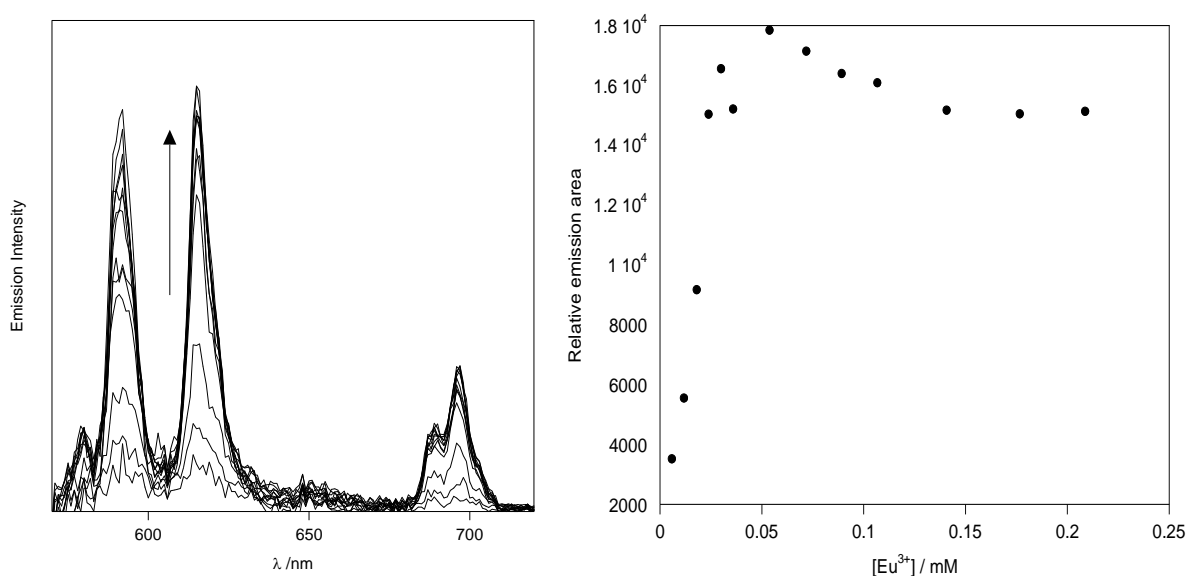
Figure 2.5: Emission spectra and plot of emission intensity vs. concentration of Eu^{3+} of ThioALNN peptide upon the titration of Eu^{3+}. Concentration of ThioALNN peptide in water = 0.18 mM.

The addition of europium (III) to thioALNN can also be monitored by circular dichroism spectroscopy (CD). The addition of europium (III) induces a slight change in the CD spectrum, and monitoring the additions also gives an indication of the concentration at which the binding sites have become saturated (figure 2.6). Increasing the concentration of europium (III) above 72 µM shows no further changes

in the CD spectrum, suggesting that the peptide structure has stabilised and the addition of further europium (III) has no further effect on the structural organisation of the peptide.
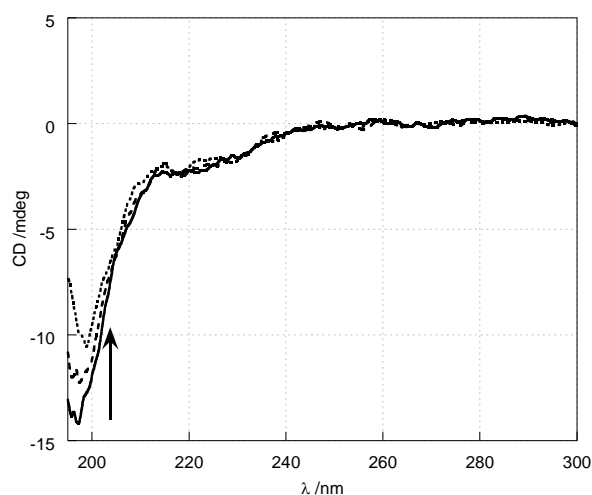
Figure 2.6: Circular dichroism spectra of ThioALNN peptide, plus the addition of europium (III) ions. [ThioALNN] = 0.18 mM (——), [1st addition Eu^{3+}] = 36 µM (−−−), [2nd addition Eu^{3+}] = 72 µM (•••••)

The longer peptide ThioKEESLADDL was also investigated as a potential lanthanide binding peptide. This peptide has been chosen for investigation as it carries a portion of the human NBS1 gene that interacts with ATM, a member of the phosphatidylinositol 3-kinase family. It is known to interfere with DNA repair mechanisms within cells. The peptide ThioKEESLADDL contains no chromophore unit similar to ThioALNN which could sensitise europium emission, therefore as with the ThioALNN peptide the emission observed is again attributed to the displacement of water molecules coordinated to the lanthanide ion. Titration of europium (III) ions into a 0.18 mM solution of ThioKEESLADDL clearly shows the binding of the

europium from the increase in europium emission observed. The binding ratio of europium to ThioKEESLADDL was found to be 1:1 (figure 2.7).
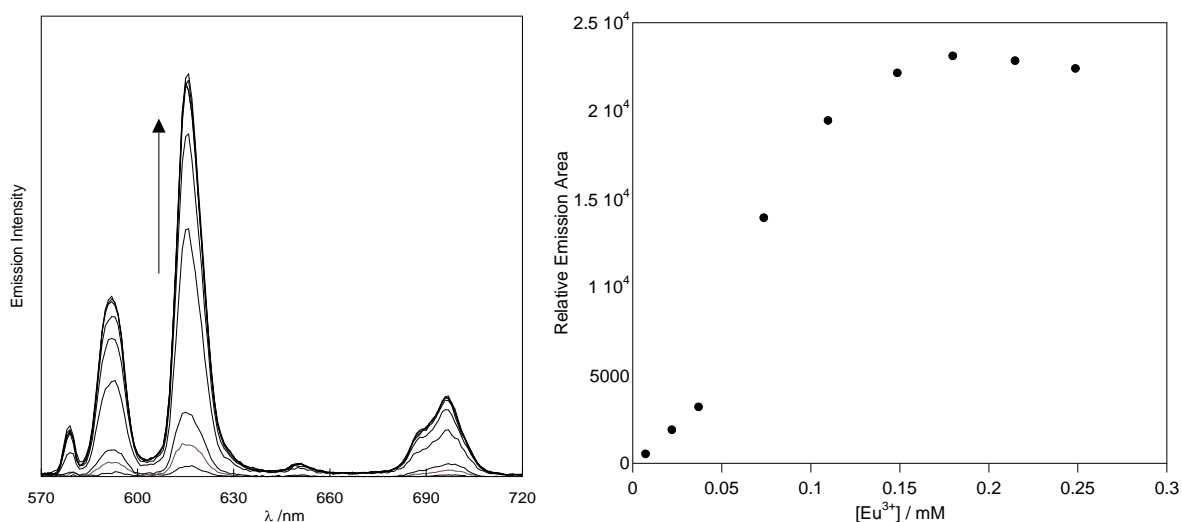
Figure 2.7: Titration of Eu^{3+} into ThioKEESLADDL solution. [ThioKEESLADDL] = 0.18 mM. λ_{exc} = 280 nm. Left: Emission spectra of titration. Right: Plot of emission intensity increase vs. [Eu^{3+}]. Data corrected for residual luminescence signal of Eu^{3+}.

Circular dichroism shows a similar trend upon addition of europium (III) to a solution of ThioKEESLADDL peptide, with a change induced in the CD spectrum upon addition of europium (figure 2.8). This is potentially due a change in the structural conformation of the peptide upon complexation of the europium ion.
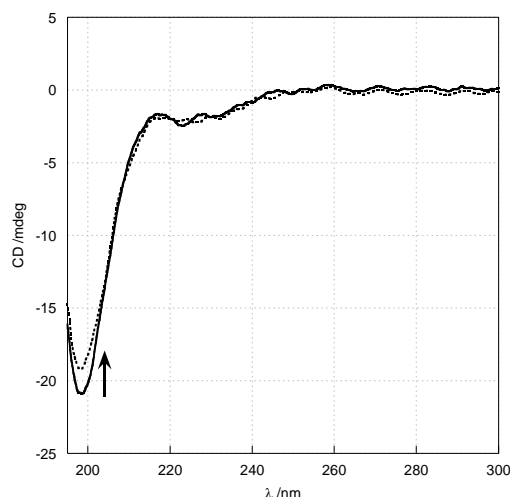
Figure 2.8: Circular dichroism of thioKEESLADDL peptide with the addition of europium (III). [ThioKEESLADDL] = 0.18 M (——), [Eu^{3+}] = 0.18 M (••••••).

The two peptides have different structures which can help to explain the different binding ratios of peptides to lanthanide ions. Lanthanide ions coordinate to hard bases, such as oxygen, therefore some of the groups on these peptides are suitable for lanthanide coordination. The carboxylates found within both of these peptide structures are the most likely to coordinate on these peptides. Comparing the numbers on these two peptides it can be seen that the ThioALNN peptide contains one carboxylic acid group whilst the ThioKEESLADDL peptide contains five. Therefore it is possible that one ThioKEESLADDL peptide can bind one lanthanide ion, as it is possible that the peptide is able to wrap around the lanthanide ion to form a complex. The ThioALNN peptide however is smaller with less available coordination sites, therefore it requires a higher number of peptides to efficiently coordinate the lanthanide ion.

2.3   Coating of gold nanoparticles with ThioALNN and ThioKEESLADDL

ThioALNN.Au   **ThioKEESLADDL.Au**
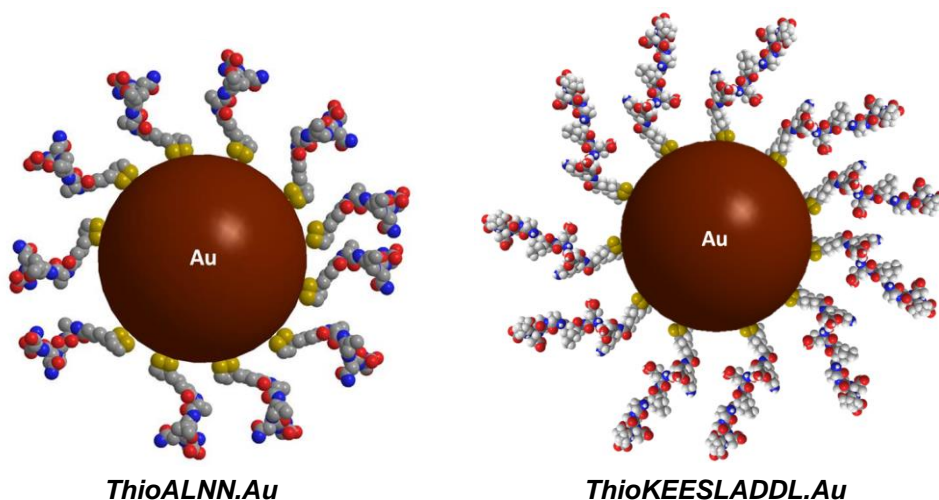
Scheme 2.1: Schematic representation of *ThioALNN.Au* and *ThioKEESLADDL.Au*

The coating of *Citrate.Au* with the peptides ThioALNN and ThioKEESLADDL was monitored by UV-Vis spectroscopy to observe any changes in the SPR band upon addition of the peptides. *Citrate.Au* was coated in ThioALNN peptide and the binding event was monitored by UV-Vis spectroscopy. The addition of ThioALNN peptide to *Citrate.Au* resulted in a 2 nm red-shift in SPR band (figure 2.9). This shift is in agreement with the shift observed in gold nanoparticles when stabilised with CALNN peptide.[18] The nanoparticles were characterised by transmission electron microscopy (TEM) which confirmed the nanoparticles were uniform in shape with a diameter of 13-15 nm (figure 2.10).
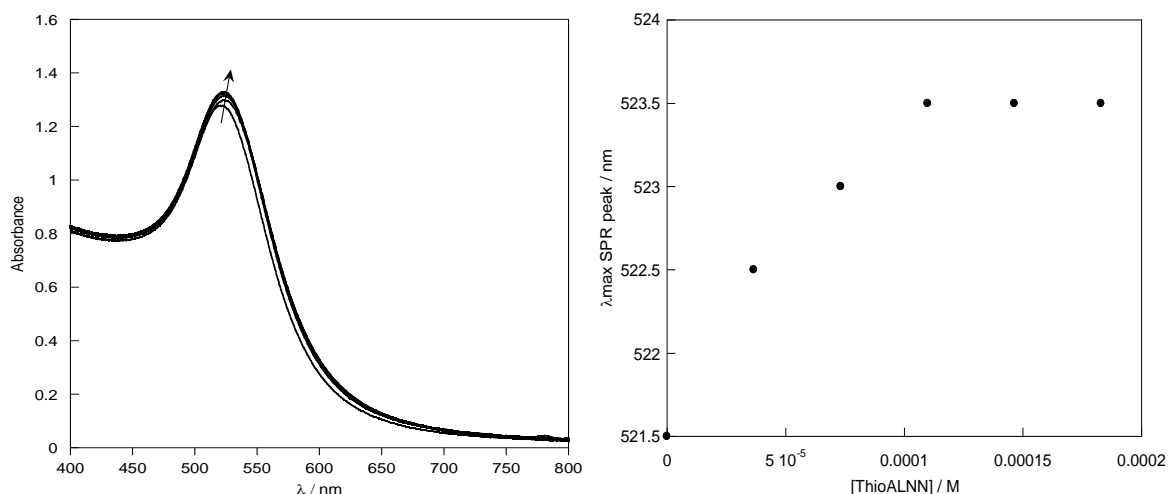
Figure 2.9: UV-Vis spectra and SPR shift plot of the titration of ThioALNN into **Citrate.Au**. [**Citrate.Au**] = 4.5 nM
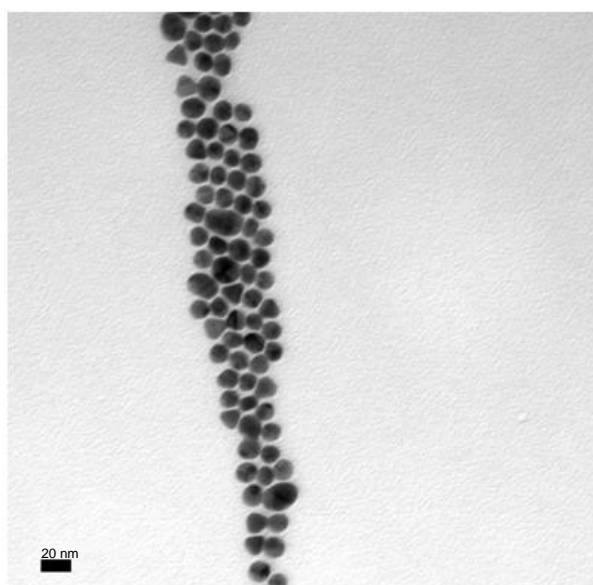
Figure 2.10: TEM image of **ThioALNN.Au**. Scale bar = 20 nm

Citrate.Au were coated with ThioKEESLADDL peptide using the same conditions as **ThioALNN.Au**. The shift in the SPR band was monitored by UV-Vis and found to be a 1.5 nm red-shift upon addition of ThioKEESLADDL (figure 2.11). These particles

were also characterised by TEM, again showing nanoparticles uniform in shape between 10-15 nm in size (figure 2.12). There are however some slightly larger particles observed in the TEM about 20 nm in size present in the *ThioKEESLADDL.Au*.
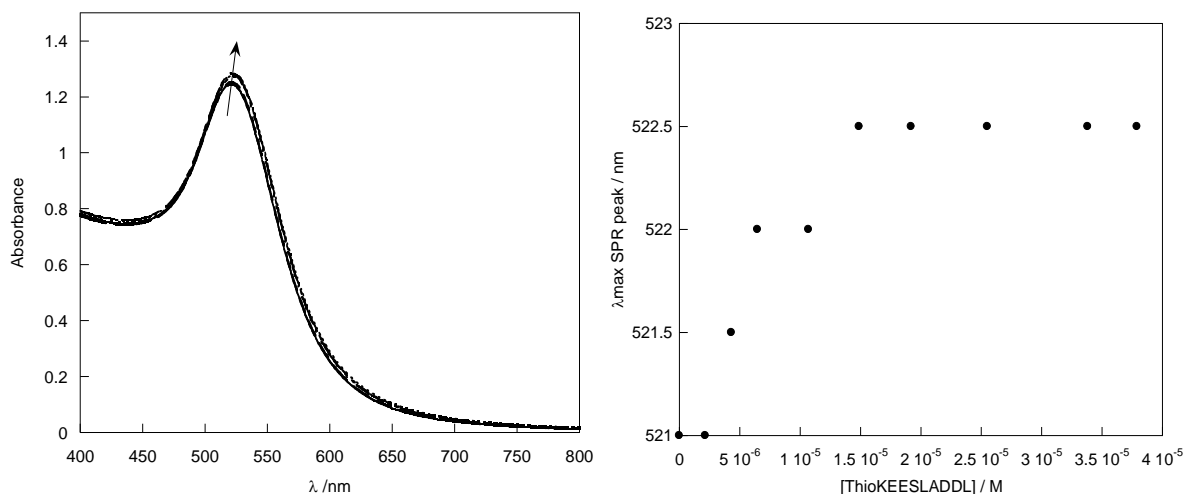
Figure 2.11: UV-Vis spectra and SPR shift plot of the titration of ThioKEESLADDL into *Citrate.Au*. [*Citrate.Au*] = 4.5 nM
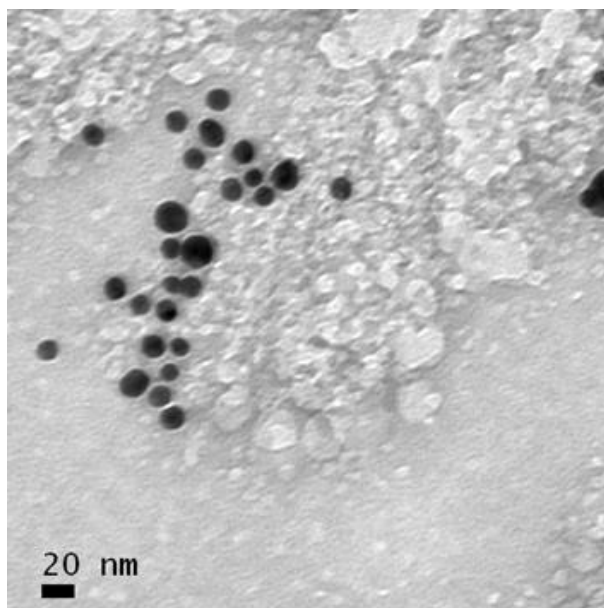
Figure 2.12: TEM image of **ThioKEESLADDL.Au**. Scale bar = 20 nm.

Studies of the size distribution of the gold nanoparticles were carried out using dynamic light scattering (DLS). The number distributions obtained by DLS (shown in table 2.1) for **Citrate.Au**, **ThioALNN.Au** and **ThioKEESLADDL.Au** agree with the size observed by TEM microscopy. The data recorded for ThioALNN also showed a small distribution at 1.2 ± 0.1 nm in both the number and intensity distribution. This is most likely an artefact which has caused the distributions to be slightly skewed.

Sample	Number Distribution	Intensity Distribution
Citrate.Au	13.7 ± 3.6 nm	30.0 ± 13.4 nm
ThioALNN.Au	* 1.2 ± 0.1 nm * 17.0 ± 3.9 nm	* 1.2 ± 0.1 nm * 27.0 ± 8.6 nm
ThioKEESLADDL.Au	10.7 ± 3.1 nm	31.3 ± 16.8 nm

Table 2.1: Dynamic light scattering data for **Citrate.Au**, **ThioALNN.Au** and **ThioKEESLADDL.Au**

2.4 The binding of europium (III) to peptide coated nanoparticles

2.4.1 The binding of europium (III) to ThioALNN.Au

ThioALNN.Au   **Eu-ThioALNN.Au**
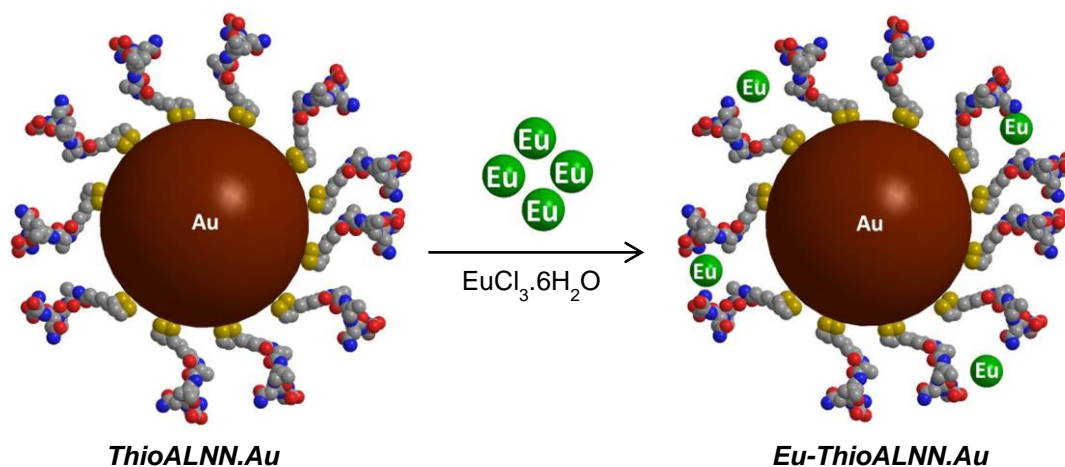
Scheme 2.2: Schematic representation of the preparation of *Eu-ThioALNN.Au*

The lanthanide binding properties of the two peptides ThioALNN and ThioKEESLADDL have been confirmed by luminescence spectroscopy studies. To further study the lanthanide binding properties of these peptides, their ability to bind lanthanides whilst tethered to gold nanoparticles has also been investigated. *Citrate.Au* was coated in ThioALNN peptide, as monitored by UV-Vis spectroscopy (figure 2.13).
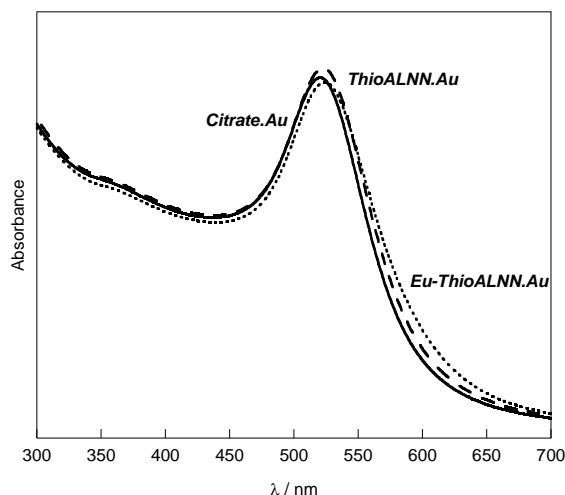
Figure 2.13: UV-Vis spectra of **Citrate.Au** (——), with the addition of ThioALNN [0.18 mM] in phosphate buffer (− −) and Eu^{3+} [0.52 mM] in water (•••).

The binding of europium to **ThioALNN.Au** was monitored by luminescence spectroscopy upon titration of EuCl$_3$.6H$_2$O. Additions of europium (III) in μl aliquots into **ThioALNN.Au** lead to a strong increase in europium signal, which reaches a plateau indicative of saturation of peptide binding sites on the nanoparticle with europium (III). A small red-shift and a decrease in the intensity in the SPR band by UV-Vis are observed upon addition of europium (III) to **ThioALNN.Au**.

46
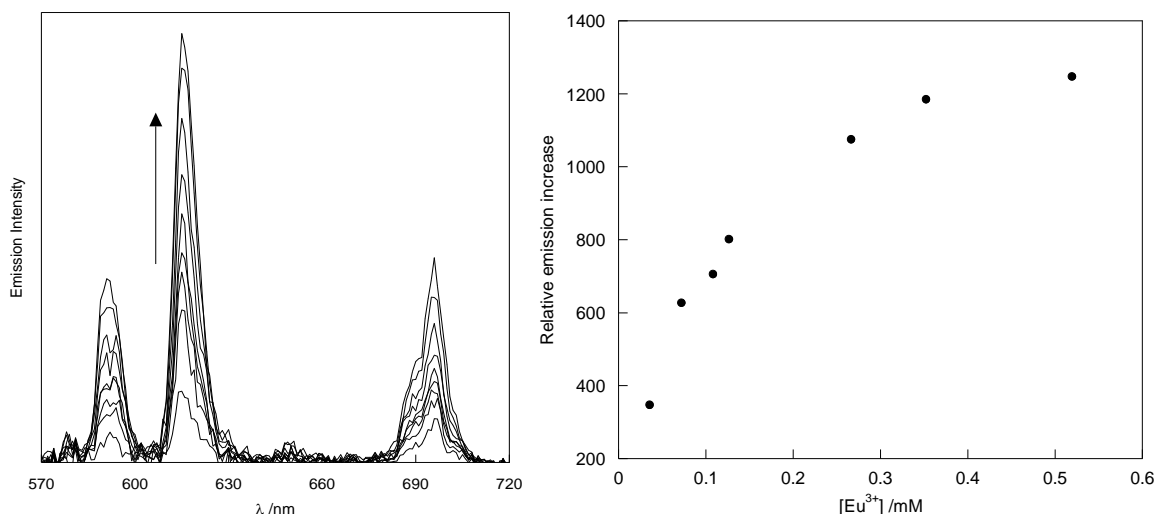
Figure 2.14: Luminescence spectra of **ThioALNN.Au** upon titration of Eu^{3+}, [AuNP] = 4.5 nM, [ThioALNN] = 0.18 mM, λ_{exc} = 280 nm. Data corrected for residual luminescence signal of Eu^{3+}.

The **Eu-ThioALNN.Au** nanoparticles are less emissive than **Eu-ThioALNN**, which could possibly be due to quenching of the lanthanide luminescence due to close proximity to the gold surface.[20] It is also possible that once bound to the gold surface, the peptide loses its structural freedom which may affect its ability to wrap around the lanthanide. This may cause the lanthanide ion to be exposed to water, which is known to quench the lanthanide emission signal. This possible explanation is supported by the different ratio of the two bands at 592 nm and 614 nm attributed to $^5D_0 \rightarrow {}^7F_2$ and $^5D_0 \rightarrow {}^7F_1$ in solutions of **Eu-ThioALNN** and **Eu-ThioALNN.Au** (figures 2.5 and 2.14), as the $^5D_0 \rightarrow {}^7F_2$ band is sensitive to the structural environment around the lanthanide ion.

47
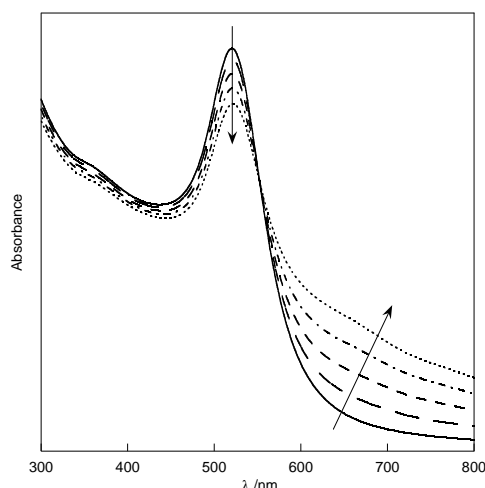
Figure 2.15: UV-Vis spectra of the titration of Eu^{3+} into *Citrate.Au* (——). [*Citrate.Au*] = 4.5 nM, [Eu^{3+}] = 0.179 - 0.682 mM. Arrows indicate peak reduction at 521 nm and peak growth at 650 nm upon additions of Eu^{3+}.

In order to establish whether the increase in europium emission intensity can be attributed to the binding of the europium ions to the peptides, a control experiment of titrating europium (III) into *Citrate.Au* was carried out. This titration of europium (III) into *Citrate.Au* leads to immediate aggregation of the particles, which is shown by the growth of a UV-Vis band at 650 nm (figure 2.15). This demonstrates the ability of the ThioALNN peptide to stabilise gold nanoparticles, as the peptide coated nanoparticles do not aggregate upon addition of the same concentrations of europium (III). Luminescence studies of this titration shows a very weak increase in europium signal upon titration of europium (III). This increase is significantly lower than that observed with the titration of europium (III) with the peptide coated gold nanoparticles, and was too weak to be corrected for residual europium emission therefore the emission increase found from this titration was not significant enough to have an effect on the results obtained for the peptide coated nanoparticles.
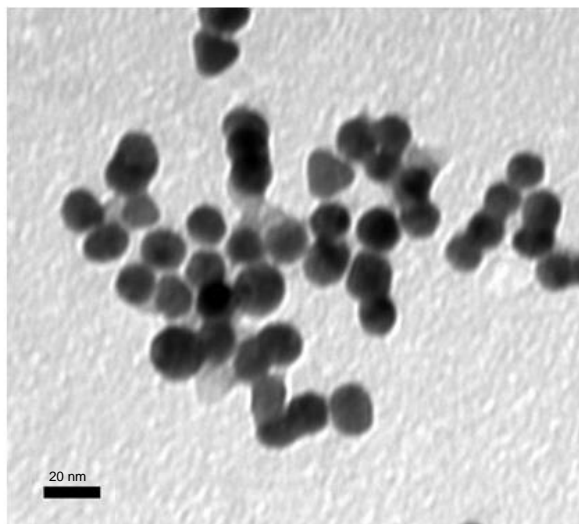
Figure 2.16: TEM image of *Eu-ThioALNN.Au*. Scale bar = 20 nm

The *Eu-ThioALNN.Au* particles are similar in size to the ThioALNN.Au, with TEM showing them as approximately 13-15 nm (figure 2.16). The particle size would be expected to remain the same.

2.4.2   The binding of europium (III) to ThioKEESLADDL.Au

ThioKEESLADDL.Au   **Eu-ThioKEESLADDL.Au**
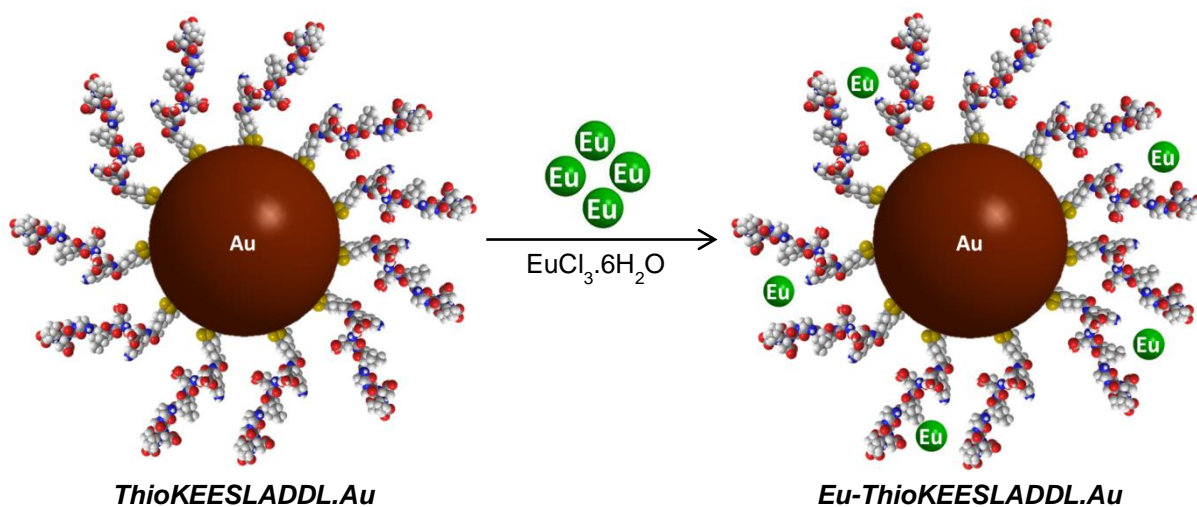
Scheme 2.3: Schematic representation of the preparation of **Eu-ThioKEESLADDL.Au**

The binding of europium (III) to **ThioKEESLADDL.Au** was investigated in a similar way to **ThioALNN.Au**. The addition of europium (III) to **ThioKEESLADDL.Au** resulted in red-shift of the SPR band of 1 nm observed by UV-Vis spectroscopy (figure 2.17).
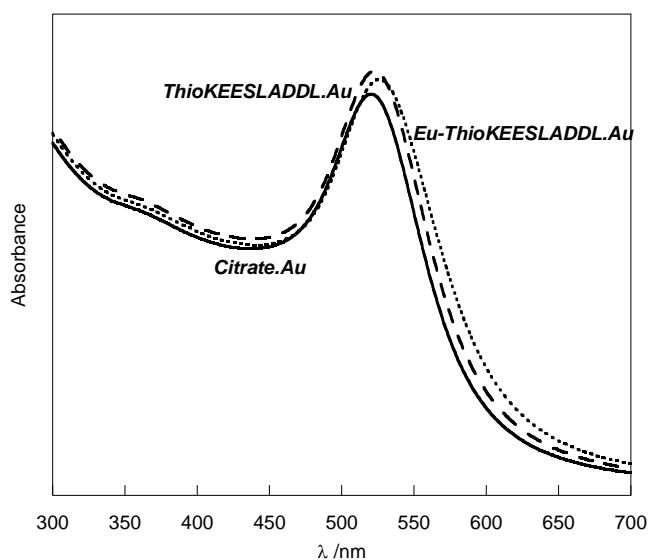
Figure 2.17: UV-Vis spectra of **Citrate.Au** (——) with the addition of ThioKEESLADDL = 0.18 mM in phosphate buffer (−−) and Eu^{3+} = 0.68 mM in water (••••)

Luminescence studies of the titration of europium (III) into **ThioKEESLADDL.Au** showed an increase in europium emission with no point of saturation upon addition of europium (III). Titration of europium (III) into ThioKEESLADDL in solution shows a 1:1 binding with a clear saturation point, which is indicative of complex formation. The peptide structure suggests that the peptide wraps around the lanthanide ion to form the complex. However in the case of the peptide immobilised on nanoparticles, the results imply that the peptide may have a different conformation making the binding of the lanthanide less strong.
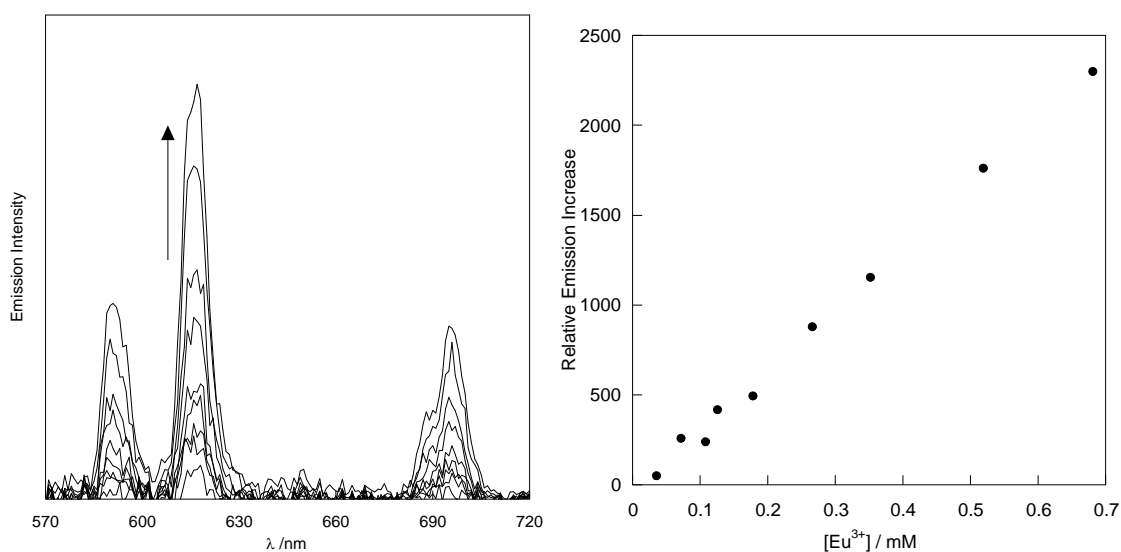
Figure 2.18: Luminescence spectra of **ThioKEESLADDL.Au** upon titration of Eu^{3+} [AuNPs] = 4.5 nM, [ThioKEESLADDL] = 0.18 mM, $\lambda_{exc} = 280$ nm. Right: Plot of emission intensity increase vs. $[Eu^{3+}]$ for **ThioKEESLADDL.Au**.
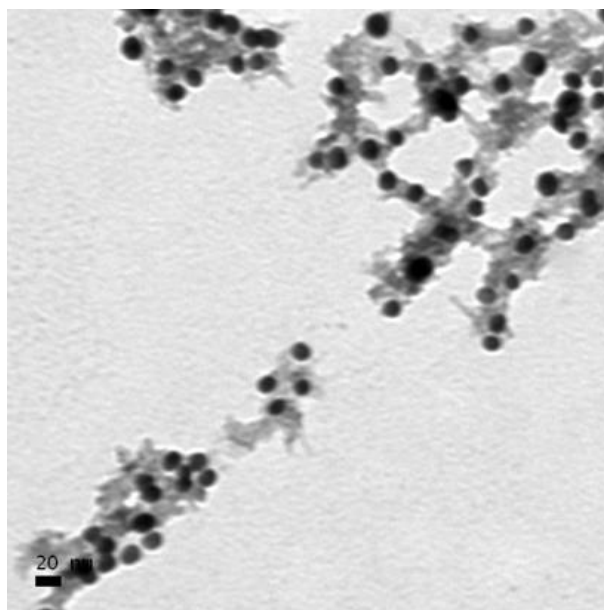
Figure 2.19: TEM image of **Eu-ThioKEESLADDL.Au**. Scale bar = 20 nm

The TEM image of the **Eu-ThioKEESLADDL.Au** (figure 2.19) shows the particles to be in a similar size range to the **Eu-ThioALNN.Au** particles (figure 2.16). The nanoparticles appear to be disperse, however they are surrounded by other artefacts which are not as dense as the gold nanoparticles. This is most likely to be excess europium (III), which has dried onto the grid once the solvent has evaporated off.

Studies of the peptide coated gold nanoparticles by circular dichroism show very weak signal for the samples (figure 2.20). Initial studies of **ThioALNN.Au** showed no change in the CD spectrum upon addition of the europium (III), nor any change from the **Citrate.Au** spectrum. The **ThioKEESLADDL.Au** spectrum however does show some variation from that **Citrate.Au** by CD spectroscopy. Whilst the overall CD signal is weak in comparison to the peptide in solution, there is a peak at approximately 225 nm present in the **ThioKEESLADDL.Au** sample which is not present in the **Citrate.Au**. This peak is likely to be caused by the presence of the peptide. The

addition of europium into the ***ThioKEESLADDL.Au*** does not cause any significant changes to the CD spectrum. From the CD spectra of the ThioKEESLADDL in solution, any changes in the CD spectrum would be anticipated would be small. The gold nanoparticles are very strongly absorbing at lower wavelengths, particularly where the peptide signal would be anticipated. Therefore it is highly likely that the light is being absorbed by the nanoparticles, which gives rise to the weak signal observed.With the weak signal within the nanoparticle samples, it would be difficult to observe any small changes between the spectra of ***ThioKEESLADDL.Au*** and ***Eu-ThioKEESLADDL.Au.***
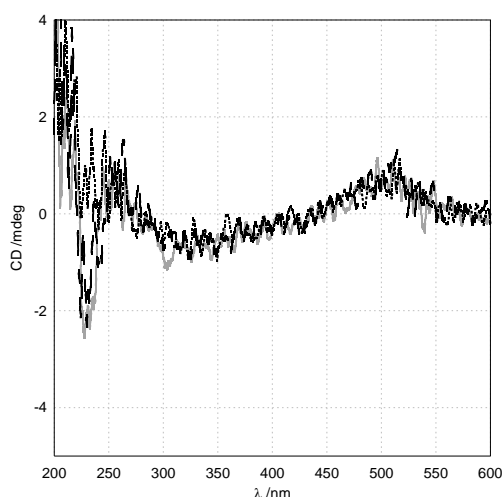
Figure 2.20: Circular dichroism spectra of ***Citrate.Au*** (••••••), ***ThioKEESLADDL.Au*** (−−−) and ***Eu-ThioKEESLADDL.Au*** (⎯⎯). [Citrate.Au] = 4.5 nM, [ThioKEESLADDL] = 0.18 mM, [Eu^{3+}] = 0.18 mM.

2.5 Conclusion

The peptides ThioALNN and ThioKEESLADDL have been found to bind lanthanide ions in solution and been successfully used to coat gold nanoparticles. Luminescent

nanoparticles were prepared with the binding of europium (III) to the peptide coated nanoparticles, which was monitored by luminescence spectroscopy. The nanoparticles were characterised by absorption spectroscopy and TEM. The peptides used contain no chromophore for sensitisation of the bound europium (III), however there is great potential to improve the luminescent properties of peptide coated nanoparticles with the inclusion of a sensitiser group.

3   Experimental

3.1   Synthesis of ThioALNN peptide
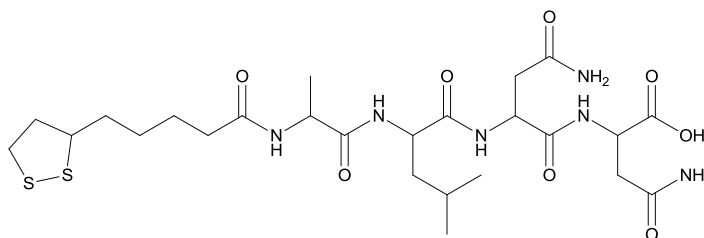
ThioALNN was synthesised using a CEM discover SPS microwave reactor. FMOC-Asn-(Trt)-Wang resin (0.208 g) was swollen in DMF (7 ml) for 15 minutes. The DMF was removed and the resin washed with DMF (5 x 7 ml). The FMOC protecting group of the amino acid was removed by adding 20 % piperidine in DMF (7 ml) and placing in the microwave reactor (Conditions: 20 W, 75 ^{o}C, 3 min). The deprotection solution was removed and the resin washed with DMF (5 x 7 ml). FMOC-L-Asn-(trt)-OH (0.5 mmol) was added to the resin in DMF, along with the activator HBTU and the activator base DIEA and then coupled in the microwave reactor (Conditions: 20 W, 75 ^{o}C, 3 min). The resin was then washed with DMF (5 x 7 ml). The deprotection and coupling was repeated for each of the amino acids, FMOC-L-Leu-OH (0.5 mmol), FMOC-L-Ala-OH.H_2O (0.5 mmol) and thioctic acid (1 mmol). After the final coupling of the thioctic acid to the peptide, the resin was washed with DCM (5 x 7 ml). The peptide was cleaved from the resin in the microwave reactor (Conditions: 20 W, 35 ^{o}C, 25 minutes) using a cleavage solution of 90 % TFA, 2 % anisole, 5 % thioanisole and 3 % EDT. The final solution was filtered, reduced in volume under N_2 and cold diethyl ether (40 ml, -20 ^{o}C) was added which caused the formation of a white precipitate. The precipitate was isolated by filtration and washed with diethyl ether,

redissolved in water (40 ml) and acetic acid (15 ml) and freeze dried. The crude peptide was then purified by semi-prep HPLC (C18 column, Acetonitrile/Water/TFA). (5.2 mg, 8.4 %) MS (MALDI) m/z 641 [M+Na]$^+$, 643 [M+2H+Na]$^+$, 657[M+K]$^+$, 659 [M+2H+K]$^+$. UV-vis (H$_2$O) λ_{max} 203 nm.

The peptide ThioKEESLADDL was purchased from United Peptide Corporation, purified by HPLC, MS m/z 1206. The peptide was used without any further purification.

3.2   Preparation of Citrate Stabilised Gold Nanoparticles, *Citrate.Au* [21]

All glassware were washed with aqua regia and dried prior to use. Hydrogen tetrachloroaurate (0.0672 g, 0.2 mmol) was dissolved in 200 ml water and heated under reflux. A solution of sodium citrate (0.228 g, 0.8 mmol) in water (20 ml) was added rapidly. The yellow solution became deep red in colour. The solution was left under reflux for a further 10 minutes and then allowed to cool. UV-vis (H$_2$O) λ_{max} 520 nm.

4   References

1 J. C. G. Bunzli, *Chem. Rev.,* 2010, **110**, 2729-2755.

2 C. P. Montgomery, B. S. Murray, E. J. New, R. Pal and D. Parker, *Acc. Chem. Res.,* 2009, **42**, 925-937.

3 K. N. Allen and B. Imperiali, *Curr. Opin. Chem. Biol.,* 2010, **14**, 247-254.

4 C. W. am Ende, H. Y. Meng, M. Ye, A. K. Pandey and N. J. Zondlo, *ChemBioChem,* 2010, **11**, 1738-1747.

5 F. Cisnetti, C. Gateau, C. Lebrun and P. Delangle, *Chem- Eur J.,* 2009, **15**, 7456-7469.

6 E. Pazos, O. Vazquez, J. L. Mascarenas and M. Eugenio Vazquez, *Chem. Soc. Rev.,* 2009, **38**, 3348-3359.

7 A. Marguerre and R. Krämer, *Bioorg. Med. Chem. Lett.,* 2009, **19**, 5757-5759.

8 T. Hirayama, M. Taki, A. Kodan, H. Kato and Y. Yamamoto, *Chem. Commun.,* 2009, **22**, 3196-3198.

9 C. S. Bonnet, P. H. Fries, S. Crouzy, O. Sénèque, F. Cisnetti, D. Boturyn, P. Dumy and P. Delangle, *Chem- Eur J.,* 2009, **15**, 7083-7093.

10 X. Su, K. McAndrew, T. Huber and G. Otting, *J. Am. Chem. Soc.,* 2008, **130**, 1681-1687.

11 N. R. Silvaggi, L. J. Martin, H. Schwalbe, B. Imperiali and K. N. Allen, *J. Am. Chem. Soc.,* 2007, **129**, 7114-7120.

12 J. Ryu, S. Y. Lim and C. B. Park, *Adv Mater,* 2009, **21**, 1577-1581.

13 J. M. Bryson, K. M. Fichter, W. Chu, J. Lee, J. Li, L. A. Madsen, P. M. McLendon and T. M. Reineke, *PNAS,* 2009, **106**, 16913-16918.

14 I. Rio-Echevarria, R. Tavano, V. Causin, E. Papini, F. Mancin and A. Moretto, *J. Am. Chem. Soc.,* 2011, **133**, 8-11.

15 S. B. Fonseca, M. P. Pereira and S. O. Kelley, *Adv. Drug Deliv. Rev.,* 2009, **61**, 953-964.

16 D. J. Lewis, C. Bruce, S. Bohic, P. Cloetens, S. P. Hammond, D. Arbon, S. Blair-Reid, Z. Pikramenou and B. Kysela, *Nanomedicine,* 2010, **5**, 1547-1557.

17 A. Davies, D. J. Lewis, S. P. Watson, S. G. Thomas and Z. Pikramenou, *PNAS,* 2012, **109**, 1862-1867.

18 R. Lévy, N. T. K. Thanh, R. C. Doty, I. Hussain, R. J. Nichols, D. J. Schiffrin, M. Brust and D. G. Fernig, *J. Am. Chem. Soc.,* 2004, **126**, 10076-10084.

19 A. C. Savage and Z. Pikramenou, *Chem. Commun.,* 2011, **47**, 6431-6433.

20 D. J. Lewis, T. M. Day, J. V. MacPherson and Z. Pikramenou, *Chem. Commun.,* 2006, **13**, 1433-1435.

21 J. Turkevich, P. C. Stevenson and J. Hillier, *Discuss. Faraday Soc.,* 1951, **11**, 55-75.

Nanoparticles coated with lanthanide complexes and peptides for cellular imaging applications

1   Introduction

Lanthanide complexes are desirable probes for cellular imaging due to their unique photophysical properties. Their long luminescent lifetimes in the millisecond range and large Stoke shifts make them useful for avoiding detection of cell autofluorescence which is often observed.[1] There have been many examples of lanthanide complexes developed for cellular imaging.[2-4] Parker *et al.* have reported a range of luminescent lanthanide probes which have been found to localise within four sub-cellular regions; lysosomes, mitochondria, nucleus and a combination of mitochondria and lysosomes.[4] They observed that the structure of the complex and the linkage of the chromophore to the lanthanide had an effect on the sub-cellular localisation of the complex.[5-7] Bünzli *et al.* have reported bimetallic lanthanide helicates as probes for cellular imaging.[8, 9] The helicates were found to be non-cytotoxic and their uptake into cells was found to proceed by endocytosis, with localisation in the endoplasmic reticulum. Europium helicates were successfully imaged by luminescence microscopy and confocal microscopy in HeLa cells (figure 3.1).[9] Incubation of cells with various concentrations of the lanthanide helicates found that dosing with higher concentrations exhibited greater luminescence.[9] The importance of concentration is evident from these studies, therefore tethering lanthanide complexes onto gold nanoparticles may provide an effective method of delivering a much greater concentration of lanthanide complexes into cells.
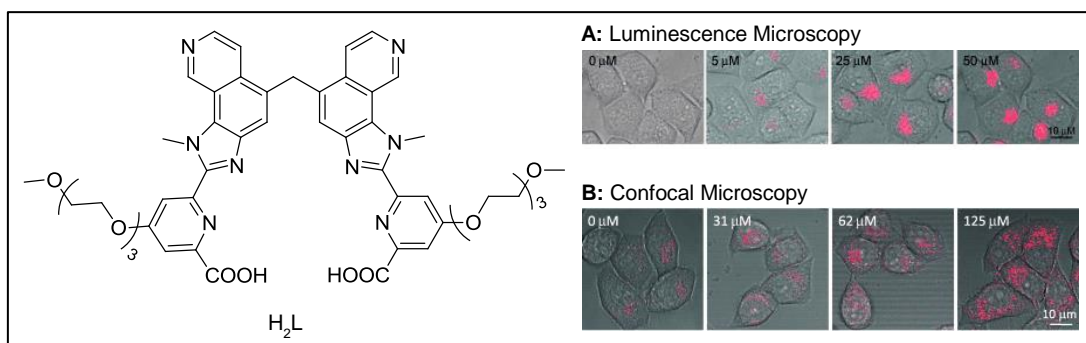
Figure 3.1: Structure of H$_2$L used to form europium helicate Eu$_2$(L)$_3$ and luminescence and confocal microscopy of Eu$_2$(L)$_3$ incubated with HeLa cells. **A:** Merged bright-field and time-resolved luminescence microscopy of HeLa cells incubated with [Eu$_2$(L)$_3$]. Cells incubated with different concentrations of [Eu$_2$(L)$_3$] at 37 °C for 6 hours, λ_{exc} = 365 nm. **B:** Confocal microscopy images of HeLa cells incubated with different concentrations of [Eu$_2$(L)$_3$] during 18 h at 37 °C; λ_{exc} = 405 nm. Confocal images reproduced from reference [9]

Gold nanoparticles provide a suitable platform for the assembly of multiple probes. They are bio-inert and can be easily functionalised with moieties containing sulphur by the formation of sulphur-gold bonds. Gold nanoparticles have been reported to be functionalised with various molecules such as peptides,[10-14] DNA,[11, 15] fluorescent dyes[16, 17] and lanthanide complexes.[18-20] One of the first examples of lanthanide coated gold nanoparticles was the attachment of a surface-active europium DTPA bis-amide complex.[18] Lanthanide coated gold nanoparticles have been used in cellular imaging and sensing applications. Lanthanide coated nanoparticles have been utilised to sense biologically relevant anions and molecules such as phosphates,[21] proteins[22] and enzymes.[23] The transfection and genotoxicity of europium and cerium coated gold and platinum nanoparticles in MRC5VA human

epithelial lung fibroblasts have been monitored by high resolution synchrotron X-ray fluorescence microscopy.[20]

The combination of lanthanide complexes and peptides attached to gold nanoparticles has only recently been reported. The delivery of gold nanoparticles in platelets in a pH dependant manner was studied by co-coating gold nanoparticles with a europium complex and a pH low insertion peptide (pHLIP).[19] In another approach, a peptide designed for multiple enzyme detection has been tethered to gold nanoparticles (figure 3.2).[23] The peptide consists of a lanthanide complex on one end of the peptide and a coumarin on the other, with two sulphurs in the middle of the peptide to anchor the peptide to gold nanoparticles. The spacer between the lanthanide complex and the coumarin contains an amino acid sequence specific to two biologically relevant enzymes, matrix metalloproteinase 2 and matrix metalloproteinase 7 (MMP-2 and MMP-7). Cleavage of the spacer between the two lumophores by the specific enzymes prevents fluorescence resonance energy transfer between the two lumophores and the gold nanoparticles causing an increase in emission. Gold nanoparticles coated with peptides and a FITC fluorophore have been used in a similar way for the detection of multiple proteinases.[24] Protease specific peptides with attached lanthanides were tethered to $Ru(bpy)_3$ doped silica nanoparticles for detection of multiple proteases by inductively coupled plasma mass spectrometry (figure 3.2).[25]
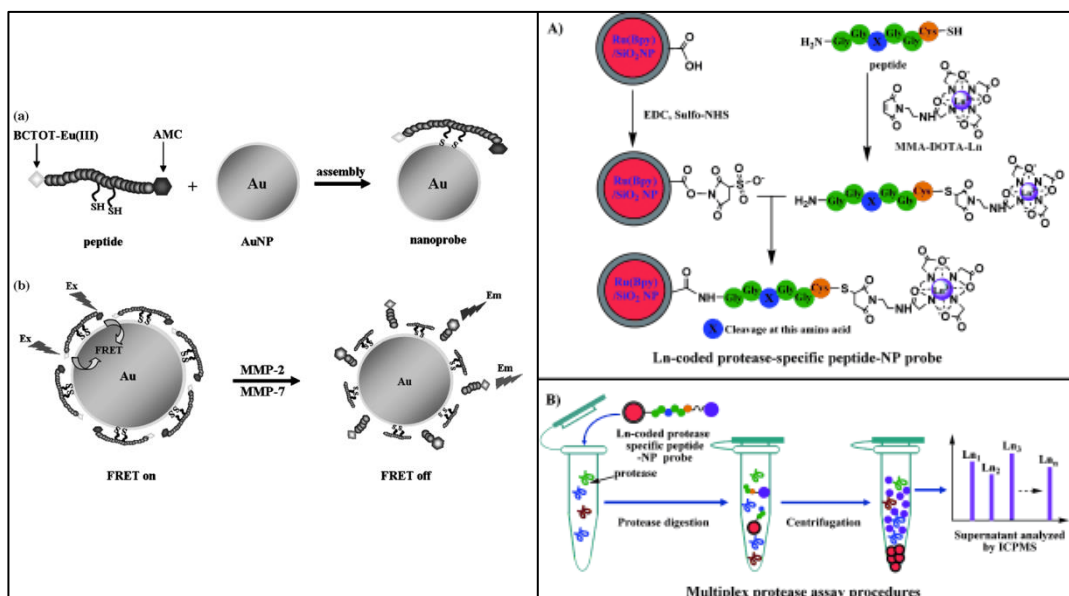
Figure 3.2: Left: Schematic of gold nanoparticles functionalised with coumarin and a europium complex for detection of the enzymes MMP-2 and MMP-7.[23] Right: Schematic of protease detection using silica nanoparticles and peptide/lanthanide complexes determined by ICP-MS.[25] Diagrams reproduced from references 23 and 25

Functionalisation of gold nanoparticles with peptides is of interest for the delivery of gold nanoparticles into cells. The addition of peptides onto nanoparticles allows for the specific targeting of certain organelles and the specific sub-cellular localisation of the nanoparticles within the cells. In this chapter, gold nanoparticles co-coated with lanthanide complexes and peptides for cellular imaging are reported. Photophysical studies of these lanthanide-peptide co-coated gold nanoparticles were carried out to investigate the effect of the binding of these two entities onto gold nanoparticles on the emissive properties of the lanthanide complex.   The particles have been characterised by UV-Vis and luminescence spectroscopy. The uptake of lanthanide/peptide gold nanoparticles into cells has been monitored by luminescence microscopy. The europium complexes used in this chapter are EuSH, EuQSH and

EuNapSAc complexes (figure 3.3). The previously reported europium complex EuSH,[18] is a DTPA bis-amide complex with two thiophenol legs for lanthanide sensitisation and gold nanoparticle attachment. The EuQSH complex is a similar DTPA bis-amide complex with one thiophenol arm and one quinoline arm. Another europium complex used is EuNapSAc (supplied by Dr Stephen Hammond) which consists of a DTPA backbone for the chelation of the lanthanide ion, two naphthalene chromophores and two alkyl chains with terminal sulphurs for attachment to gold (figure 3.3). The sulphur atoms are protected with acetyl groups to prevent the formation of disulphide bonds.
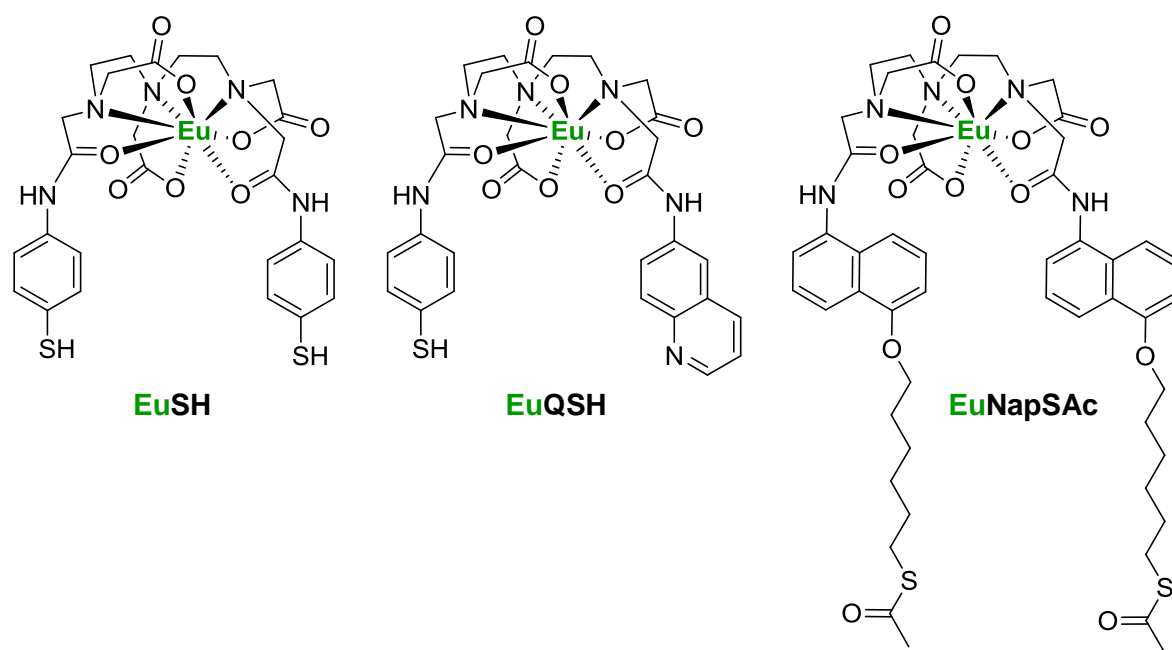
Figure 3.3: Structure of the europium complexes EuSH, EuQSH and EuNapSAc

The peptides used in this chapter are based on known sequences which have been used for cellular targeting. Two of the sequences chosen, were based on known nuclear localisation sequences (NLS).[10, 11, 13, 26] The third sequence is a peptide

sequence that is known to interact with the enzyme *ataxia telangiectasia mutated* (ATM), and is believed to inhibit ATM-mediated DNA damage response and enhance radiosensitivity.[27]
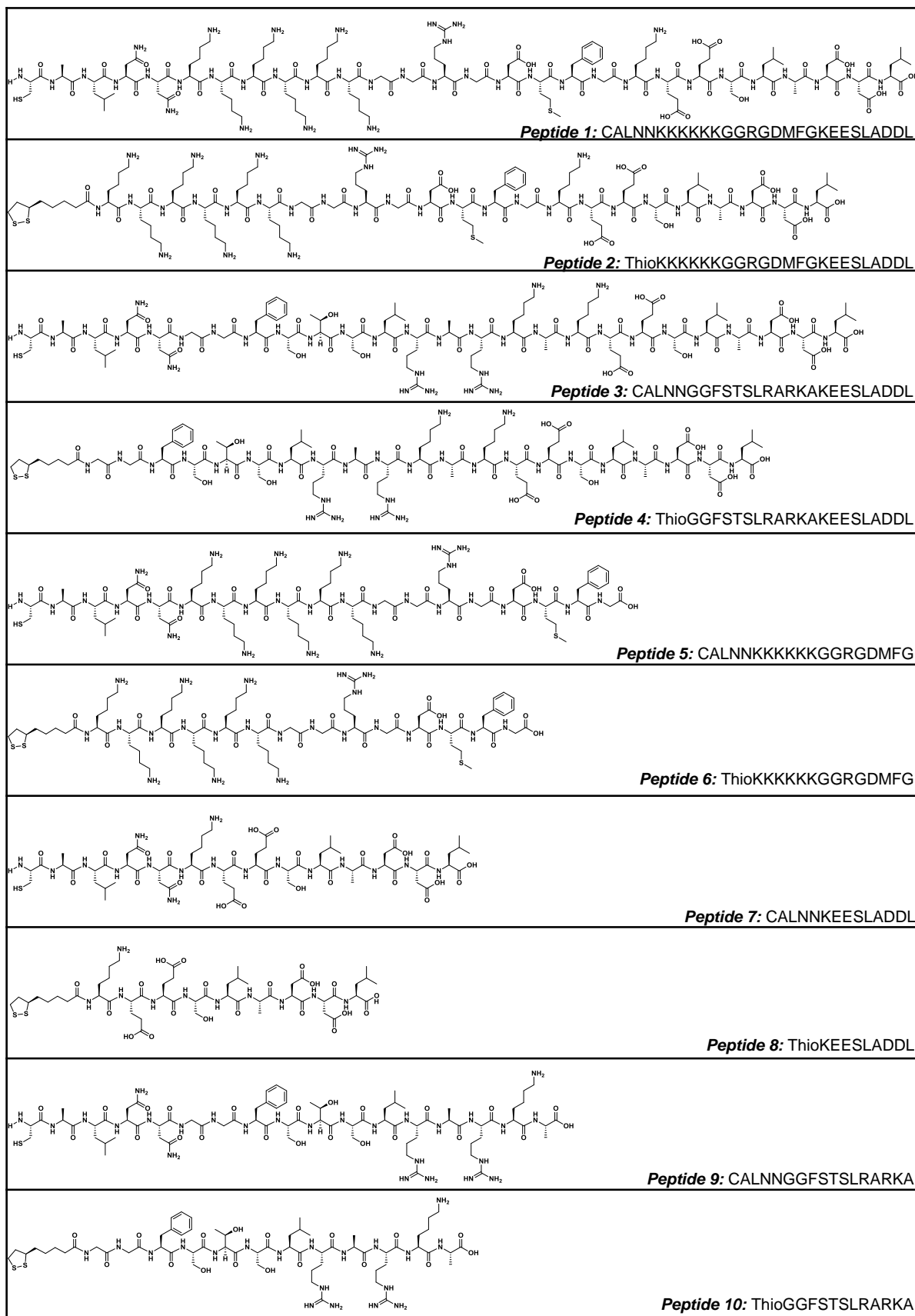
Figure 3.4: Structures of peptides discussed in this chapter.

Peptide 1: CALNNKKKKKKGGRGDMFGKEESLADDL

Peptide 2: ThioKKKKKKGGRGDMFGKEESLADDL

Peptide 3: CALNNGGFSTSLRARKAKEESLADDL

Peptide 4: ThioGGFSTSLRARKAKEESLADDL

Peptide 5: CALNNKKKKKKGGRGDMFG

Peptide 6: ThioKKKKKKGGRGDMFG

Peptide 7: CALNNKEESLADDL

Peptide 8: ThioKEESLADDL

Peptide 9: CALNNGGFSTSLRARKA

Peptide 10: ThioGGFSTSLRARKA

2   Results and Discussion

2.1   Synthesis of lanthanide complexes

2.1.1   Synthesis of SH ligand and LnSH (Ln = Eu, Tb, Gd, Nd) complexes
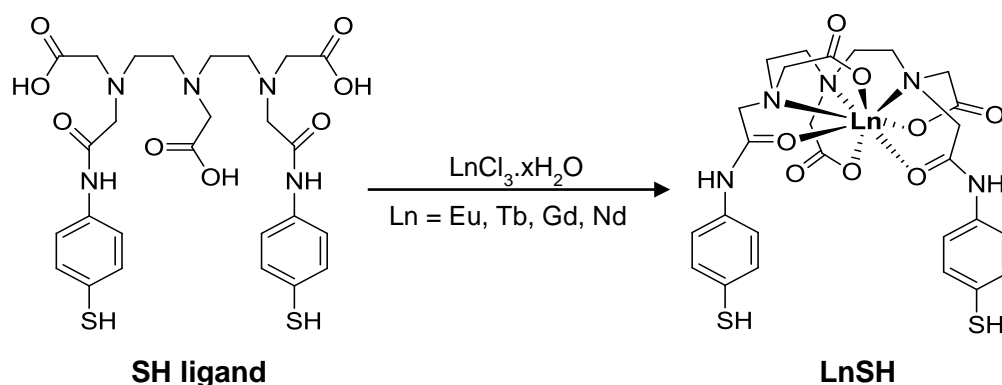
Scheme 3.1: Reaction scheme for the preparation of LnSH, where Ln = Eu, Tb, Gd and Nd.

The SH ligand was synthesised by a condensation reaction in pyridine of 4-aminothiophenol with DTPA-bis anhydride following a published procedure.[18] The ligand was characterised by NMR and mass spectrometry.

The LnSH (Ln = Tb, Nd, Gd) complexes were prepared by reacting the SH ligand with $LnCl_3.xH_2O$ in degassed methanol. Acetonitrile was used to precipitate out the complex from the methanol, and the complex was isolated by filtration. EuSH was prepared by first preparing the potassium salt of the SH ligand by adding KOH into a solution of the SH ligand in methanol. Then $EuCl_3.6H_2O$ was added to form the complex. The complexes were characterised by UV-Vis and mass spectrometry and the results showed agreement with the previous data reported.[18, 28]

The UV-Vis spectra of the LnSH complexes in methanol showed a peak at approximately 266 nm, which is characteristic of the π-π* transition of the

phenylamide group of the ligand. Luminescence studies of a solution of EuSH in methanol show the characteristic europium f-f transitions $^5D_0 \rightarrow {^7F_J}$ where J = 0, 1, 2, 3, 4 at 580, 590, 614, 650 and 695 nm. The solution was excited at 270 nm, to correspond with the absorbance of the ligand. The excitation spectrum of the EuSH complex followed the profile of the UV-Vis spectrum of the ligand, which illustrates the energy transfer between the thiophenol groups of the ligand to the lanthanide.

The emission spectrum of the TbSH complex and the NdSH complex was also recorded. A solution of TbSH complex dissolved in methanol showed the characteristic transition $^5D_4 \rightarrow {^7F_J}$ where J = 0, 1, 2, 3, 4, 5, 6 at 490, 546, 583, 620, 649, 667, and 680 nm. The most intense transition was $^5D_4 \rightarrow {^7F_5}$ seen at 546 nm. The excitation spectrum of the TbSH solution was also recorded, with the profile matching that of the UV-Vis spectrum as with the EuSH complex. The emission spectrum of NdSH in methanol shows the typical transitions of neodymium $^4F_{3/2} \rightarrow {^4I_J}$ where J = 9/2, 11/2 and 13/2. The phosphorescence signal of the GdSH complex measured at 77 K in methanol showed agreement with the spectrum previously reported.[28]

2.1.2 Synthesis of QSH ligand and LnQSH (Ln = Eu, Gd, Nd)
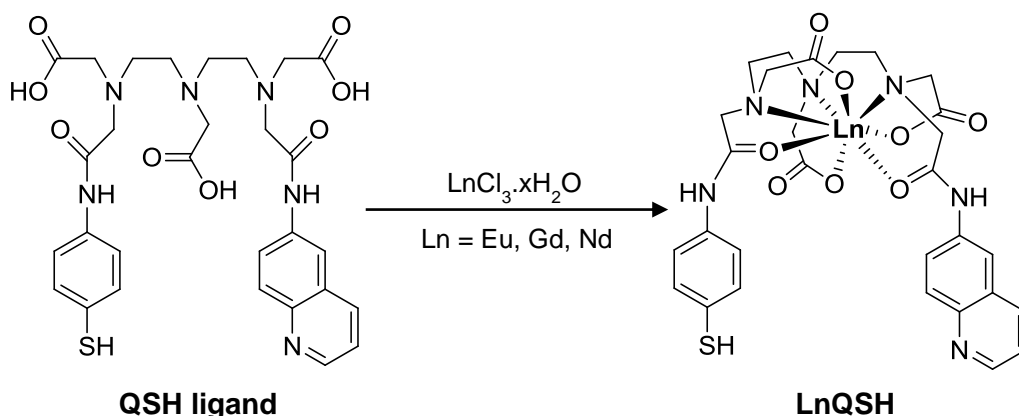
QSH ligand   **LnQSH**

Scheme 2: Reaction scheme for the preparation of LnQSH

The QSH ligand was synthesised by initially reacting 6-aminoquinoline with a 1:1 molar ratio of DTPA bis-anhydride in pyridine, then 4-aminothiophenol is added to the reaction mixture. The reaction yields a combination of three different products; a DTPA ligand with two quinoline groups, a DTPA ligand with two thiophenol groups (SH ligand) and the desired product DTPA with one quinoline arm and one thiophenol arm (QSH ligand). Purification of the final product is achieved by preparative HPLC using a 0.05 % TFA, acetone/water gradient. A reducing agent, tris (2-carboxyethyl) phosphine hydrochloride (TCEP) was added to the crude product before purification by HPLC to reduce any disulphide bonds which could affect the purification. The final product was characterised by NMR and mass spectrometry.

The complexes LnQSH (Ln = Eu, Gd, Nd) were prepared by adding $LnCl_3.nH_2O$ to a solution of the QSH ligand. The pH was adjusted to 5 and the final complex was precipitated out of solution using acetonitrile. The complexes were characterised by mass spectrometry and elemental analysis.

Photophysical studies of EuQSH were carried out and are shown in figure 3.5. The emission spectrum of the EuQSH complex in methanol shows the characteristic europium transitions $^5D_0 \rightarrow {}^7F_J$ where J = 0, 1, 2, 3, 4. The excitation spectrum of EuQSH shows a peak at 330 nm suggesting that the luminescence observed is caused by sensitisation of the lanthanide by the quinoline sensitiser. The luminescence lifetime recorded for this complex in methanol was found to be 0.78 ms. This is a similar lifetime to that of the EuSH complex.
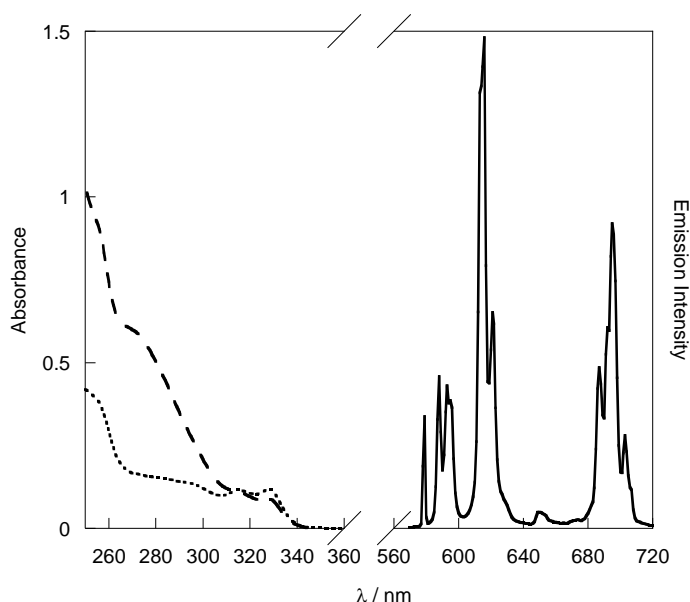
Figure 3.5: Emission (——), excitation (••••••) and UV-Vis (−−−) spectra of EuQSH complex in methanol. Emission λ_{exc} = 330 nm corrected for PMT response. Excitation λ_{em} = 614 nm.

Studies of the luminescent properties of the NdQSH complex showed the characteristic emission profile attributed to the neodymium f-f transitions $^4F_{3/2} \rightarrow {}^4I_J$ where J = 9/2, 11/2 and 13/2.
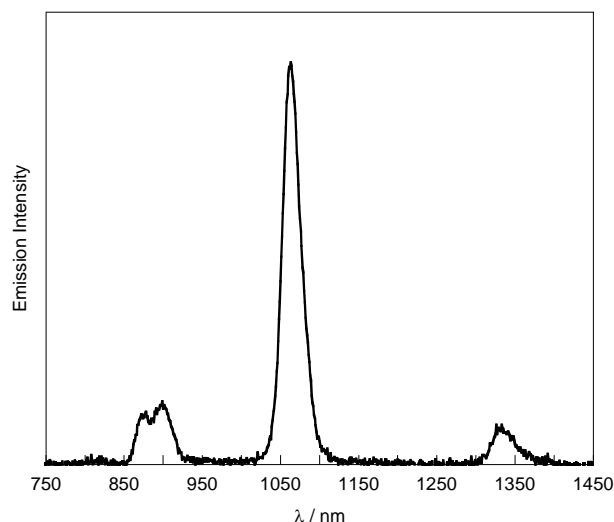
Figure 3.6: Emission spectrum of NdQSH complex in methanol. λ_{exc} = 330 nm.

The yttrium complex was prepared following the same procedure as the LnQSH complexes. The YQSH complex was characterised by mass spectrometry and ^{1}H NMR. The yttrium complex was prepared for analysis by ^{1}H NMR spectrometry as it possesses similar coordination properties to the lanthanides, but does not cause peak broadening in NMR spectrum which is typically observed with the lanthanides. Comparison of the ^{1}H NMR spectra of the QSH ligand and the YQSH complex shows some differences attributed to the complexation of the yttrium. The eight protons on the DTPA backbone appear in the NMR of the ligand as one singlet, but upon complexation the protons appear as two singlets each integrating for four protons. The aromatic protons of the quinoline and the thiophenol group exhibit some changes in the ^{1}H NMR upon complexation, with the majority of peaks shifting downfield upon complexation with yttrium.

2.2   Coating of gold nanoparticles with lanthanides complexes and peptides

2.2.1   Lanthanide complexes on gold nanoparticles

EuS.Au
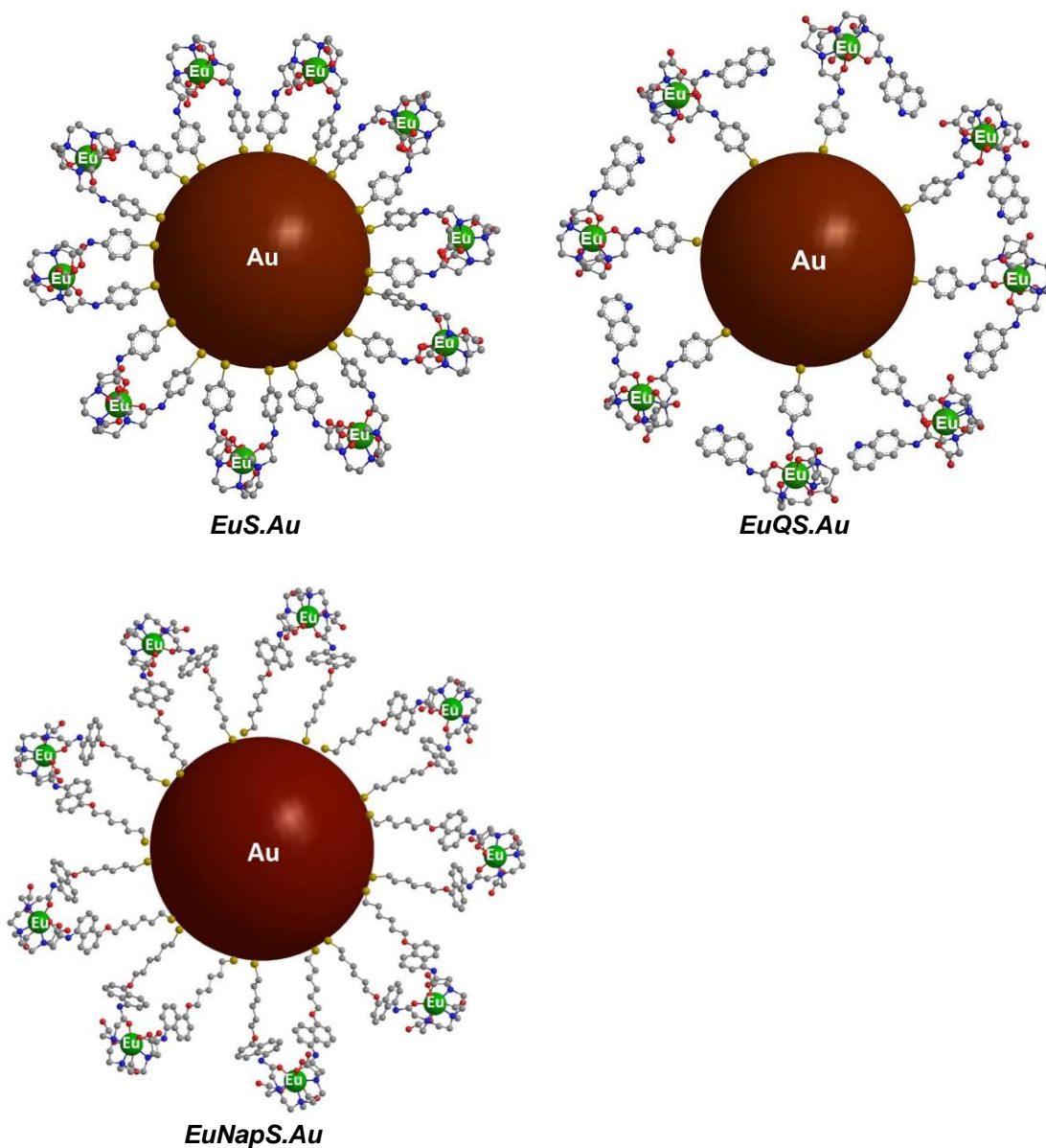
EuQS.Au

EuNapS.Au

Figure 3.7: Schematic representation of **EuS.Au**, **EuQS.Au** and **EuNapS.Au**.

The lanthanide complexes used within this chapter for the co-coating of **Citrate.Au** with lanthanide complexes and peptides are EuSH, EuQSH and EuNapSAc. The previously reported EuSH complex has been successfully used to prepare

luminescent gold nanoparticles.[18] The addition of the EuSH complex to gold nanoparticles results in 5 nm shift in the SPR band monitored by UV-Vis spectroscopy. Luminescence spectroscopy of *EuS.Au* shows the characteristic europium emission spectrum, with a luminescence lifetime similar to that of the europium complex in water. Coating *Citrate.Au* with EuQSH complex shows a similar trend, with a red-shift in the SPR band of 6 nm and the characteristic europium emission being observed. The luminescence lifetime recorded of *EuQS.Au* is similar to that of the complex in water, showing no quenching. Full characterisation of *EuS.Au* and *EuQS.Au* can be found in chapter 4. Another europium complex utilised for this work to prepare luminescent gold nanoparticles is EuNapSAc, prepared by Dr. Stephen Hammond. The addition of the EuNapSAc complex to gold nanoparticles causes a 5 nm red-shift in the SPR band. The luminescence lifetime of this complex on gold nanoparticles (*EuNapS.Au*) has been found to be 0.5 ms.[29]

2.2.2   Coating of gold nanoparticles with peptides

The surface coating of *Citrate.Au* with various peptides was monitored by UV-Vis spectroscopy to establish the overall shifts in the SPR band in the presence of the peptides, and to provide a comparison of the concentrations of peptide needed to obtain this shift. The two individual NLS peptides and the inhibitor peptide were used on their own to coat *Citrate.Au*, and also a combination of the NLS peptides and the inhibitor peptide were also used. The peptides sequences are either terminated in a

CALNN sequence or a thioctic acid group to provide sulphurs for attachment to the gold nanoparticles.

Peptide	Sequence	Molecular Weight	Function
Peptide 1	CALNNKKKKKKGGRGDMFGKEESLADDL	3081.58	NLS + Inhibition
Peptide 2	ThioKKKKKKGGRGDMFGKEESLADDL	2754.32	NLS + Inhibition
Peptide 3	CALNNGGFSTSLRARKAKEESLADDL	2767.09	NLS + Inhibition
Peptide 4	ThioGGFSTSLRARKAKEESLADDL	2439.82	NLS + Inhibition
Peptide 5	CALNNKKKKKKGGRGDMFG	2080.52	NLS
Peptide 6	ThioKKKKKKGGRGDMFG	1753.25	NLS
Peptide 7	CALNNKEESLADDL	1534.67	Inhibition
Peptide 8	ThioKEESLADDL	1207.40	Inhibition
Peptide 9	CALNNGGFSTSLRARKA	1766.02	NLS
Peptide 10	ThioGGFSTSLRARKA	1438.75	NLS

Table 3.1: Peptide sequences used for coating nanoparticles and their functions. The peptides are either functional nuclear localisation signals (NLS) or a peptide which inhibits ATM-mediated DNA damage response. The larger peptides 1-4 contain a combination of two different peptides.

The peptides were all found to be soluble in phosphate buffer. *Citrate.Au* were coated with these peptides with the addition of μL aliquots of the peptide solution in buffer, monitoring the SPR band of the gold nanoparticles by UV-Vis spectroscopy. Titration of various peptides into *Citrate.Au* showed red-shifts in the SPR ranging from 2 - 4 nm (figure 3.8). Peptides 5 and 6 were found to cause severe aggregation of *Citrate.Au* at concentrations as low as 10 ηM and were also found to cause aggregation upon addition to partially coated *EuNapS.Au* which meant that they were not used in any further experiments. The aggregation observed upon the addition of these peptides is most likely to be caused by the six positively charged lysines that are present in the peptide structure.
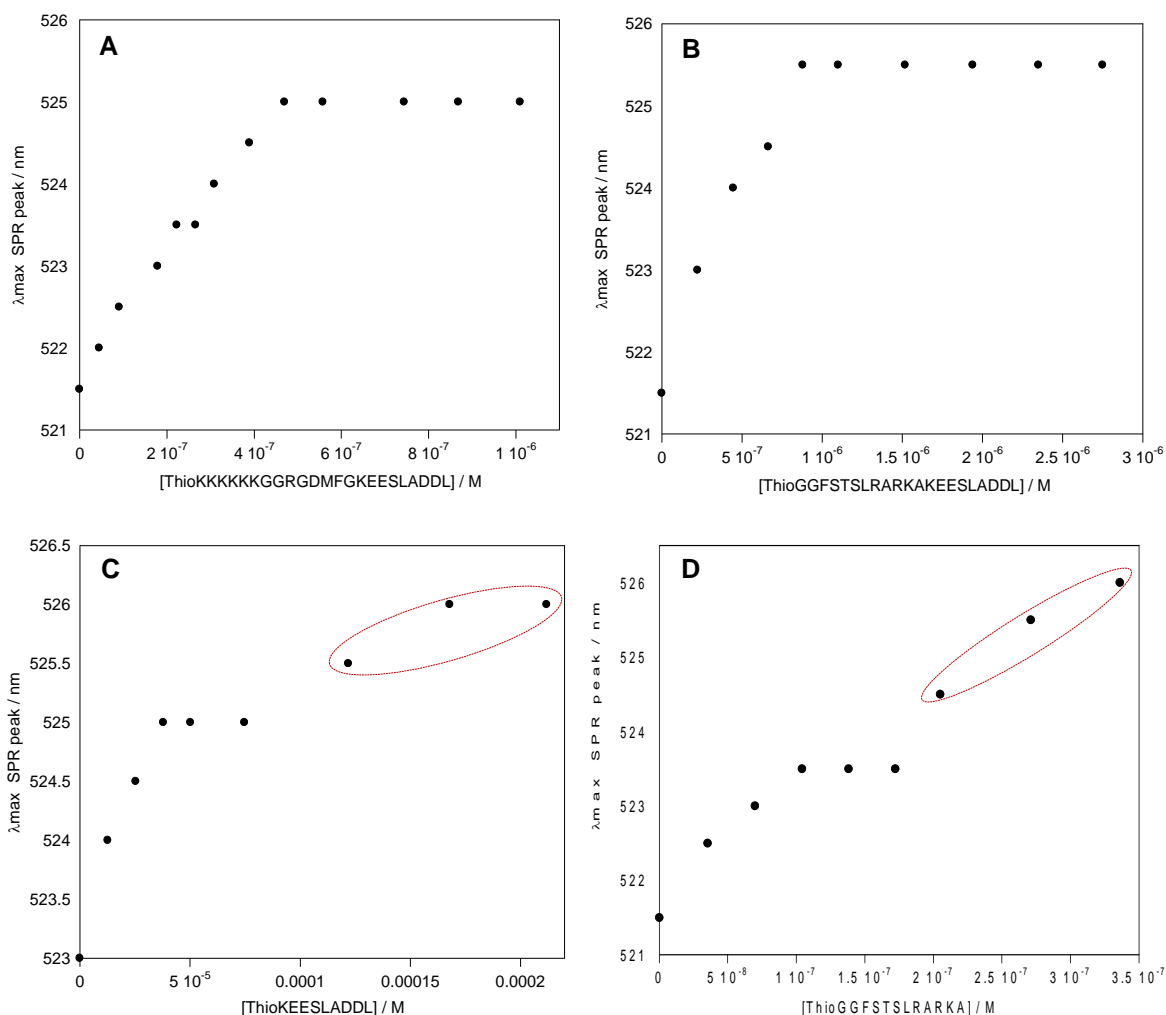
Figure 3.8: Titration of different peptides into **Citrate.Au**. Circled points show excess peptide leading to nanoparticle aggregation. [**Citrate.Au**] = 1.2 nM. **A:** ThioKKKKKKGGRGDMFGKEESLADDL (Peptide 2). **B:** ThioGGFSTSLRARKAKEESLADDL (Peptide 4). **C:** ThioKEESLADDL (Peptide 8). **D:** ThioGGFSTSLRARKA (Peptide 10)

Comparing the SPR shifts of the thioctic-terminated peptides, a larger red-shift for the longer peptides (peptides 2 and 4) is observed, compared with peptides 8 and 10. Interestingly, even though peptide 6 causes aggregation of the **Citrate.Au** at very low concentrations, peptide 2 can be added to **Citrate.Au** and result in stable **Peptide 2.Au** nanoparticles at a concentration of 0.45 μM (figure 3.8A). Peptide 2

contains the same peptide sequence as peptide 6 except for an additional KEESLADDL sequence on the end of the peptide. This extra portion of peptide tethered onto the end seems to aid the stabilisation of *Citrate.Au* and prevent aggregation upon addition. This also appears to be the case with peptide 4 with the extra KEESLADDL portion, meaning that higher concentrations of approximately 0.9 µM of peptide can be added to the *Citrate.Au* causing no aggregation (figure 3.8B), compared with the smaller peptide 10 which can only be added to *Citrate.Au* at a concentration of 0.1 µM (figure 3.8D). Addition of an excess amount of the smaller peptides into gold nanoparticles appears to give rise to aggregation of the particles after the SPR band reaches a plateau, whilst the longer peptides are stable once the saturation point has been reached and do not exhibit a further shift in the SPR upon titration of excess peptide. From the titration of ThioKEESLADDL (peptide 8) into *Citrate.Au* it can be seen that a higher concentration of 45 µM of peptide can be added to the *Citrate.Au* compared with the two shorter NLS sequences (peptides 6 and 10) (figure 3.8C). The longer peptides give rise to a larger red-shift in the SPR peak of between 3-4 nm compared to the smaller peptides, which only lead to a 2 nm red-shift. This result is similar to the ThioALNN peptide discussed in chapter 2.

2.3   Gold nanoparticles co-coated with lanthanide complexes and peptides

Luminescent gold nanoparticles designed for cellular targeting and imaging were prepared by coating *Citrate.Au* in combinations of different europium complexes and

peptides. Co-coating of **_Citrate.Au_** was achieved by simply adding to the **_Citrate.Au_**

a methanolic stock solution of lanthanide complex and a solution of peptide dissolved

in a phosphate buffer (scheme 3.3). The lanthanide complexes were added taking

into account the concentrations required to fully coat the **_Citrate.Au_** and the

concentration required to give partial shift in the SPR band. The peptides used were

a selection of the peptides shown in table 3.1. The binding of the lanthanide

complexes and peptides were monitored by the shift in the SPR band as observed by

UV-Vis spectroscopy.
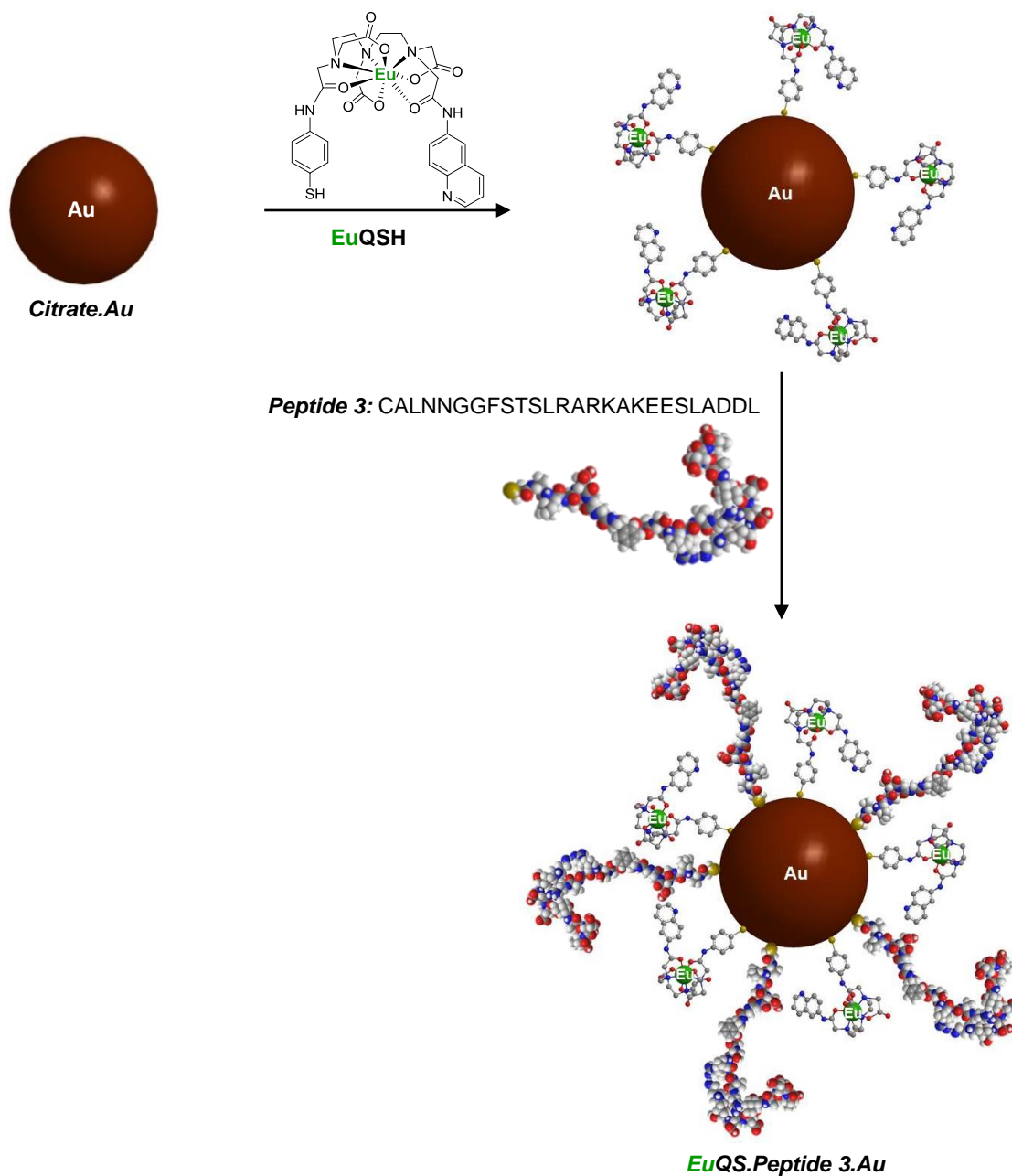
Scheme 3.3: Schematic representation of coating gold nanoparticles with a europium complex and peptide. The first step involves the partial coating of gold nanoparticles by the titration of μL quantities of the europium complex in methanol. The second step is the titration of the peptide dissolved in phosphate buffer added in μL aliquots.

The ***Citrate.Au*** nanoparticles were co-coated with the lanthanide complex and peptides by firstly adding small aliquots of a methanolic solution of the complex to

give a partial shift in the SPR band. The peptides were then added and the resulting SPR shift was monitored by UV-Vis spectroscopy. Removal of any excess peptide or complex was carried out by passing the resulting solution through a Sephadex G25 size exclusion column. Coated gold nanoparticles were then characterised by luminescence spectroscopy.

2.3.1 Co-coating of gold nanoparticles with EuSH and peptides

The europium luminescence signal of the nanoparticles with different peptides and the EuSH complex show interesting results (figure 3.9). Even though the same concentration of EuSH complex was used to partially coat a 1.2 nM solution of **Citrate.Au**, the addition of the peptides leads to a decrease in the europium emission observed. All the solutions were isoabsorptive at the excitation wavelength, therefore the only difference in the nanoparticle samples was the presence of the different peptides.
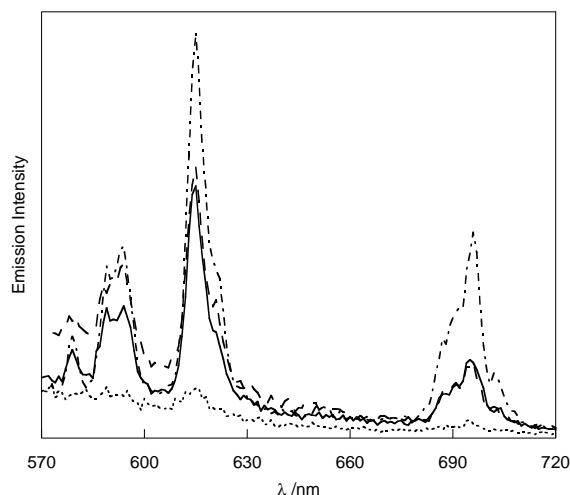
Figure 3.9: Luminescence spectra of **EuS.Au** (–·–·–), **EuS.Peptide 2.Au** (–––), **EuS.Peptide 4.Au** (••••••), **EuS.Peptide 10.Au** (——). λ_{exc} = 270 nm. The nanopartcles were prepared by mixing [EuSH] = 4.5 µM. [AuNPs] = 1.2 nM. [Peptide 2] =1.6 µM. [Peptide 4] =6.8 µM. [Peptide 10] = 52 nM

The emission spectra of the partially coated **EuS.Au** shows greater luminescence than the particles that have additional peptide on the surface. The most dramatic decrease in europium luminescence signal is with **EuS.Peptide 4.Au**, with a 70 % decrease compared with **EuS.Au**. **EuS.Peptide 4.Au** shows a greater decrease in europium emission compared to **EuS.Peptide 2.Au** and **EuS.Peptide 10.Au**. The luminescence signal for **EuS.Peptide 2.Au** and **EuS.Peptide 10.Au** are similar with a 9 % and 28 % decrease respectively from the europium signal observed from **EuS.Au** suggesting that the presence of these peptides has a similar effect on the emissive properties of the complex. Peptide 10 and peptide 4 are similar peptide sequences, with peptide 4 having a longer amino acid sequence. However the concentrations of these peptides added to coat the gold nanoparticles is significantly less for peptide 10 than peptide 4 which may mean that the greater concentration of

peptide added to coat the particles, the more that the peptide has an effect on the emission of the complex.

2.3.2   Co-coating of gold nanoparticles with EuNapSAc and Peptides

A similar examination of the effect of the peptide on the europium signal of EuNapSAc coated nanoparticles shows little effect (figure 3.10). Any apparent increase in the emission can be attributed to an increase in the baseline of the emission spectra. The different effect on the emissive properties of the two different complexes is likely to be due to the different heights of the two complexes, as the EuNapSAc complexes has long alkyl chains to hold the lanthanide ion away from the nanoparticle surface.
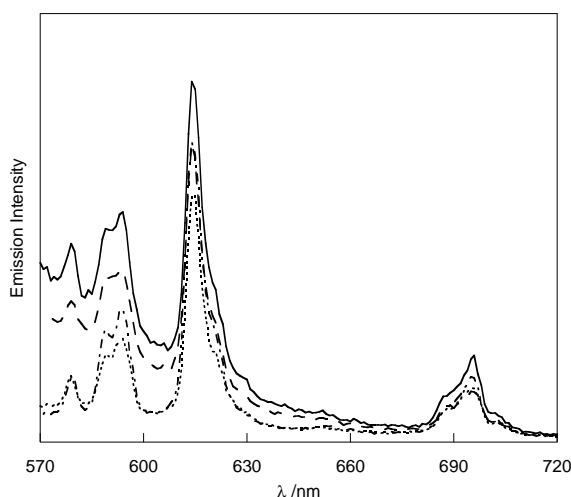
Figure 3.10: Luminescence spectra of partially coated **EuNapS.Au** (− · −·· −),
EuNapS.Peptide 2.Au (−−−), **EuNapS.Peptide 4.Au** (••••••), and **EuNapS.Peptide 10.Au** (——).
λ_{exc} = 310 nm. The nanoparticles were prepared by mixing [EuNapSAc] = 1 µM. [**Citrate.Au**] = 1.3nM,
[Peptide 2] = 1.6 µM, [Peptide 4] =6.6 µM, [Peptide 10] = 52 nM

The europium complexes predominately studied with peptides for cellular microscopy were EuQSH and EuNapSAc as they can be excited at wavelengths greater than 310 nm which is more desirable for the optics found in the microscope.

Examination of the **EuNapS.Au** with two of the CALNN terminated peptides shows a different trend than previously observed with the thioctic terminated peptides. Preparation of **EuNapS.Peptide 1.Au** was achieved by firstly the titration of µL aliquots of EuNapSAc dissolved in methanol to **Citrate.Au** give a red-shift in the SPR band of 3 nm. A further 1 nm red-shift is observed upon addition of the CALNNKKKKKGGRGDMFGKEESLADDL (peptide 1) (figure 3.11). This suggests that both the europium complex and the peptide are bound to the surface of the gold nanoparticles. The addition of a further excess of complex causes little change in the UV-Vis spectrum of the EuNapSAc peptide coated gold nanoparticles (figure 3.11).
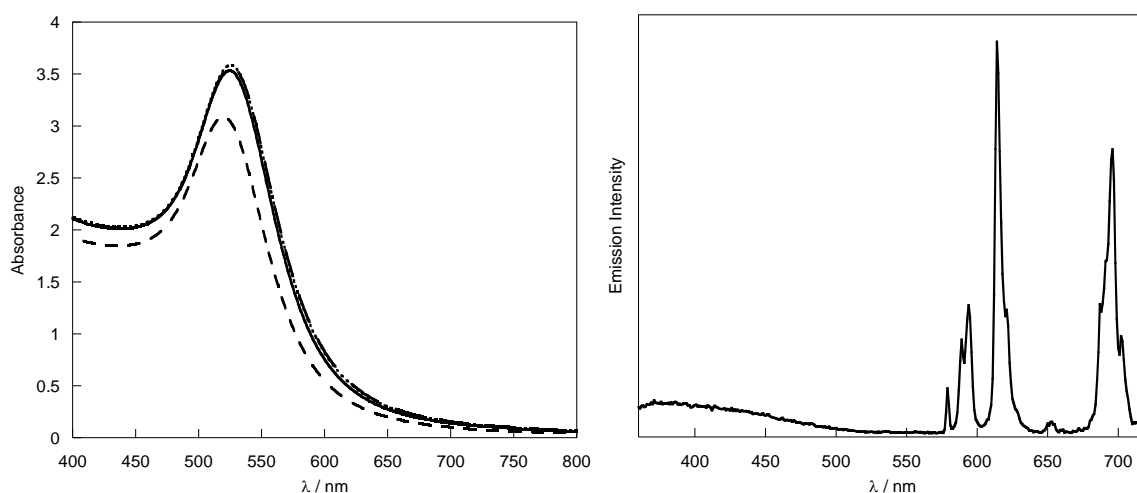
Figure 3.11: UV-Vis and emission spectrum of EuNapSAc CALNNKKKKKGGRGDMFGKEESLADDL (peptide 1) gold nanoparticles **EuNapS.Peptide1.Au**. UV-Vis (left) **Citrate.Au** (−−−−) with the addition of 9.4 µM EuNapSAc (——) and 0.03 µM peptide 1 (••••••). A further addition of 44 µM EuNapSAc was added to the sample (— —). Emission spectrum (right) λ_{exc} = 310 nm, gold nanoparticles purified to

remove excess complex and peptide by size exclusion chromatography. Emission spectrum corrected for PMT response.

Comparison of the EuNapSAc complex with different peptides shows an interesting result. The addition of the peptides cause a decrease in the emission of the europium compared with **EuNapS.Au** (figure 3.12). Peptide 1 causes a significant decrease in the europium emission, with the emission being reduced to a third of that observed with **EuNapS.Au**. However, the addition of CALNNGGFSTSLRARKAKEESLADDL (peptide 3) causes very little difference in the europium emission signal compared with **EuNapS.Au**.

The luminescence lifetimes show that the EuNapSAc complex has a higher lifetime of 720 µs in water than on gold nanoparticles which was found to be 590 µs. The presence of the peptide 1 with the EuNapSAc complex causes a decrease in the luminescence lifetime both in water and on gold nanoparticles with lifetimes of 640 µs and 530 µs respectively (table 3.2). The recorded lifetime of 630 µs for **EuNapS.peptide 3.Au** is higher than the lifetime of 590 µs for **EuNapS.Au**. The emission intensity of **EuNapS.peptide 3.Au** is similar to that of the **EuNapS.Au**, which suggests that the peptide does not greatly affect the emissive properties of the europium complex on nanoparticles. Peptide 1 contains a section of positively charged lysine residues which may be a contributing factor to the poor emission observed as they might interact unfavourably with the europium complex.

	Lifetime	χ^2
EuNapS.Au	590 µs	0.99779
EuNapSAc in water	720 µs	0.99946
EuNapS.Peptide 1.Au	530 µs	0.99401
EuNapSAc Peptide 1 in water	640 µs	0.99933
EuNapS.Peptide 3.Au	630 µs	0.9897
EuNapSAc Peptide 3 in water	700 µs	0.99944

Table 3.2: Comparison of luminescence lifetime of the EuNapSAc complex with peptides in water and on gold nanoparticles.
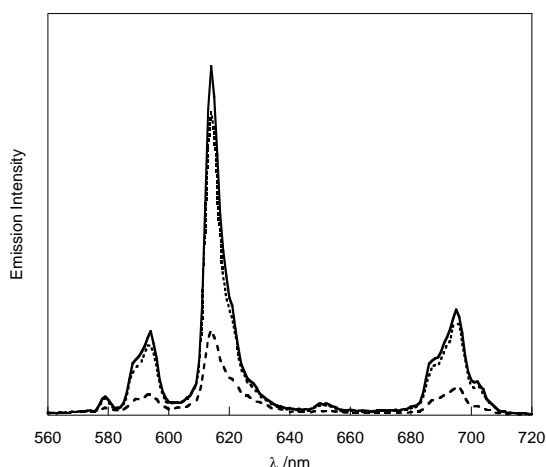
Figure 3.12: Comparison of emission spectra of *EuNapS.Au* (——), *EuNapS.Peptide 1.Au* (− − −) and *EuNapS.Peptide 3.Au* (•••••). λ_{exc} = 310 nm. The nanopartcles were prepared by mixing [*Citrate.Au*] = 9.3 nM, [EuNapSAc] = 9.5 µM, [Peptide 1] = 34 nM, [Peptide 3] = 1.2 µM.

Comparing the luminescence spectra of the luminescent nanoparticles *EuNapS.Peptide 1.Au*, *EuNapS.Peptide 2.Au*, *EuNapS.Peptide 3.Au* and *EuNapS.Peptide 4.Au* shows an interesting result. The europium emission from the samples containing peptides 2, 3 and 4 show no difference in the europium emission

in comparison with the ***EuNapS.Au*** containing the same concentration of EuNapSAc. However ***EuNapS.Peptide 1.Au*** shows a significant decrease in emission compared with ***EuNapS.Au***. The main difference between peptide 1 and 2 is the surface attachment, with peptide 1 having a terminal CALNN group and peptide 2 having a thioctic acid group. This makes the overall length of peptides different which potentially means that different amino acids at different distances from the gold surface compared with the EuNapSAc complex. The potential problem with this peptide is the group of positively charged lysines which may interact unfavourably with the europium complex. The different terminal surface attachment group may cause these charged groups to be at different heights from the nanoparticle surface. Therefore these lysine groups may be in different proximities to the EuNapSAc complex.

2.3.3   *Co-coating gold nanoparticles with EuQSH and Peptides*

The effect of peptides 1-4 has also been investigated on the EuQSH complex. Comparing the luminescence spectra of ***EuQS.Peptide 1.Au***, ***EuQS.Peptide 2.Au***, ***EuQS.Peptide 3.Au*** and ***EuQS.Peptide 4.Au*** shows the presence of the different peptides has different effects on the luminescence (figure 3.13). It is clear from the luminescence spectra that the europium emission signal is considerably reduced in the presence of peptide 1, with four-fold increased emission signal observed for ***EuQS.peptide 2.Au*** and ***EuQS.peptide 4.Au*** and an eight-fold increase observed with ***EuQS.peptide 10.Au***. This is similar to the trend shown with the EuNapSAc complex. ***EuQS.Peptide 2.Au*** and ***EuQS.Peptide 3.Au*** have similar europium

emission whilst ***EuQS.Peptide 4.Au*** has a two-fold greater emission intensity in comparison. Overall from the luminescence spectra of these nanoparticle samples, it can be seen that the trends are very similar for the EuQSH complex and the EuNapSAc complex in the presence of these peptides.
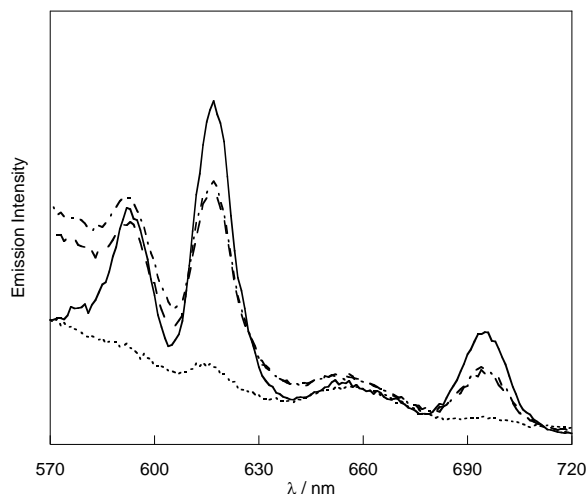
Figure 3.13: Luminescence spectra of ***EuQS.Peptide 1.Au*** (······), ***EuQS.Peptide 2.Au*** (- - - -), ***EuQS.Peptide 3.Au*** (- •- •-) and ***EuQS.Peptide 4.Au*** (——). λ_{exc} = 330 nm. The nanopartcles were prepared by mixing [***Citrate.Au***] = 9.3 nM, [EuQSH] = 53 µM, [Peptide 1] = 38 nM, [Peptide 2] = 0.12 µM, [Peptide 3] = 2.5 µM, [Peptide 4] = 3.7 µM

2.4 Preparation and characterisation of europium and peptide coated platinum nanoparticles

Platinum nanoparticles were also investigated as a potential scaffolds for lanthanide complexes and peptides. Unlike gold nanoparticles, platinum nanoparticles do not possess a surface plasmon resonance that can be monitored to determine the coating. An advantage of this however is that the platinum nanoparticles are not as strongly absorbing as the gold nanoparticles, which can be better for measuring the

photophysical properties of the lanthanide on the surface. Citrate stabilised platinum nanoparticles, **Citrate.Pt**, were prepared by the citrate reduction of chloroplatinic acid hexahydrate under reflux. The particles produced were spherical and approximately 6 nm in diameter. Platinum nanoparticles can be coated in a similar way to **Citrate.Au**, utilising functionalising moieties containing sulphur groups. Platinum nanoparticles however do not possess a surface plasmon resonance that can be monitored by UV-Vis spectroscopy, therefore this technique cannot be used to monitor the surface coating. The EuNapSAc complex was used to coat **Citrate.Pt**, with peptides 1 and 3. The prepared platinum nanoparticles were characterised by TEM and luminescence spectroscopy (figure 3.14).
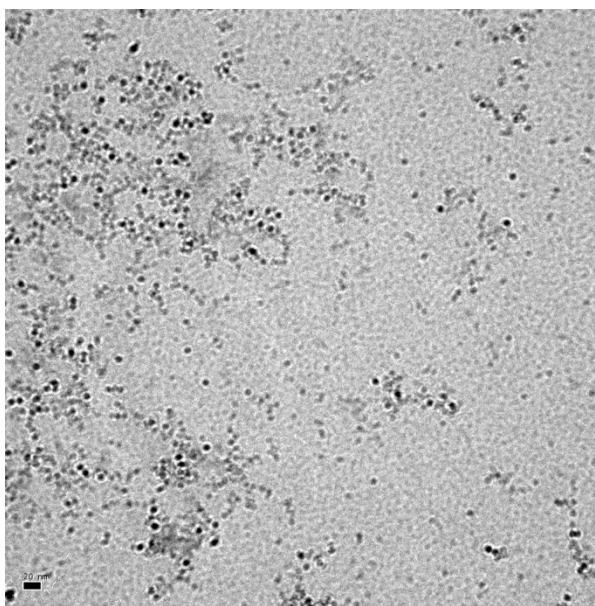
Figure 3.14: TEM image of **EuNapS.Peptide 3.Pt**. Scale bar = 20 nm

Luminescence studies of the EuNapSAc complex with platinum nanoparticles show an interesting trend (figure 3.15). **EuNapS.Pt** and EuNapSAc in water are of similar

emission intensity, suggesting that the platinum nanoparticles do not affect the emissive properties of the complex. The addition of peptide 3 causes a dramatic increase in the europium emission, with the emission intensity doubling with the presence of peptide 3. Peptide 1 has the opposite effect, with its addition to EuNapSAc coated platinum nanoparticles causing the europium emission to decrease. The trend in the emissive properties of EuNapSAc complex in the presence of peptide 1 and peptide 3 is similar in both gold and platinum nanoparticles.
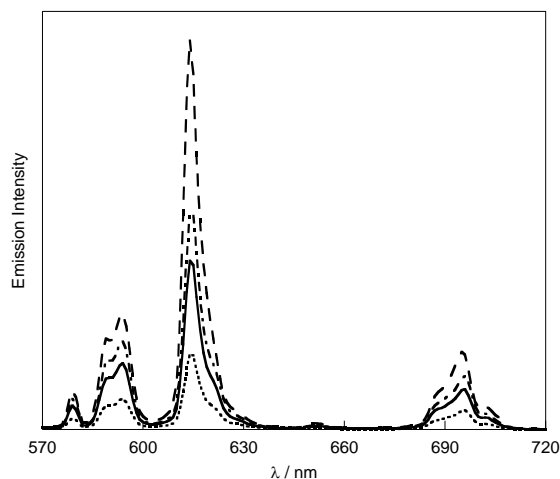
Figure 3.15: Emission spectra of **EuNapS.Pt** (——), EuNapSAc in water (–·–·–) **EuNapS.peptide 1.Pt** (••••••) and **EuNapS.peptide 3.Pt** (– – –). λ_{exc} = 310 nm. The nanoparticles were prepared by mixing [**Citrate.Pt**] = 17.2 nM, [EuNapSAc] = 0.75 µM, [Peptide 1] = 40 nM, [Peptide 3] = 2 µM.

	Lifetime	χ^2
EuNapS.Pt	580 μs	0.99677
EuNapSAc in water	720 μs	0.99946
EuNapS.Peptide 1.Pt	540 μs	0.99455
EuNapSAc Peptide 1 in water	640 μs	0.99933
EuNapS.Peptide 3.Pt	820 μs	0.99799
EuNapSAc Peptide 3 in water	700 μs	0.99944

Table 3.3: Comparison of luminescence lifetime of the EuNapSAc complex with peptides in water and on platinum nanoparticles.

Studies of the luminescence lifetime of the platinum nanoparticles show a similar trend to that of the co-coated gold nanoparticles. The lifetime of 820 μs recorded for **EuNapS.Peptide 3.Pt** is significantly higher than the complex on platinum nanoparticles, **EuNapS.Pt**, with a lifetime of 580 μs. It is also higher than EuNapSAc in water and EuNapSAc with peptide 3 in water, with lifetimes of 720 μs and 700 μs respectively. As with the gold nanoparticles, **EuNapS.Peptide 1.Pt** has a lower lifetime of 540 μs compared with **EuNapS.Pt**.

2.5 Cellular imaging with lanthanide and peptide coated gold and platinum nanoparticles

Citrate.Au were coated in EuNapSAc complex and peptides for dosing cancer cells for luminescence imaging. The cell line dosed with gold nanoparticles was the A549 cell line, which is a human adenocarcinoma alveolar basal epithelial cell line. Cells were seeded in phenol red free Dulbecco's modified eagle's medium to prevent any

fluorescence caused by the cell media, as cell media containing phenol red is likely to give rise to some fluorescence which could lead to false positive results when trying to detect luminescence from the cells incubated with the lanthanide coated nanoparticles. The cells were then incubated for 24 hours with the gold nanoparticles and fixed with 100 % methanol at -20 ^{o}C. Figure 3.16 shows the bright field and fluorescence images of A549 cells incubated with **EuNapS.peptide 1.Au**. There is luminescence observed from the cells imaged, suggesting some uptake of nanoparticles into the cells. A steady state emission spectrum was recorded from the cell sample and the emission recorded from the cells was attributed to europium. Similar luminescence was observed upon incubation of A549 cells with **EuNapS.peptide 3.Au** (figure 3.17).
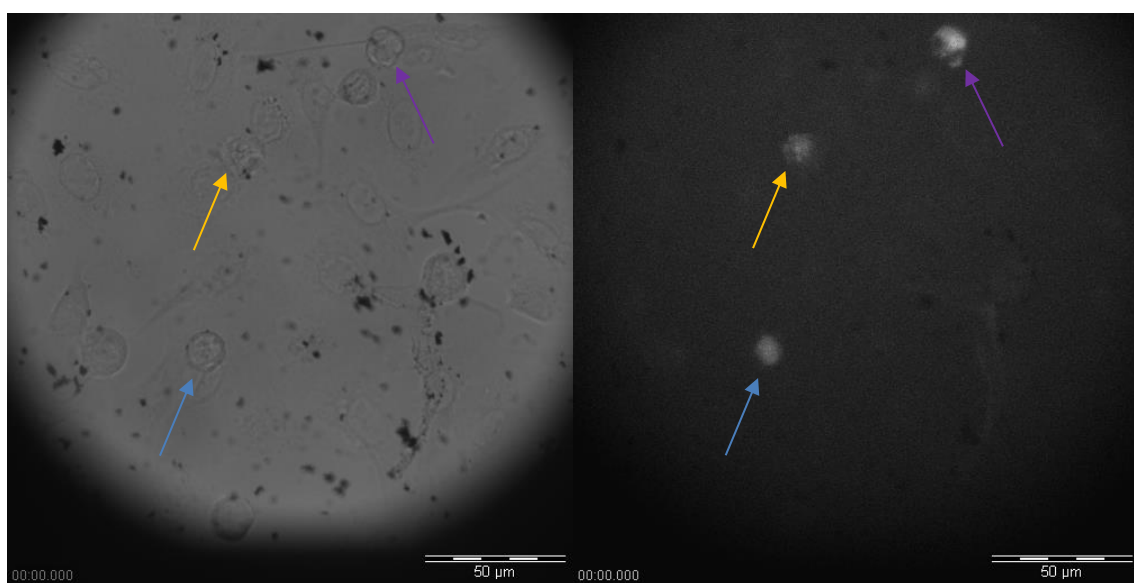
Figure 3.16: **EuNapS.Peptide 1.Au**, A549 cells. Left: Bright-field image, Right: Luminescence imaging λ_{exc} = 320 nm. Arrows indicate the position of cells that exhibit luminescence upon excitation.
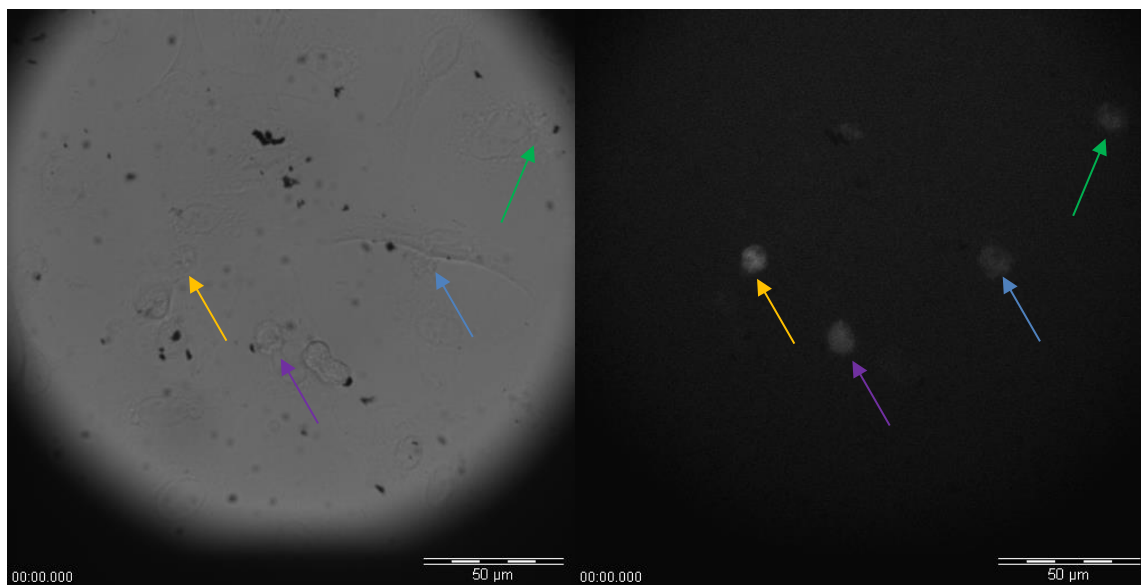
Figure 3.17: **EuNapS.Peptide 3.Au**, A549 cells. Left: Bright-field image, Right: Luminescence imaging λ_{exc} = 320 nm. Arrows indicate the position of cells that exhibit luminescence upon excitation.
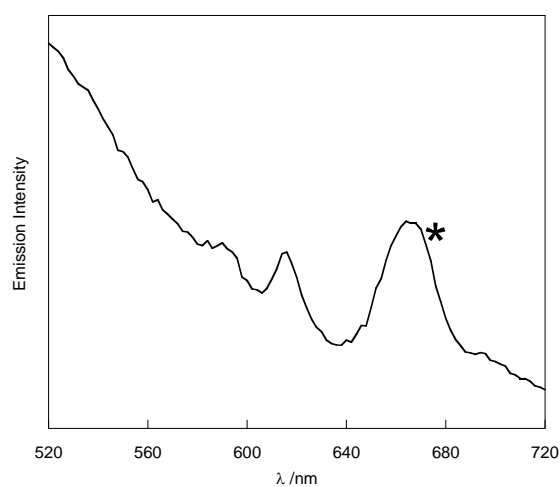
Figure 3.18: Emission spectrum from luminescence microscopy of **EuNapS.peptide 1.Au** in A549 cells. λ_{exc} = 330 nm. *scattering peak

90
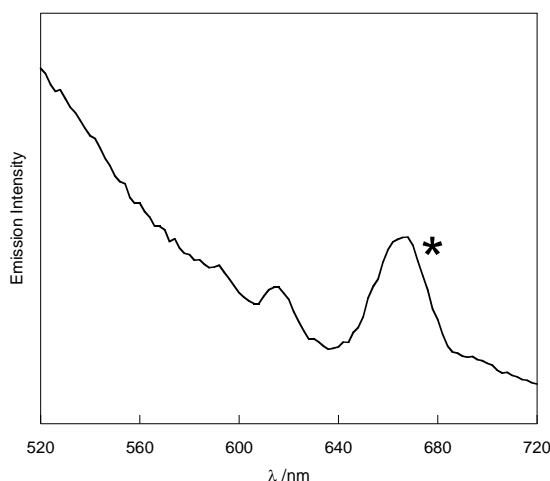
Figure 3.19: Emission spectrum from luminescence microscopy of **_EuNapS.peptide 3.Au_** in A549 cells. λ_{exc} = 330 nm. *scattering peak

Luminescence microscopy was also carried out with gold nanoparticles coated with a combination of EuQSH and peptides 1-4. However there was no luminescence observed with these nanoparticles. The EuQSH peptide nanoparticles also exhibited weaker emission in solution than the EuNapSAc peptide nanoparticles which may explain why they could not be observed in cells. Figure 3.20 shows A549 cells dosed with **_EuQS.peptide 3.Au_**. The cells are clearly visible in the bright field image, but none of these show any luminescence when excited at 330 nm.
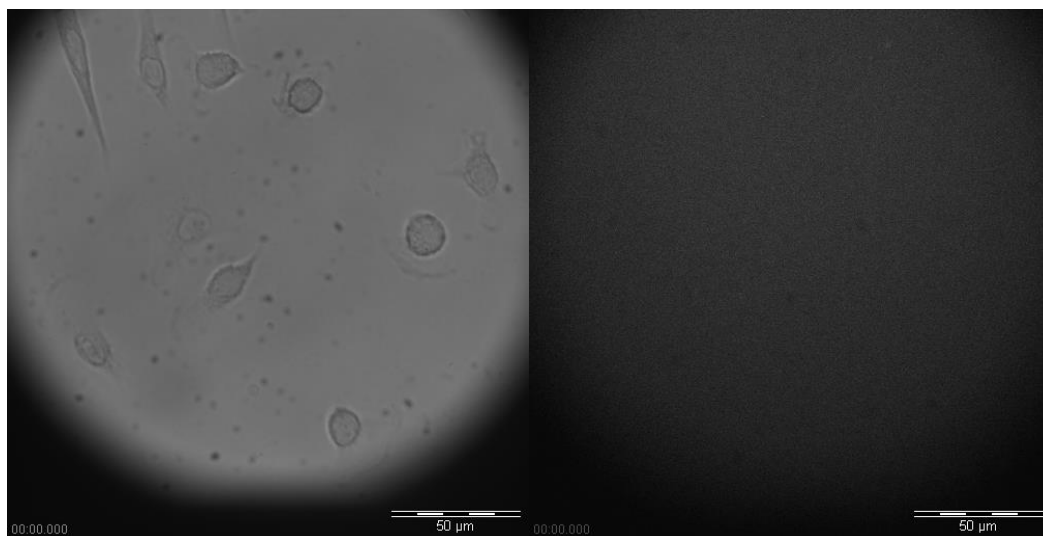
Figure 3.20: ***EuQS.Peptide 3.Au***, A549 cells. Left: Bright-field image, Right: Luminescence image λ_{exc} = 330 nm

Citrate.Pt were also coated in the EuNapSAc complex and peptides 1 and 3. ***EuNapS.Peptide 1.Pt*** and ***EuNapS.Peptide 3.Pt*** were incubated with A549 cells for luminescence imaging. From the images in figure 3.21, it can be seen that the cells exhibit some luminescence for cellular imaging, but the luminescence was very weak compared with ***EuNapS.Peptide 1.Au*** and ***EuNapS.Peptide 3.Au***.
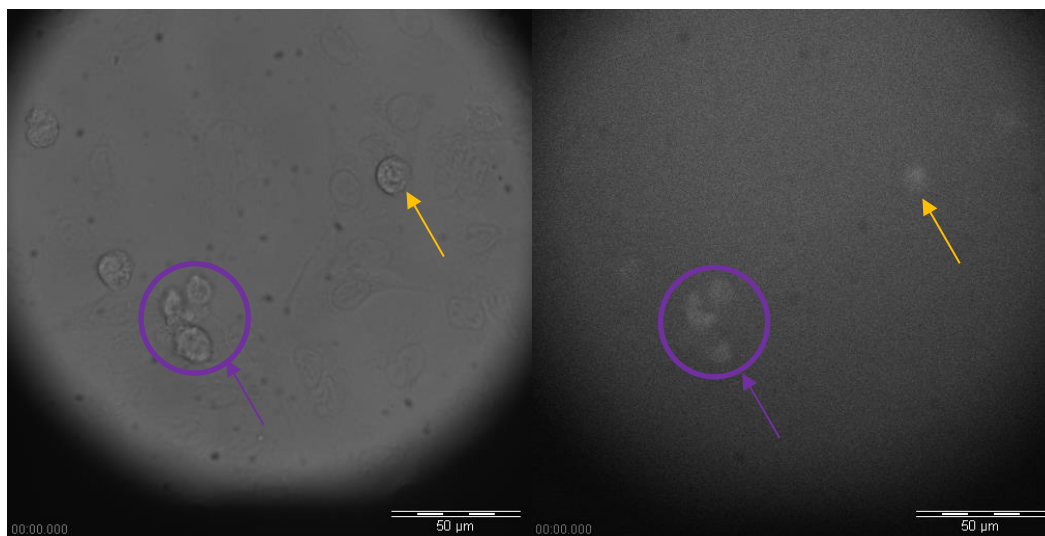
Figure 3.21: ***EuNapS.Peptide 3.Pt***, A549 cells. Left: Bright-field image, Right: Luminescence image λ_{exc} = 320 nm. Arrows indicate the position of cells that exhibit luminescence upon excitation.

2.6 Conclusion

Gold and platinum nanoparticles coated with europium complexes and peptides have been prepared and characterised by UV-Vis and luminescence spectroscopy. The different structures of the peptides have different effects on the emissive properties of the lanthanide complexes on gold nanoparticles. On comparison of the longer peptides, peptide 3 shows the least effect on the luminescent properties of the lanthanide complexes and peptide 1 showing the most pronounced effect. The highest europium luminescence was observed with the EuNapSAc complex in the presence of the peptides on gold nanoparticles. To investigate these lanthanide and peptide coated nanoparticles as lanthanide imaging probes, selected nanoparticles were incubated with cells. Luminescence microscopy images showed europium luminescence with the cells incubated with ***EuNapS.Peptide1.Au***, ***EuNapS.Peptide 3.Au***, ***EuNapS.Peptide 1.Pt*** and ***EuNapS.Peptide 3.Pt***. This

suggests that the EuNapSAc complex is a good luminescent probe for cellular imaging. Whilst these nanoparticles show promise as imaging probes in cells, further investigation could be carried out into designing lanthanide complexes that are unaffected by the presence of the peptide on the gold nanoparticle surface, The lanthanide complex would have to include a strongly chelating component to ensure the lanthanide remains firmly bound, and would also require sulphur(s) for binding to the gold nanoparticles. The ratio of peptide and lanthanide complex could also be examined further to investigate the highest ratio of lanthanide complexes that can be added, whilst still having enough peptide to transport the nanoparticles into cells. These are all factors which could be investigated in order to improve the potential of these lanthanide and peptide coated gold nanoparticles as cellular imaging probes.

3   Experimental

3.1   Preparation of DTPA bis-anhydride
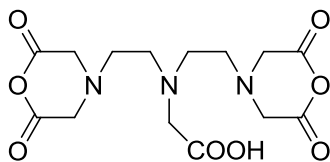
Acetic anhydride (220 ml, 2.33 mol) was added slowly via a dropping funnel to a stirring suspension of H_5DTPA (160.6 g, 0.41 mol) in pyridine (150 ml) at $65^{\circ}C$. The solution was stirred for 5 h and the solid was isolated by suction filtration and washed with acetic anhydride (2 x 50 ml). Acetonitrile (250 ml) was added to the solid and the solution refluxed for 1 h. Once the solution had cooled, the white solid was isolated by suction filtration and washed with acetonitrile (2 x 50 ml) and diethyl ether (2 x 50 ml). The final solid was dried *in vacuo.* (134.69 g, 92 %) ^{1}H NMR (300 MHz, D_2O) δ (ppm) 3.98 (8H, s, NC$\underline{H}_2$CO), 3.63 (2H, s, NC$\underline{H}_2$COOH), 3.48 (4H, t, NC$\underline{H}_2$CH$_2$N), 3.18 (4H, t, NCH$_2$C$\underline{H}_2$N).

3.2   Preparation of 1,11-(bis(4amidothiophenol)-1,11-dioxo-3,6,9-triaza-3,6,9-triscarboxymethyl) undecane (SH ligand)[18, 28]
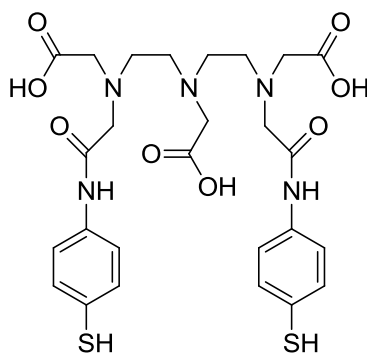
4-aminothiophenol (2. g, 16 mmol) was added to a solution of DTPA bis-anhydride (1.02 g, 2.8 mmol) in pyridine (10 ml) and stirred under nitrogen for 24 h. The resulting cloudy yellow solution was filtered, and the pyridine removed to give a thick yellow oil. Water (8 ml) was added to the oil and the crude ligand was isolated by lowering the pH to 3 using conc. HCl. The water was decanted from the flask, and the remaining solid was washed with water (2 x 20 ml) and acetonitrile (2 x 20 ml) and stirred in acetonitrile (50 ml) until a pale yellow powder is formed. The precipitate was isolated by suction filtration, and washed with acetonitrile (2 x 10 ml) and diethyl ether (2 x 20 ml).

Hydrazine monohydrate (3 ml) was added dropwise to a solution of crude product in pyridine (20 ml). The pyridine was then removed by rotary evaporation and the product was redissolved in water and filtered. The solution was acidified to pH 3 with the addition of conc. HCl. The bottom layer was isolated and washed with acetonitrile (2 x 25 ml), then stirred in acetonitrile (2 x 50 ml) until an off white precipitate had formed. The powder was collected by filtration and washed with acetonitrile (2 x 10 ml) and diethyl ether (2 x 20 ml) and then dried *in vacuo*. (0.34 g, 40 %) ^{1}H NMR (300 MHz, MeOD-D$_4$) δ (ppm) 7.41 (4H, d, Ar$\underline{H}$), 7.15 (4H, d, Ar$\underline{H}$), 4.10 (2H, s, central - C$\underline{H}_2$COOH), 3.62 (4H, s C$\underline{H}_2$COOH), 3.59 (4H, s, -CH$_2$CONH), 3.50 (4H, t, NC$\underline{H}_2$CH$_2$N), 3.23 (4H, t, NCH$_2$C$\underline{H}_2$N). ^{13}C NMR (400 MHz, MeOD-D$_4$) 174.6 (2xC, CH$_2$$\underline{C}$OOH), 171.5 (1xC, CH$_2$$\underline{C}$OOH), 136.9 (2xC, Ar$\underline{C}$), 130.8 (4xC, Ar$\underline{C}$), 127.8 (2xC, Ar$\underline{C}$), 122.2 (4xC, Ar$\underline{C}$), 59.1 (2xC, $\underline{C}$H$_2$CO), 56.3 (2xC, N$\underline{C}$H$_2$COOH), 55.2 (2xC, central- N$\underline{C}$H$_2$COOH), 55.0 (2xC, NCH$_2$$\underline{C}H_2$N), 51.1 (2xC, N$\underline{C}H_2CH_2$N). MS (ES$^+$): m/z 631 [M+Na]$^+$

3.3 Preparation of LnSH (Ln = Tb, Nd, Gd and Eu)[28]

LnSH: SH ligand (0.2 g, 0.3 mmol) was added to a solution of $LnCl_3.xH_2O$ (0.3 mmol) in degassed methanol (3 ml) and the solution was sonicated until the ligand had completely dissolved. Acetonitrile (20 ml) was added to the solution which caused the complex to precipitate out. The precipitate was collected under nitrogen and washed with acetonitrile (2 x 10 ml) and diethyl ether (2 x 10 ml). The final complex was dried *in vacuo.*

TbSH: Yield 97 %, MS (ES$^+$) m/z 786.3 $[M+Na]^+$, UV-Vis (MeOH), λ_{max} nm (log ε): 266 nm (4.4)

NdSH: Yield 84 %, MS (ES$^+$) m/z 749.4 $[M+H]^+$, UV-Vis (MeOH), λ_{max} nm (log ε): 267 nm (4.4)

GdSH: Yield 92 %, MS (ES$^+$) m/z 784 $[M+Na]^+$, UV-Vis (MeOH), λ_{max} (log ε): 267 nm (4.3)

EuSH: SH ligand (0.036 g, 0.06 mmol) was dissolved in degassed methanol (1 ml). A solution of KOH (0.0105 g, 0.18 mmol) in degassed methanol was added to the H_3L^1 solution and stirred for 12 h. The solvent was removed to give the white potassium salt of the SH ligand, which was re-dissolved in degassed water (1 ml). $EuCl_3.6H_2O$ (0.0218 g, 0.08 mmol) was added to the solution, which caused the formation of a white precipitate. The precipitate was isolated by suction filtration and washed with

acetone (2 x 5 ml) and diethyl ether (2 x 5 ml). The final solid was dried *in vacuo.*

Yield 53 %, UV-Vis (MeOH), λ_{max} (log ε): 266 nm (4.2).

3.4 Preparation of 1-(6-amidoquinoline), 11-(4-amidothophenol)-1,11-dioxo-3,6,9-triaza-3,6,9-triscarboxymethyl undecane (QSH ligand)
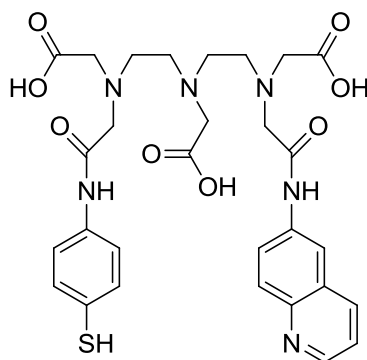
DTPA bisanhydride (2.45 g, 7 mmol) was stirred in pyridine (100 ml). 6-aminoquinoline (0.99 g, 7 mmol) was added to the solution and stirred at room temperature under nitrogen for 45 minutes. 4-aminothiophenol (0.87 g, 7 mmol) was added to the reaction mixture and stirred for 2 hours at room temperature under nitrogen. Water (80 ml) was added and stirred for 30 minutes. Solvent was removed *in vacuo* to give a yellow solid. The solid was dissolved in degassed water, and the pH was reduced to pH 3 with conc. HCl under nitrogen which caused the formation of a yellow precipitate. The water was decanted off and the precitipate was washed with 50 ml degassed water and 50 ml degassed acetonitrile. The precipitate was stirred in 200 ml degassed acetonitrile overnight. The solid was collected by suction filtration

under nitrogen and washed with degassed acetonitrile (2 x 25 ml) and diethyl ether (2 x 25 ml) to yield a bright yellow solid. (0.893 g, 21 %).

This crude product was purified by prep HPLC (C12 column, Acetone/Water/0.05 % TFA). Briefly, the crude product was dissolved in 1:1 THF: water, with tris (2-carboxyethyl) phosphine hydrochloride (TCEP) added in excess to reduce any disulphide bonds. The sample injection size was 100 mg/ml. (0.157 g, 17.5 %)

^{1}H NMR (300 MHz, D_2O) δ (ppm) 8.46 (1H, d, Ar$\underline{H}$), 8.00 (1H, d, Ar$\underline{H}$), 7.74 (2H, d, Ar$\underline{H}$), 7.51 (1H, dd, Ar$\underline{H}$), 7.23 (1H, q, Ar$\underline{H}$), 6.02 (2H, d, Ar$\underline{H}$), 6.68 (2H, d, Ar$\underline{H}$), 3.18 (2H, s, NC$\underline{H_2}$CO), 3.08 (2H, s, NC$\underline{H_2}$CO), 2.95 (6H, t, NC$\underline{H_2}$COOH), 2.51 (8H, s, NC$\underline{H_2}$C$\underline{H_2}$N)

3.5   Preparation of LnQSH (Ln = Eu, Nd and Gd)

LnQSH: $LnCl_3.xH_2O$ (0.06 mmol) was added to a solution of the QSH ligand (0.06 mmol) in 5 ml water and stirred under nitrogen. The pH was adjusted to 5 with the dropwise addition of tetrabutylammonium hydroxide (40 % w/w). The volume of the solution was reduced to 1 ml *in vacuo*. Degassed acetonitrile (30 ml) was added to precipitate LnQSH. The precipitate was collected by suction filtration under nitrogen and washed with acetonitrile (5 ml) and diethyl ether (5 ml). The final solid was dried on a high vacuum line.

EuQSH: Yield = 91 % MS (ES$^+$) m/z 777 [M+H]$^+$; CHN analysis: Anal. Calc. for $C_{29}H_{31}N_6O_8SEu$. C: 44.84; N: 10.83; H: 4.03. Found C: 44.30; N: 10.85; H: 4.23.

NdQSH: Yield = 58 % CHN analysis: Anal. Calc. for $C_{29}H_{31}N_6O_8SNd$ C: 45.48; N: 10.98; H: 4.08. Found C: 45.29; N: 10.91; H: 4.16

GdQSH: Yield = 76 % CHN analysis: Anal. Calc. for $C_{29}H_{31}N_6O_8SGd(H_2O)_3$ C: 41.67; N: 10.06; H: 4.47. Found C: 41.60; N: 10.01; H: 4.05

YQSH: Yield = 88 % MS (ES⁻) m/z 711 [M-H]⁻ ^{1}H NMR (300 MHz, MeOD) δ (ppm) 8.46 (1H, s, Ar$\underline{H}$), 8.15 (1H, s, Ar$\underline{H}$), 8.00 (1H, d, Ar$\underline{H}$), 7.64 (2H, q, Ar$\underline{H}$), 7.21 (1H, m, Ar$\underline{H}$), 7.02 (2H, d, Ar$\underline{H}$), 6.08 (2H, d, Ar$\underline{H}$), 2.96 (4H, s, NC$\underline{H}_2$COOH), 2.91 (2H, s, central - NC$\underline{H}_2$COOH), 2.78 (4H, s, NC$\underline{H}_2$CO), 2.49 (4H, s, NC$\underline{H}_2$CH$_2$N), 2.30 (4H, s, NCH$_2$C$\underline{H}_2$N)

3.6   Preparation of citrate stabilised platinum nanoparticles (*Citrate.Pt*)

All glassware was washed with Aqua Regia and dried prior to use. Chloroplatinic acid hexahydrate (9.3 mg, 17.9 mmol) was dissolved in 150 ml water and heated under reflux. A solution of sodium citrate (18 mg, 61.2 mmol) in water (18 ml) was added rapidly. The solution was refluxed for 4 hours and then allowed to cool.

4   References

1 V. V. Zherdeva and A. P. Savitsky, *Biochemistry (Moscow),* 2012, **77**, 1553-1574.

2 C. P. Montgomery, B. S. Murray, E. J. New, R. Pal and D. Parker, *Acc. Chem. Res.,* 2009, **42**, 925-937.

3 A. Thibon and V. C. Pierre, *Anal. Bioanal. Chem.,* 2009, **394**, 107-120.

4 E. J. New, D. Parker, D. G. Smith and J. W. Walton, *Curr. Opin. Chem. Biol.,* 2010, **14**, 238-246.

5 B. S. Murray, E. J. New, R. Pal and D. Parker, *Org. Biomol. Chem.,* 2008, **6**, 2085-2094.

6 E. J. New, D. Parker and R. D. Peacock, *Dalton Trans.,* 2009, **4**, 672-679.

7 F. Kielar, G. Law, E. J. New and D. Parker, *Org. Biomol. Chem.,* 2008, **6**, 2256-2258.

8 E. Deiters, B. Song, A. Chauvin, C. D. B. Vandevyver and J. C. G. Bunzli, *New J. Chem.,* 2008, **32**, 1140-1152.

9 E. Deiters, B. Song, A. S. Chauvin, C. D. B. Vandevyver, F. Gumy and J. C. G. Bunzli, *Chem- Eur J.,* 2009, **15**, 885-900.

10 A. G. Tkachenko, H. Xie, D. Coleman, W. Glomm, J. Ryan, M. F. Anderson, S. Franzen and D. L. Feldheim, *J. Am. Chem. Soc.,* 2003, **125**, 4700-4701.

11 P. C. Patel, D. A. Giljohann, D. S. Seferos and C. A. Mirkin, *PNAS,* 2008, **105**, 17222-17226.

12 N. G. Bastuİs, E. SaÌnchez-TilloÌ, S. Pujals, C. Farrera, C. LoÌpez, E. Giralt, A. Celada, J. Lloberas and V. Puntes, *ACS Nano,* 2009, **3**, 1335-1344.

13 P. Nativo, I. A. Prior and M. Brust, *ACS Nano,* 2008, **2**, 1639-1644.

14 R. Lévy, N. T. K. Thanh, R. C. Doty, I. Hussain, R. J. Nichols, D. J. Schiffrin, M. Brust and D. G. Fernig, *J. Am. Chem. Soc.,* 2004, **126**, 10076-10084.

15 Y. Song, X. Xu, K. W. MacRenaris, X. Zhang, C. A. Mirkin and T. J. Meade, *Angew. Chem. Int. Ed.,* 2009, **48**, 9143-9147.

16 J. Wang, J. Moore, S. Lauhle, M. Nantz, S. Achilefu and K. A. Kang, *Nanotechnology,* 2012, **23**, 095501.

17 T. Biver, N. Eltugral, A. Pucci, G. Ruggeri, A. Schena, F. Secco and M. Venturini, *Dalton Trans.,* 2011, **40**, 4190-4199.

18 D. J. Lewis, T. M. Day, J. V. MacPherson and Z. Pikramenou, *Chem. Commun.,* 2006, **13**, 1433-1435.

19 A. Davies, D. J. Lewis, S. P. Watson, S. G. Thomas and Z. Pikramenou, *PNAS,* 2012, **109**, 1862-1867.

20 D. J. Lewis, C. Bruce, S. Bohic, P. Cloetens, S. P. Hammond, D. Arbon, S. Blair-Reid, Z. Pikramenou and B. Kysela, *Nanomedicine,* 2010, **5**, 1547-1557.

21 J. Massue, S. J. Quinn and T. Gunnlaugsson, *J. Am. Chem. Soc.,* 2008, **130**, 6900-6901.

22 S. Comby and T. Gunnlaugsson, *ACS Nano,* 2011, **5**, 7184-7197.

23 X. Wang, Y. Xia, Y. Liu, W. Qi, Q. Sun, Q. Zhao and B. Tang, *Chem- Eur J.,* 2012, **18**, 7189-7195.

24 X. Wang, J. Geng, D. Miyoshi, J. Ren, N. Sugimoto and X. Qu, *Biosensors and Bioelectronics,* 2010, **26**, 743-747.

25 X. Yan, L. Yang and Q. Wang, *Angew. Chem. Int. Ed.,* 2011, **50**, 5130-5133.

26 C. Kim, P. Ghosh and V. M. Rotello, *Nanoscale,* 2009, **1**, 61-67.

27 M. J. Cariveau, X. Tang, X. Cui and B. Xu, *Molecular Pharmacology,* 2007, **72**, 320-326.

28 D. J. Lewis, P. B. Glover, M. C. Solomons and Z. Pikramenou, *J. Am. Chem. Soc.,* 2011, **133**, 1033-1043.

29 S. P. Hammond, PhD, University of Birmingham, 2009.

Dual lanthanide coated gold nanoparticles: preparation and photophysical characterisation.

1   Introduction

The self-assembly of multiple probes onto gold surfaces is particularly desirable for use as sensors and multimodal imaging agents. Probes with a variety of functions can be assembled onto the same nanoparticle to give the nanoparticle multimodal properties,[1] or work as sensors for the detection of multiple analytes and biological molecules in solutions containing complex mixtures of molecules.[2] The assembly of probes on surfaces can also facilitate energy transfer between donor and acceptor molecules. There have been many examples of gold nanoparticle functionalised with donor and acceptor molecules designed for Förster resonance energy transfer (FRET). FRET systems are often utilised for sensing biologically relevant analytes, metal ions, proteins and enzymes. Gold nanoparticles have been widely researched in this field as they are able to act as fluorescence quenchers. Fluorophores have been attached to gold nanoparticles, which induces fluorescence quenching by FRET between the fluorophore and the gold nanoparticles. The fluorophore acridine orange has been non-covalently absorbed onto gold nanoparticles which induce fluorescence quenching in close proximity to the surface (figure 4.1A). These nanoparticles can be used in the sensing of biological thiols, as thiols are able to displace the fluorophore from the nanoparticle causing an increase in fluorescence observed.[3] Release of the fluorophore from the gold nanoparticle surface reduces the FRET between the fluorophore and the gold nanoparticles and causes the fluorescence to increase. A similar principle has been applied to the detection of

hydrogen peroxide, glucose and uric acid using gold nanoparticles conjugated with an enzyme horseradish peroxidase.[4] Hydrogen peroxide is able to catalyse the binding of a tyramide moiety labelled with tetramethyl rhodamine to the enzyme horseradish peroxidase (HRP) or bovine serum albumin (BSA) (figure 4.1B and C). The binding of the labelled tyramide to the enzyme conjugated to gold nanoparticles causes the fluorescence of the rhodamine to be quenched. Thus the presence of hydrogen peroxide can be detected by the decrease in fluorescence observed from the rhodamine once it is bound to HRP or BSA.

Scheme A: Sensing for biothiols with Acridine Orange-AuNPs FRET system.

Scheme B: Sensing for hydrogen peroxide using a BSA and HRP coated gold nanoparticles and tyramide labelled TMR FRET system

Scheme C: Reaction scheme of the enzymatic reaction of hydrogen peroxide with BSA and HRP − AuNP and tyramide labelled TMR
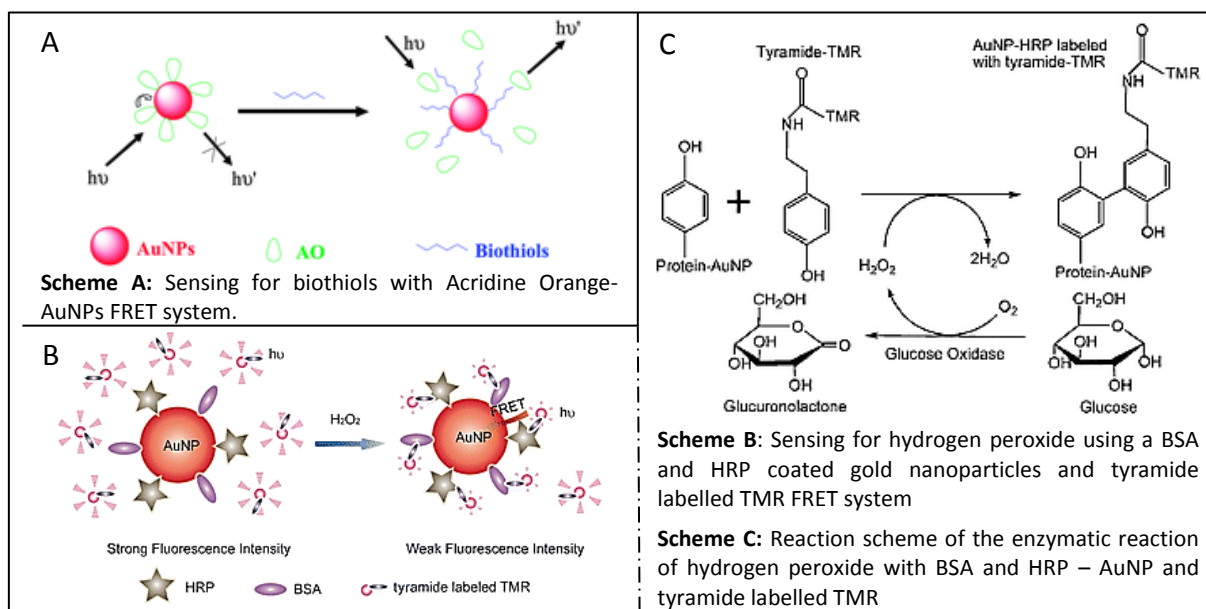
Figure 4.1: Schematic representations of two different FRET systems using gold nanoparticles (**A** and **B**). **A:** Acridine orange labelled gold nanoparticles for the sensing of biothiols.[3] **B:** BSA and HRP coated gold nanoparticles with tyramide labelled TMR for the detections of hydrogen peroxide. **C:** Reaction scheme of the enzymatic reaction for the detection of hydrogen peroxide.[4] Figures reproduced from references 3 and 4

The development of multimodal gold nanoparticles has recently become of interest to many researchers. The ease of modification and large surface area of gold nanoparticles gives great potential for the attachment of several different functionalising moieties to the same nanoparticle. This allows for the development of probes that can be used for multiple imaging applications[5-7] as well as drug delivery[8] and therapeutics.[9] One example of this is the gadolinium-enriched DNA coated gold nanoparticles Cy3-DNA-Gd@AuNP developed by Meade *et al.*[7] The nanoparticle conjugates contain gadolinium for use as an MRI contrast agent, and also the fluorescent dye Cy3 to allow the uptake of the nanoparticles to be monitored by fluorescence microscopy (figure 4.2).
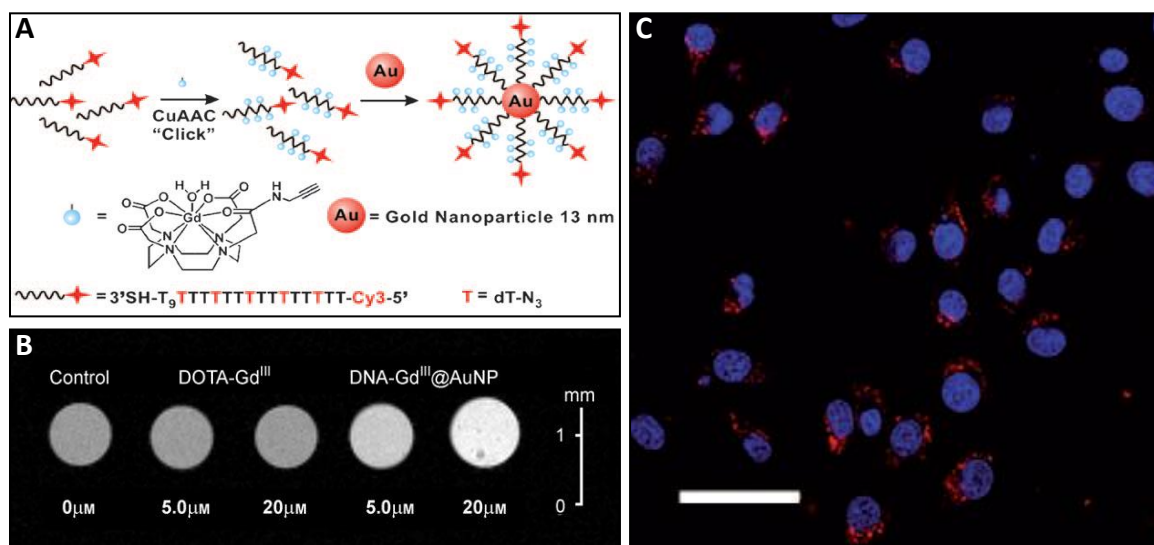
Figure 4.2: Development and characterisation of DNA-Gd@AuNP.[7] **A:** Synthesis scheme of Cy3-DNA-Gd@AuNP. **B:** T_1-weighted MR image of NIH/3T3 cells incubated with 20 mM and 5.0 mM (Gd[III] concentrations) Cy3-DNA-Gd@AuNP and DOTA-Gd[III] for 24 h at 14.1 T (600 MHz) and 25 °C. **C:** Confocal fluorescence micrograph of NIH/3T3 cells incubated with 0.2 nM particle concentration of Cy3-DNA–Gd@AuNPs for 4.0 h and a 24 h leach in fresh media and 1 mM DAPI (4',6-diamidino-2-phenylindole) for 10 min. Image shows merge of the blue (DAPI) and red (Cy3-DNA-Gd@AuNPs) channels. Scale bar = 50 µm. Figure reproduced from reference [7]

Gadolinium DOTA complexes are attached using click chemistry onto a thiol-containing poly-dT DNA oligomer for attachment to citrate-stabilised gold nanoparticles. Upon incubation of NIH/3T3 cells with 20 µM Cy3-DNA-Gd@AuNP, the conjugate was found to give a 43 % reduction in T_1 compared with the free Gd-DOTA complex at the same concentration. Fluorescence imaging shows the accumulation of these particles in cells after 4 hours incubation, which shows that the Cy3-DNA-Gd@AuNP conjugates are a versatile multimodal imaging agent (figure 4.2C). Gold nanoparticles are also known to be a suitable contrast agent for computed tomography (CT), which the authors suggest make these Cy3-DNA-Gd@AuNP conjugates suitable for CT as well as fluorescence and MRI.

With emission in the visible and near-infrared regions and long luminescence lifetimes, lanthanides can be used as imaging agents using a variety of techniques. The paramagnetic properties of gadolinium also make it widely used as an MRI contrast agent. By combining different lanthanides into a single probe, it is possible that the different photophysical or paramagnetic properties can be exploited allowing different techniques to be used in their detection.[10]

Lanthanides have been previously found to exhibit energy transfer between two different lanthanide DTPA-bis amide complexes in solution upon the formation of macrocycles by disulphide bonds.[11] The macrocycles exhibit weak energy transfer between the lanthanide ions when the two complexes are assembled into macrocycles but as yet this energy transfer phenomenon has not been reported on gold nanoparticles.

Typically lanthanide complexes are designed with the inclusion of a chromophore for the sensitisation of lanthanide ions, as lanthanide ions are typically poor absorbers. However some examples of the self-assembly of lanthanide complexes with a chromophore on gold nanoparticles have been reported. The addition of a diketonate to gold nanoparticles coated in a macrocyclic europium complex causes a 'switch on' effect in the lanthanide luminescence (figure 4.3A).[12] The diketonate acts a sensitising unit for the lanthanide, as the macrocycle contains no chromophore. The pH dependent self-assembly of the diketonate with the europium complex allows energy transfer from the diketonate to the europium ion to produce luminescent gold nanoparticles. This principle has also been applied to the sensitisation of near-infrared lanthanides with xylenol orange (figure 4.3B).[13] The mixture of nucleotides and lanthanide ions has been found to form supramolecular networks which go on to form nanoparticles. Energy transfer occurs between the nucleotides and the lanthanide ions. These supramolecular networks that are formed upon mixing are able to encapsulate gold nanoparticles, as well as proteins and fluorescent dyes.[14]
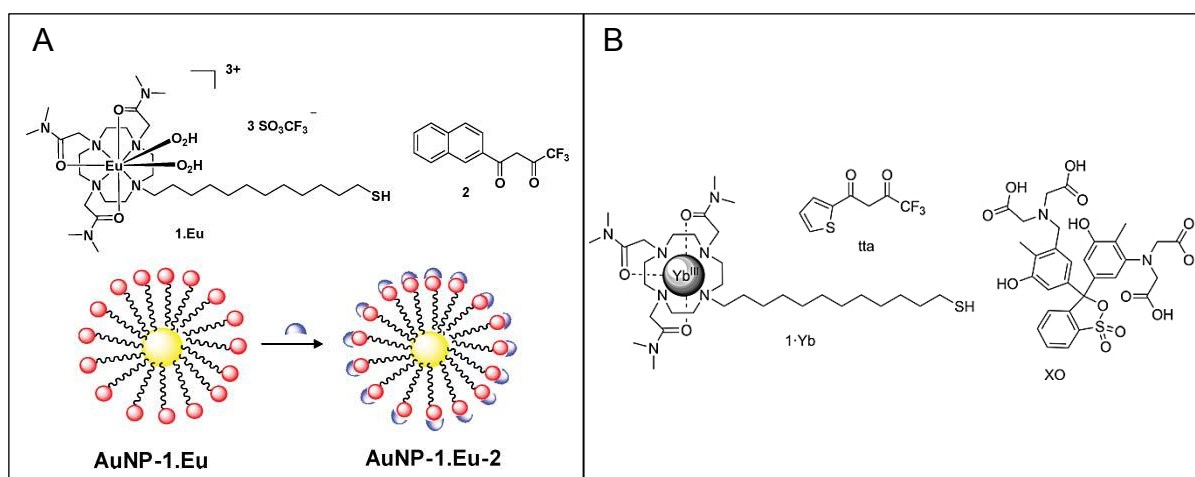
Figure 4.3: Macrocyclic lanthanide compounds developed for attachment to gold nanoparticles, with antennae for self-assembly. **A:** A macrocyclic europium complex with a diketonate antenna for

lanthanide sensitisation.[12] **B:** A macrocyclic ytterbium complex with xylenol orange. Figures reproduced from reference [13]

This chapter describes the coating of gold nanoparticles with europium and gadolinium complexes. The lanthanide complexes are based on two different DTPA bis-amide ligands shown in figure 4.4. The asymmetric lanthanide complex LnQSH contains a quinoline chromophore on one arm of the DTPA bis-amide complex and an amidothiophenol group on the other arm to provide the thiol for attachment to gold nanoparticles. The LnSH complex contains two amidothiophenol arms attached to a DTPA backbone to provide two thiols for surface attachment to gold. The EuSH complex has previously been reported on gold nanoparticles.[15] By co-coating gold nanoparticles in a combination of different lanthanide complexes, it is possible to develop multi-modal probes utilising the different photophysical properties of the lanthanide ions. Gold nanoparticles were coated in both the europium and gadolinium analogues of LnSH and for comparison the europium and gadolinium analogues of LnQSH. The coated gold nanoparticles exhibit the characteristic properties of the lanthanide complexes attached.

The europium complexes previously reported in chapter three EuNapSAc will be discussed for comparison with the two DTPA-bisamide complexes EuSH and EuQSH. The structure of this complex is shown in figure 4.5.
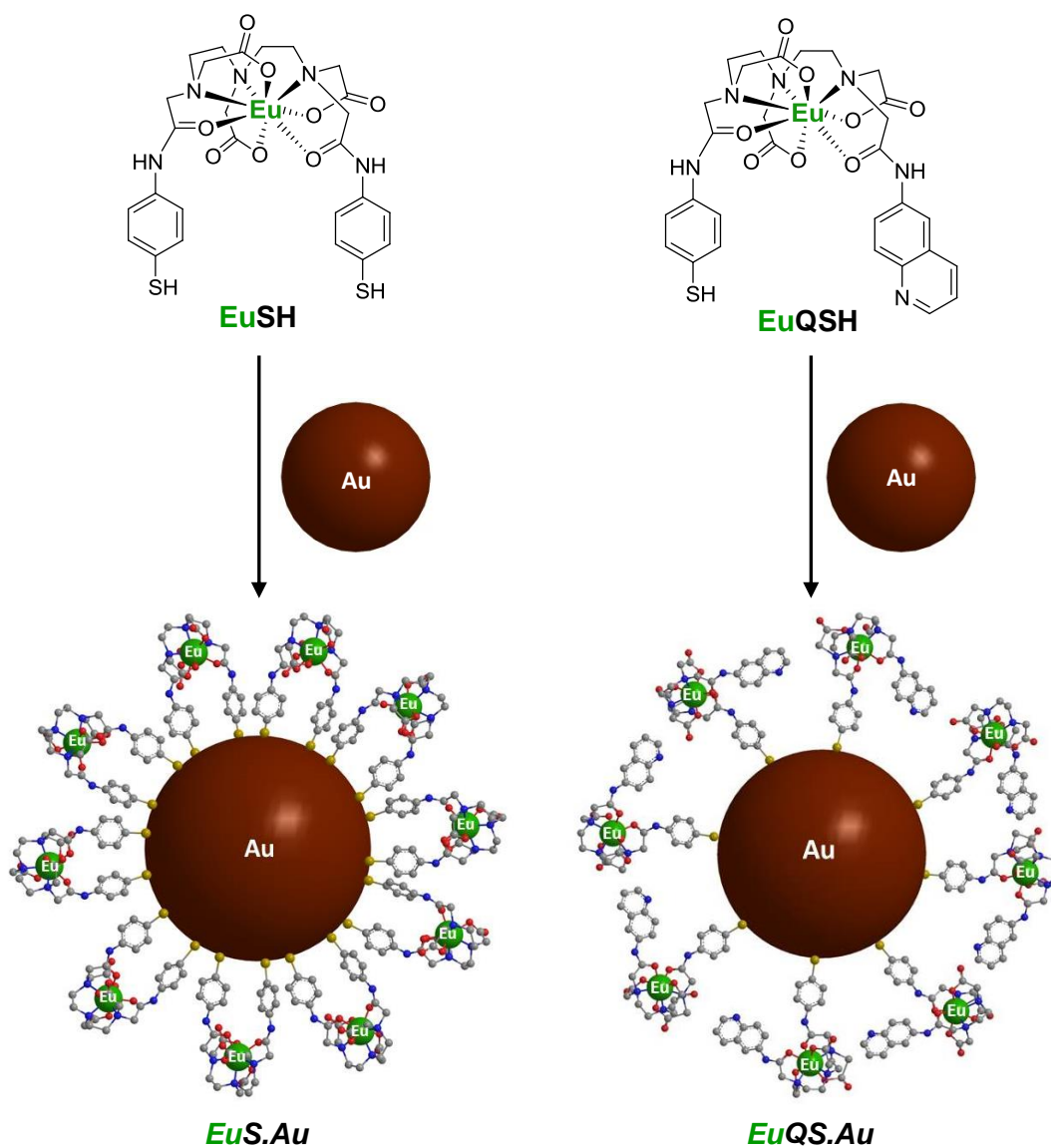
Figure 4.4: Structure of the lanthanide complexes EuSH and EuQSH and a schematic of europium coated nanoparticles.
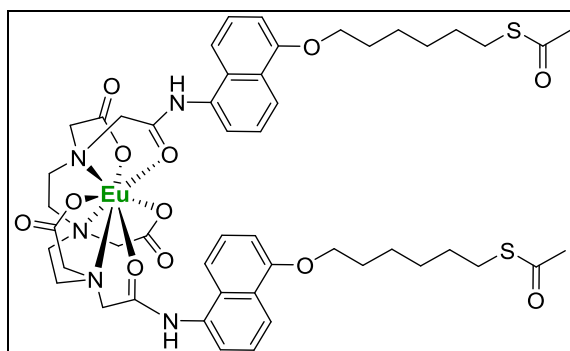
Figure 4.5: Structure of EuNapSAc complex

EuS.GdS.Au

EuQS.GdQS.Au

EuS.GdQS.Au

EuQS.GdS.Au
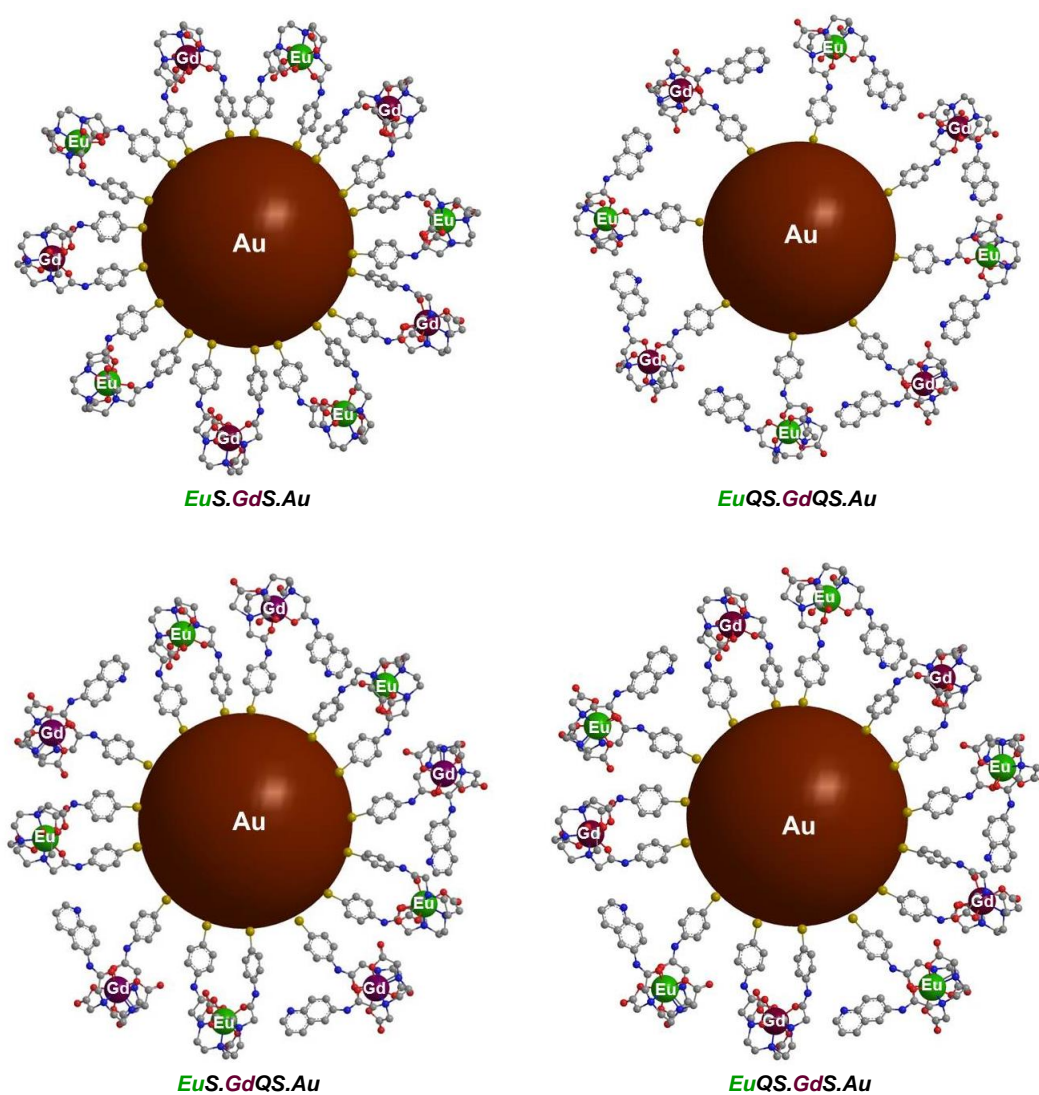
Figure 4.6: Dual coated gold nanoparticles developed and discussed in this chapter

2   Results and Discussion

2.1   Preparation and characterisation of *EuS.Au* and *EuQS.Au*

EuS.Au have been prepared following the published procedure.[15] The nanoparticles were purified by size exclusion chromatography, and the UV-Vis spectra of the sample before and after purification shows the same profile but with small dilution observed due to the chromatography technique (figure 4.7). The nanoparticles have been examined by UV-Vis spectroscopy and luminescence studies. The luminescence lifetime of the complex on gold nanoparticles however was found to be longer than reported, with a lifetime on nanoparticles found to be 0.5 ms. This lifetime is longer than the reported 0.8 µs lifetime and similar to the lifetime of the complex in water. Analysis of *EuS.Au* with inductively coupled plasma optical emission spectroscopy (ICP-OES) shows the number of complexes per particle to be approximately 3600 ± 300.
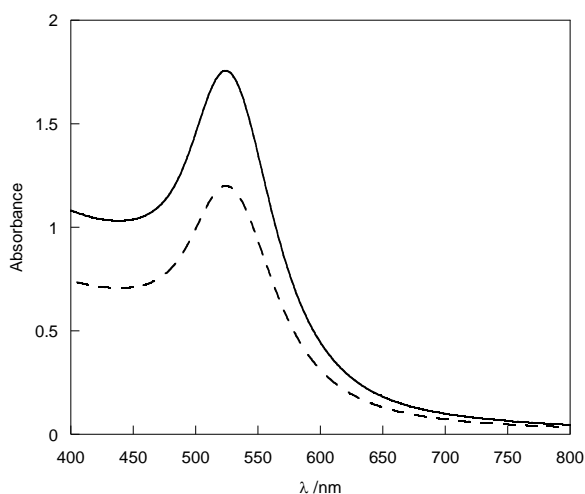
Figure 4.7: UV-Vis spectra of *EuS.Au* before (——) and after (− − −) size exclusion chromatography.

Citrate.Au were coated with EuQSH. The synthesis and photophysical characterisation of EuQSH complex in methanol is described in chapter 3. Titration of a methanolic solution of EuQSH into ***Citrate.Au*** gives rise to a 6 nm shift in the surface plasmon resonance of the gold nanoparticles (figure 4.8).
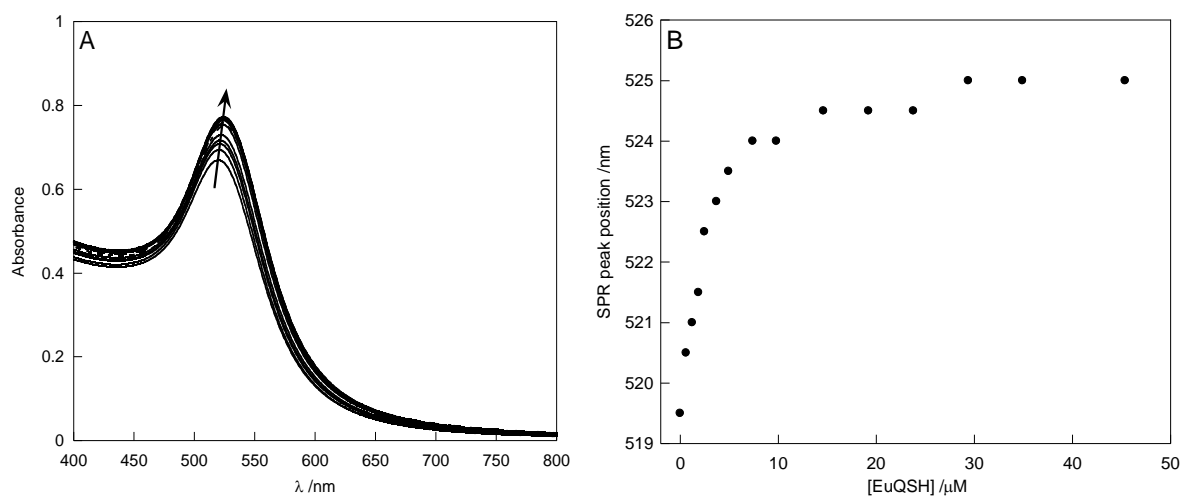
Figure 4.8: UV-Vis titration of EuQSH into ***Citrate.Au*** and plot of shift in SPR peak position (**B**). [Citrate.Au] = 2.3 nM. Stock solution of [EuQSH] = 1 mM in methanol.

The luminescence lifetime of EuQSH complex in solution shows similar trends to that of the EuSH complex, with the lifetime in methanol measured as 0.8 ms decreasing to 0.53 ms in water. This is as expected as water has a higher effect on quenching lanthanide luminescence. The luminescence lifetime of the complex recorded on gold nanoparticles, ***EuQS.Au*** was also found to be 0.53 ms which is the same as the complex in water. Upon examination of the UV-Vis spectra before and after purification by size exclusion chromatography, the SPR peak position remains at the same wavelength (figure 4.9). This suggests that the coating on the surface of the

gold nanoparticles remains unchanged after the purification of **EuQS.Au** and the EuQSH complex is still bound to the gold.
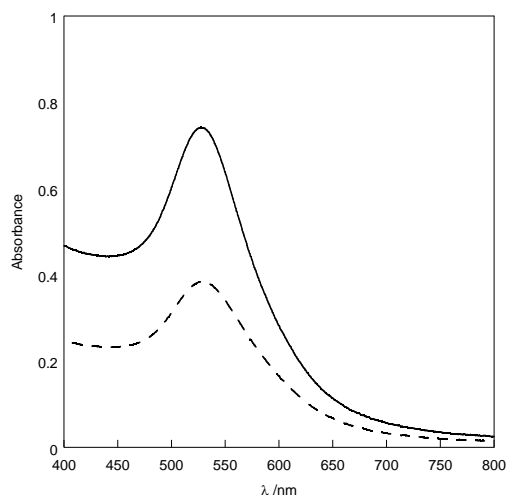
Figure 4.9: UV-Vis spectra of **EuQS.Au** before (⎯⎯) and after (− − −) size exclusion chromatography

The EuNapSAc complex used in chapter 3 has a reported luminescence lifetime of 0.5 ms on gold nanoparticles.[16] The lifetime of this free complex in methanol is 0.82 ms,[17] whilst in water it was found to decrease to 0.59 ms.

The luminescence lifetime of the DTPA bis-amide complexes on bound to gold nanoparticles are very similar regardless of the chromophore. This is probably because the chelation of the lanthanide is the same throughout the complexes, and the complexes all have similar lifetimes in other solutions such as water and methanol. This agrees with other comparisons of DTPA bis-amide with different chromophores which have similar lifetimes.[18]

The binding affinity of the EuSH and EuQSH complexes to gold nanoparticles was investigated by isothermal titration calorimetry (ITC). ITC is a sensitive technique for

measuring the thermodynamics parameters of two molecules during complexation. It is typically used for the monitoring protein-protein interactions,[19] but more recently it has been utilised for monitoring the binding of peptides and small molecules to gold nanoparticles.[20-23] The heat released upon titration of the complexes into a solution of *Citrate.Au* is measured to provide information on the binding interaction. The stock solutions of EuSH and EuQSH were dissolved in water containing 10 % methanol. *Citrate.Au* were centrifuged twice and re-suspended in a 10 % methanol solution to ensure the two solutions were identical so that the change in heat measured was only caused by the binding event of the complex on gold nanoparticles.
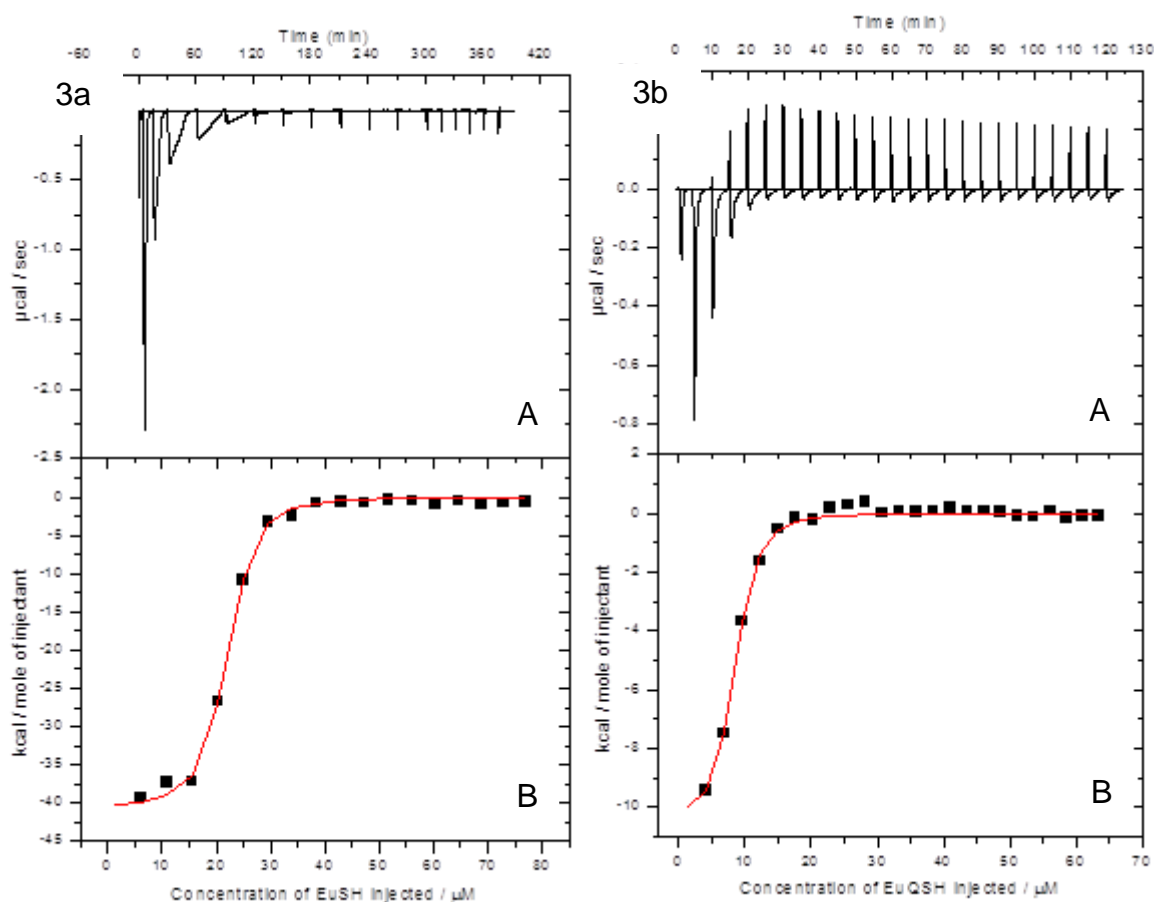
Figure 4.10: Isothermal titration calorimetry analysis of the binding of EuSH with **Citrate.Au** (left) and EuQSH with **Citrate.Au** (right) in water with 10 % methanol. Eu complex was added in µl quantities of a 1 mM stock solution to **Citrate.Au** (concentration = 4.5 nM). *Graph A* in both figures is the raw ITC data for complex - nanoparticle interaction. *Graph B* is the binding curve from the raw data. The squares represent the integrated area of heat change upon binding and the line is the curve fit to the binding isotherm.

	K (M^{-1})	N	ΔH (cal mol^{-1})	ΔS (cal mol^{-1} K^{-1})
EuS.Au	$3.09 \times 10^{6} \pm 4.10 \times 10^{5}$	4610 ± 41.1	$-4.08 \times 10^{4} \pm 616.9$	-107
EuQS.Au	$2.63 \times 10^{6} \pm 4.61 \times 10^{5}$	1690 ± 34.9	$-1.055 \times 10^{4} \pm 330.0$	-6.01

Table 4.1: Isothermal calorimetry data for the binding studies of **EuS.Au** and **EuQS.Au** at 25°C

The ITC data show similar binding constants for the two complexes with gold nanoparticles. This could potentially be anticipated as both complexes are of similar structure with only a small difference in one of the arms of the DTPA being a quinoline in the EuQSH rather than a thiophenol. The EuSH complex with two sulphurs has the slightly higher binding constant, possibly due to the presence of the extra sulphur. The stoichiometry of complexes to gold nanoparticles (given by the value N) obtained from this ITC data are quite different for the two complexes. EuSH complex shows a much larger value of 4610 ± 41.1, whilst EuQSH has a stoichiometry of 1690 ± 34.9. As this technique measures the gold-sulphur interaction between the complex and nanoparticle, it could be anticipated that the EuSH complex would have a higher number of interactions per particle as it contains two sulphurs. Comparisons of the two values of ΔH, which is the enthalpy change upon binding of the complexes to nanoparticles, show that there is a greater enthalpy change upon binding of the EuSH to gold nanoparticles compared with EuQSH. This is again most likely to be due to a greater number of interactions causing a large change in enthalpy.

2.2   Preparation and characterisation of *EuS.GdQS.Au*
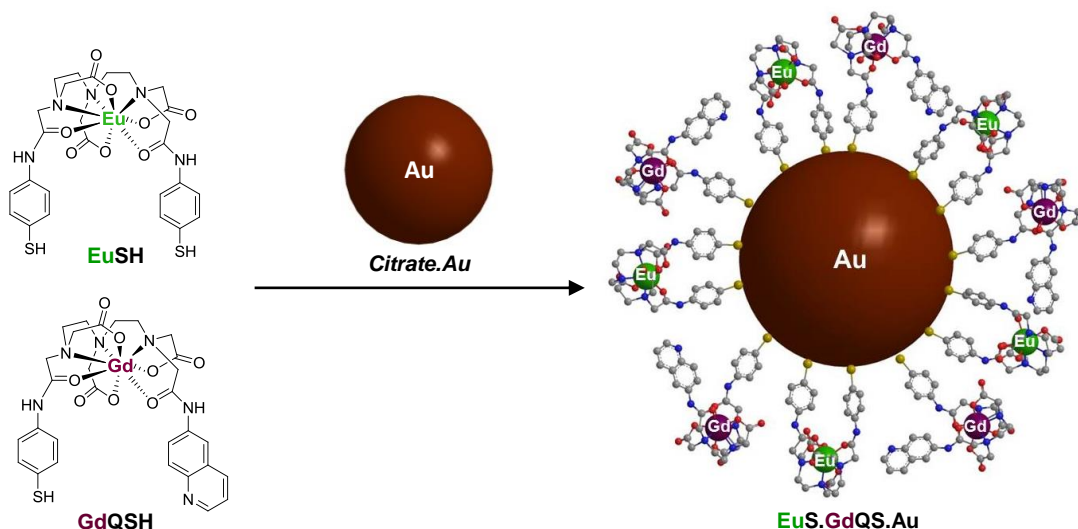
Scheme 4.1: Schematic representation of the preparation of *EuS.GdQS.Au*

The effect of a combination of two different lanthanide complexes on gold nanoparticles was studied by the examination of their photophysical properties. The europium complex EuSH and the gadolinium complex GdQSH were added to *Citrate.Au*, with the coating of the *Citrate.Au* monitored by UV-Vis spectroscopy. The nanoparticles were coated by initially titrating in µl aliquots of a 1 mM stock solution of EuSH in methanol. Monitoring the SPR band of the gold nanoparticles, a 6 nm red-shift is observed upon fully coating the *Citrate.Au* with the complexes. For partially coating *Citrate.Au*, a 1 mM stock solution of EuSH in methanol was added at a concentration which resulted in a 3 nm red-shift of the SPR band of the gold nanoparticles. A 1 mM stock solution of GdQSH in methanol was then titrated in µl aliquots until no further red-shift in the SPR band was observed. Figure 4.11 shows the UV-Vis spectra of the *EuS.GdQS.Au*. The initial addition of 2.5 µM EuSH to *Citrate.Au* gives a red-shift in the SPR of 3 nm, with a further 0.5 nm red-shift upon addition of 15 µM GdQSH complex (figure 4.11A). However coating *Citrate.Au* with

117

GdQSH complex first at a concentration of 6.6 µM gives the initial red-shift of 3 nm, and a further red-shift of 2 nm is observed upon the addition of 9.8 µM EuSH complex (figure 4.11B).
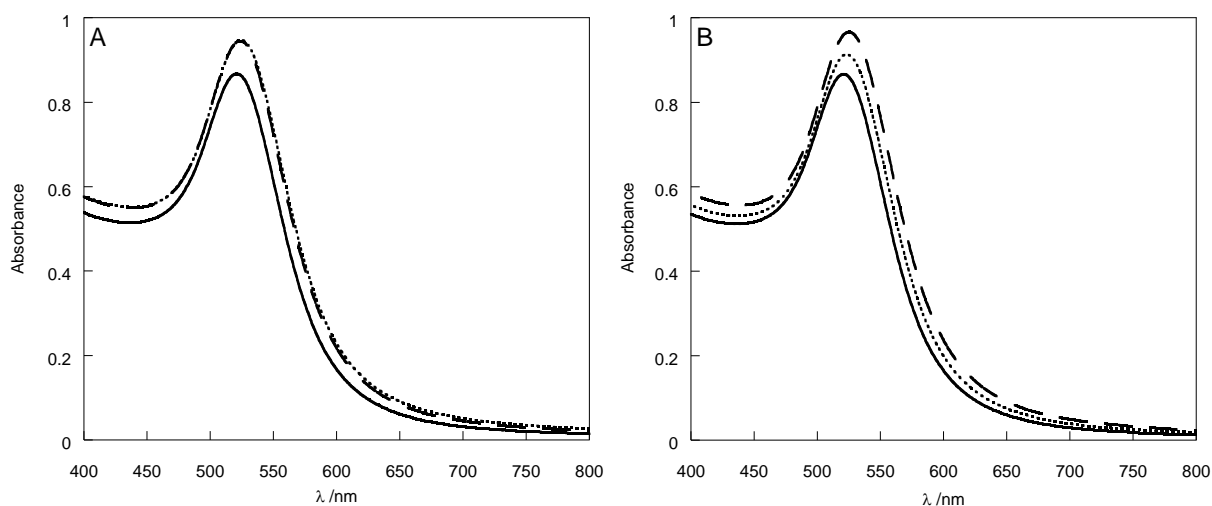
Figure 4.11: UV-Vis spectroscopy of **EuS.GdQS.Au**. **A:** **Citrate.Au** (——), with EuSH (- - -) and GdQSH (•••••) [EuSH] = 2.5 µM, [GdQSH] = 15 µM, [AuNPs] = 2.25 nM; **B:** **Citrate.Au** (——), with GdQSH (•••••) and EuSH (- - -) [GdQSH] = 6.6 µM, [EuSH] = 9.8 µM, [AuNPs] = 2.25 nM

Luminescence spectroscopy of the solution of **EuS.GdQS.Au** shows characteristic europium emission upon excitation of the phenol chromophore at 270 nm. The europium emission profile remains after purification of the nanoparticles by size exclusion chromatography. Interestingly, upon excitation of the quinoline chromophore of the GdQSH complex at 310 nm, strong europium emission is still observed (figure 4.13). This suggests that the quinoline sensitiser of the GdQSH complex is in close proximity of the europium ion to allow excitation to occur. This is confirmed by the excitation spectrum of the **EuS.GdQS.Au** when monitoring the europium emission at 614 nm, as it mirrors the profile of the GdQSH complex rather than the profile of the EuSH complex (figure 4.12). The excitation profile has a lower

intensity in the region of 270-290 nm compared with the absorption of the QSH ligand. This suggests that there is little contribution of the phenol group which absorbs in this region, to the excitation of the lanthanide.
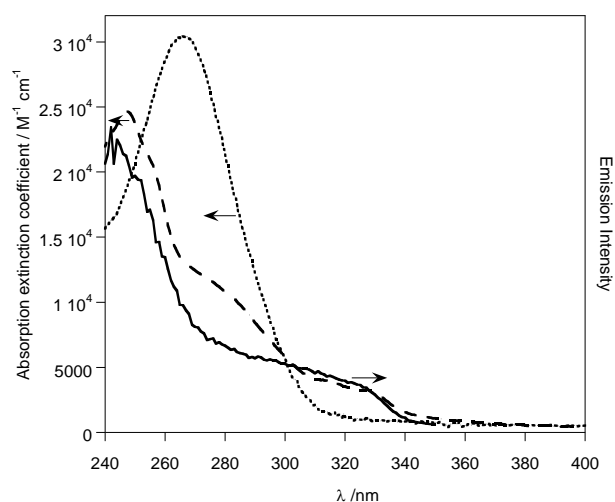
Figure 4.12: Excitation spectrum of **EuS.GdQS.Au** (——) and UV-Vis spectrum of GdQSH (- - - -) and EuSH (•••••••). λ_{em} = 614 nm.

Comparisons of isoabsorptive solutions of **EuS.GdQS.Au** and **EuS.Au** show that the europium emission intensity is greatly increased in the presence of the GdQSH complex at both excitation wavelengths 270 nm and 310 nm. This suggests that the GdQSH is responsible for this europium emission intensity increase. Some of the luminescence spectra obtained, particularly on weakly emitting samples, show a peak attributed to second-order scattering. These have been indicated with an asterix within the figures, and are described in the figure captions.
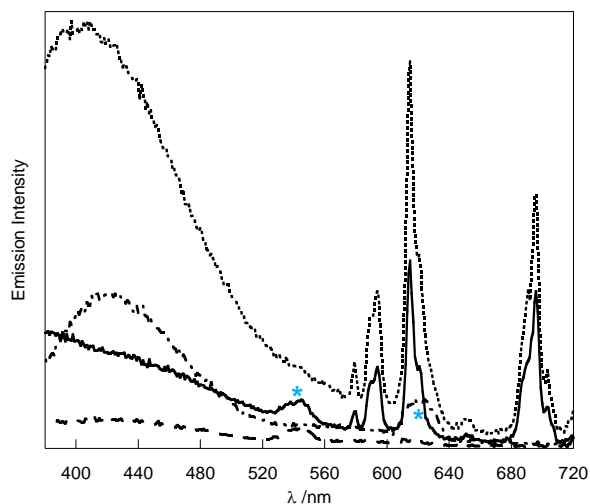
Figure 4.13: Emission spectra of **EuS.GdQS.Au** λ_{exc} = 270 nm (——), **EuS.GdQS.Au** λ_{exc} = 310 nm (••••••), **EuS.Au** λ_{exc} = 270 nm (− − −), **EuS.Au** λ_{exc} = 310 nm (−·−·−) [EuSH] = 2.5 μM; [GdQSH] = 15 μM; [AuNPs] = 2.25 nM. Emission spectra corrected for PMT response. Some small second-order scattering peaks are observed at 540 nm and 620 nm, more visible in the **EuS.Au** samples.

The luminescence lifetime of the **EuS.GdQS.Au** was found to be 0.54 ms. This is similar to the lifetime of **EuQS.Au**. To examine the role that the gold nanoparticles play in this energy transfer between the two complexes, a control solution of EuSH and GdQSH in water has been characterised along with **EuS.GdQS.Au** and **EuS.Au**. The comparison of **EuS.GdQS.Au**, EuSH GdQSH in water and **EuS.Au** is shown in figure 4.14. By comparing a solution of **EuS.GdQS.Au** with a solution of EuSH and GdQSH in water at the same concentrations of complexes used in **EuS.GdQS.Au** preparation, it can be observed that the emission intensity of **EuS.GdQS.Au** is over double that of the free complexes in water upon excitation of the quinoline moiety at λ_{exc} = 310 nm (figure 4.14B). The two complexes mixed in solution show a small increase in europium emission intensity suggesting that some energy transfer may

be occurring in solution. This solution of EuSH and GdQSH in water exhibits weak europium emission upon excitation at λ_{exc} = 310 nm, possibly due to the formation of disulphide bonds between the two complexes. The emission spectrum for **EuS.Au** shows no europium emission at the concentrations used to prepare **EuS.GdQS.Au** at either excitation wavelengths λ_{exc} = 270 nm or 310 nm.
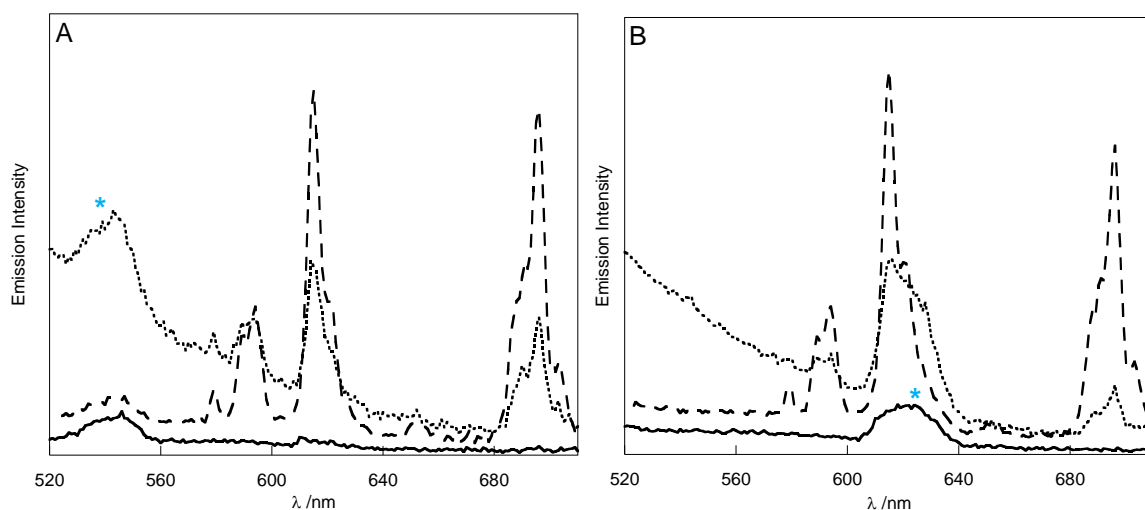
Figure 4.14: Emission spectra of **EuS.GdQS.Au** (- - - -), EuSH GdQSH in water (••••••) and **EuS.Au** (——). **A:** λ_{exc} = 270 nm. **B:** λ_{exc} = 310 nm. [EuSH] = 2.5 µM; [GdQSH] = 1.5 µM; [AuNPs] = 2.25 nM. Emission spectra corrected for PMT response. * indicates second-order scattering peaks (A at 540 nm and B at 620 nm (the broad peaks at 620 nm in the EuSH GdQSH in water and **EuS.Au**.spectra)

Preliminary experiments found that the europium emission intensity increase of **EuS.GdQS.Au** occurs over a period of time. To investigate this, **EuS.GdQS.Au** was also monitored by UV-Vis spectroscopy over time to monitor any changes to the SPR band as the complexes attach to the nanoparticle surface. An initial scan of **Citrate.Au** was taken by UV-Vis spectroscopy, then a methanolic solution of EuSH and GdQSH was added in one addition and further scans run repeatedly over several

hours. Figure 4.15 shows the UV-Vis spectra of a solution of **EuS.GdQS.Au** monitored over time, with a plot of the shift in λ_{max} of the SPR band taken from the derivative of the curve. After the initial red-shift upon addition of the complexes to **Citrate.Au**, the SPR band exhibits a further 1 nm red-shift over time. This suggests that there is a large interaction initially on the nanoparticle surface, and then further rearrangement may occur over a longer period of time.
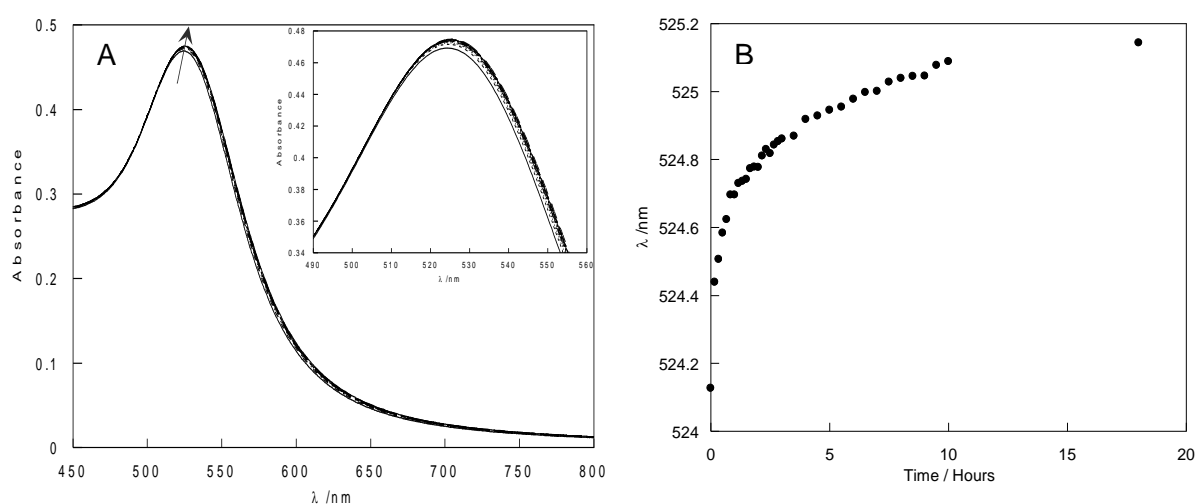
Figure 4.15: UV-Vis spectra and plot of SPR band λ_{max} shift of **EuS.GdQS.Au** taken over 18 hours. Inset: SPR band between 490-560 nm. [EuSH] = 6.6 µM, [GdQSH] = 6.6 µM, [AuNPs] = 1.3 nM.

The europium emission intensity of the **EuS.GdQS.Au** was also monitored over time. This was carried out by monitoring the strongest peak at 614 nm which is attributed to the $^5D_0 \rightarrow {}^7F_2$ transition of europium. Figure 4.16 shows the increase in europium emission intensity over 24 hours. The initial mixing of the two complexes with and without gold nanoparticles show the same emission spectra, with no europium emission observed. Integration of the peak area of the emission spectra of **EuS.GdQS.Au** and EuSH GdQSH in water shows the **EuS.GdQS.Au** emission

intensity is nearly four times greater than the two complexes mixed in water after 24 hours. Hydrazine monohydrate was added to both solutions to reduce any disulphide bonds formed between the two different complexes, which could allow for the quinoline sensitiser of the GdQSH complex to become in close proximity to the europium ion of the EuSH complex. Therefore the gold nanoparticle appears to provide a good scaffold for the assembly of these two complexes in close enough proximity to allow energy transfer to occur.
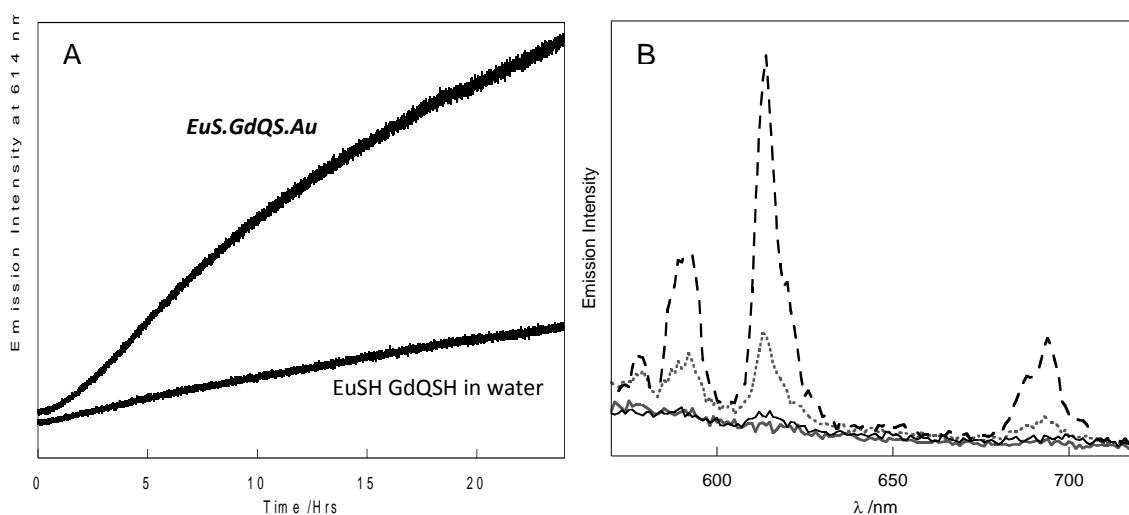
Figure 4.16: Timebased emission studies of *EuS.GdQS.Au* and EuSH GdQSH in water. λ_{exc} = 320 nm; λ_{em} = 614 nm. **A:** Europium emission intensity monitored at 614 nm. **B**: steady state emission spectra of *EuS.GdQS.Au* at 0 hrs (——) and 24 hrs (– – –) and EuSH GdQSH in water at 0 hrs (——) and 24 hrs (••••••). [EuSH] = 6.6 µM, [GdQSH] = 6.6 µM, [AuNPs] = 1.3 nM.

In order to confirm that this phenomenon occurs with the two complexes on the same nanoparticle, fully coated *EuS.Au* and *GdQS.Au* were prepared and combined in order to investigate their photophysical properties. The nanoparticle samples were passed through a size exclusion chromatography column to remove any excess complex in solution. Upon excitation of a mixture of *EuS.Au* and *GdQS.Au* at

$\lambda_{exc} = 320$ nm, the nanoparticles exhibit no europium emission. This suggests that the two complexes need to be on the same nanoparticle in order for the europium ion to be sensitised by the quinoline. It is likely that the increase in europium emission observed is not caused by transmetallation of the lanthanide complexes, as this is likely to occur upon mixing of **EuS.Au** and **GdQS.Au**.

Further studies into the energy transfer on gold nanoparticles were carried out by adding just the QSH ligand onto gold nanoparticles with EuSH, in order to ascertain whether energy transfer occurs without the presence of the gadolinium in the complex. **Citrate.Au** were coated in EuSH complex at a concentration of 2.9 µM as previously described giving a red-shift in the SPR band of the gold nanoparticles of 3 nm. Then a solution of the free QSH ligand in methanol was titrated into the nanoparticles to give a final concentration of QSH of 9.9 µM, resulting in a further 1 nm red-shift. The emission spectra of the **EuS.QS.Au** when exciting the phenol group of the EuSH at $\lambda_{exc} = 270$ nm and exciting the quinoline at $\lambda_{exc} = 310$ nm both show the characteristic emission profile for europium (figure 4.17A). The excitation spectrum of a solution of **EuS.QS.Au** monitoring the europium band at 614 nm also agrees with the UV-Vis profile for the QSH ligand, suggesting that the europium emission is being sensitised by the quinoline chromophore of the QSH ligand (figure 4.17B).
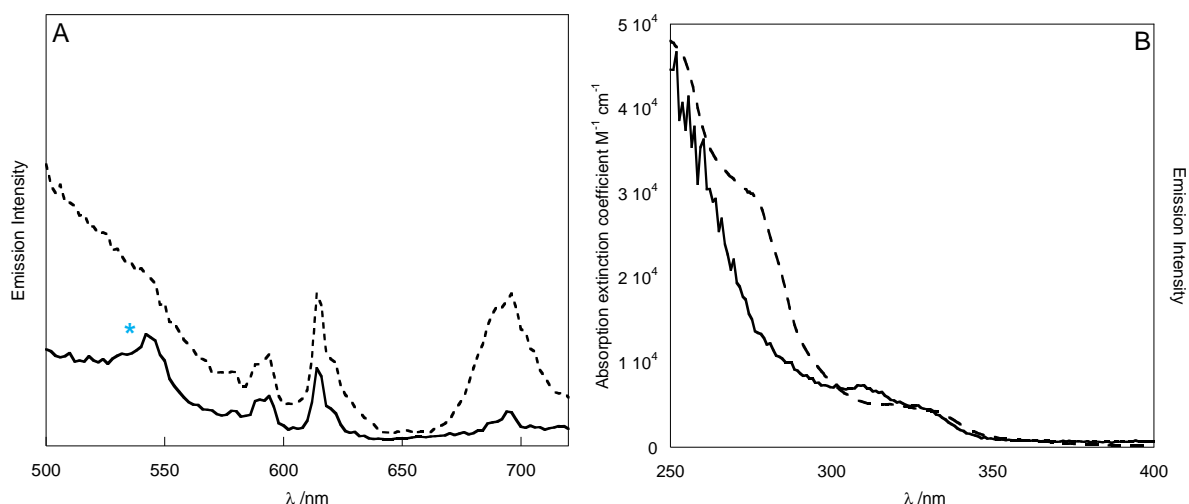
Figure 4.17: Photophysical studies of **EuS.QS.Au** after size exclusion chromatography. [EuSH] = 2.9 µM, [QSH ligand] = 9.9 µM, [AuNPs] = 2.25 nM. **A:** Emission spectra of nanoparticles λ_{exc} = 270 nm (——) and λ_{exc} = 310 nm (−−−). **B:** Excitation spectrum of **EuS.QS.Au** (——) λ_{em} = 614 nm and UV-vis spectrum of QSH ligand (−−−). * indicates second-order scattering peak at 540 nm

For comparison, **EuS.GdS.Au**, **EuQS.GdQS.Au** and **EuQS.GdS.Au** were prepared following a similar procedure to **EuS.GdQS.Au**. The nanoparticles were prepared and their photophysical properties were investigated to examine the effects of the co-coating **Citrate.Au** with these combinations of lanthanide complexes. These experiments are discussed in sections 2.3, 2.4 and 2,5.

2.3 Preparation and characterisation of *EuS.GdS.Au*
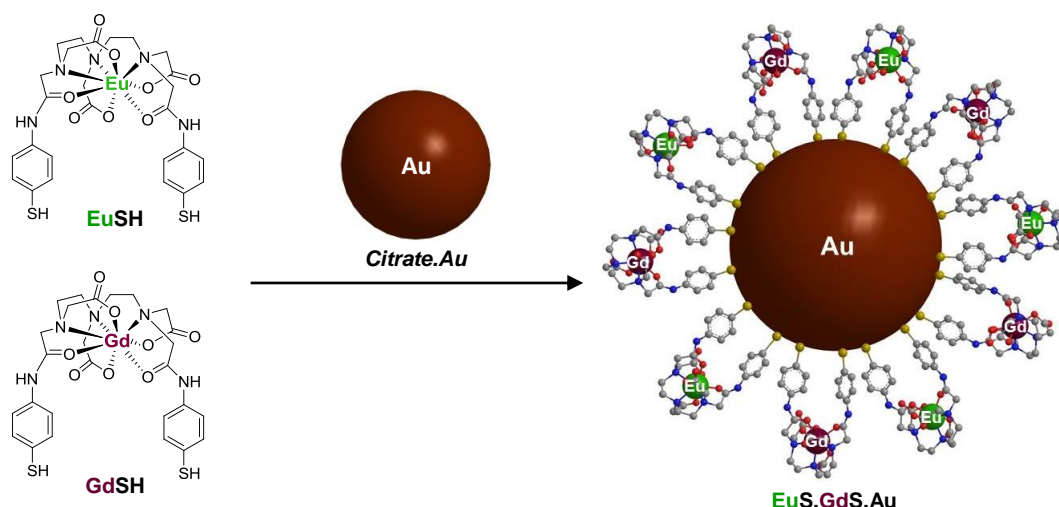
Scheme 4.2: Schematic representation of the preparation of *EuS.GdS.Au*

To prepare mixed complex coated gold nanoparticles, *Citrate.Au* were coated with the europium and gadolinium complex EuSH and GdSH. The gold nanoparticles are coated by adding µl additions of a methanol stock solution of the complexes and purified by size exclusion chromatography. The final concentrations titrated into *Citrate.Au* were 9.9 µM EuSH and 6.6 µM GdSH. The additions of the two complexes to *Citrate.Au* were monitored by UV-Vis spectroscopy, with the position of the maximum absorption wavelength of the SPR band red-shifting upon addition of the methanolic lanthanide complex solution. The initial shift upon addition of the EuSH complex is 4 nm, with a small red-shift of approximately 0.5 nm upon addition of the GdSH complex (figure 4.18). The final SPR shift observed is a 4.5 nm red-shift, which is less than that of fully coated *EuS.Au* which has a red-shift in the SPR band of 6-7 nm.[15]
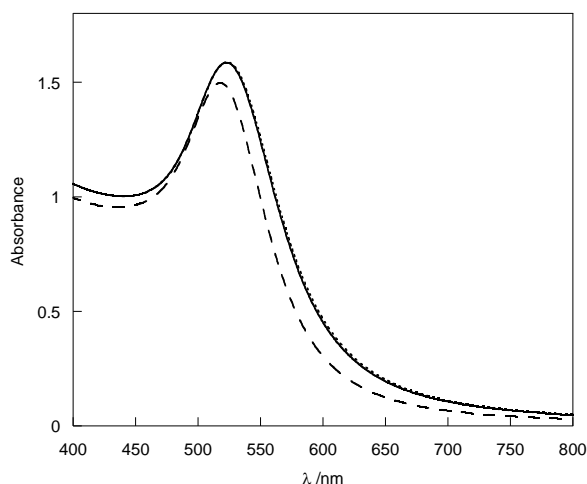
Figure 4.18: UV-Vis spectra of the preparation of **EuS.GdS.Au. Citrate.Au** (‒ ‒ ‒) with the addition of EuSH (——) and GdSH (••••••) [EuSH] = 9.9 µM, [GdSH] = 6.6 µM, [AuNPs] = 4.5 nM

Figure 4.19 shows **EuS.GdS.Au** before purification by size exclusion chromatography and **EuS.Au** at the same concentration of EuSH as used in the preparation of **EuS.GdS.Au**. The emission of the **EuS.GdS.Au** is of similar intensity to **EuS.Au**, even though the signal is weak in comparison to other samples prepared. This suggests that the mixing of EuSH and GdSH has little effect on the emissive properties of the EuSH complex on gold nanoparticles, as the nanoparticles exhibit the characteristic photophysical properties of europium. The luminescence lifetime of the europium complex on the dual coated gold nanoparticles is 0.56 ms, which is similar to **EuS.Au**.
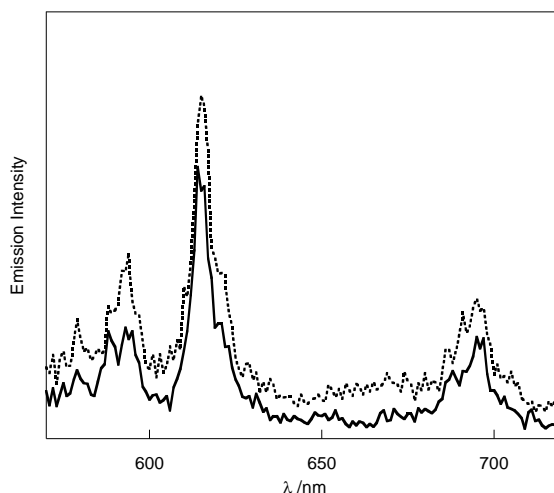
Figure 4.19: Emission spectra of **EuS.GdS.Au** (——) before purification by size exclusion chromatography and **EuS.Au** (······). λ_{exc} = 270 nm. [EuSH] = 9.9 µM, [GdSH] = 6.6 µM. [AuNPs] = 4.5 nM,

2.4 Preparation and characterisation of *EuQS.GdQS.Au*
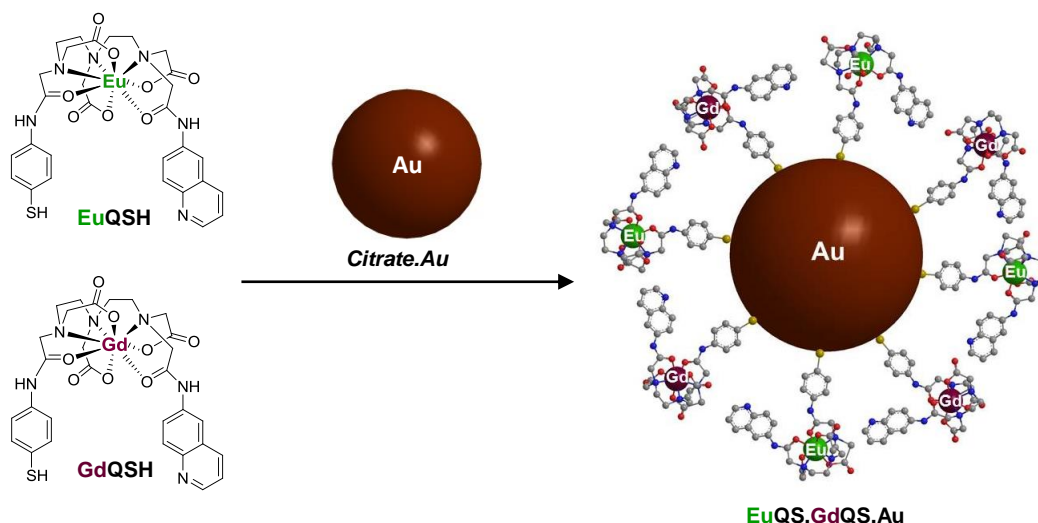
Scheme 4.3: Schematic representation of the preparation of **EuQS.GdQS.Au**

Citrate.Au were coated in the lanthanide complexes EuQSH and GdQSH. The coating of **Citrate.Au** with the lanthanide complexes was again monitored by the shift

in the SPR band of the gold nanoparticles. A 1 mM stock solution of EuQSH in methanol was titrated into **Citrate.Au** to give a red-shift of 3 nm, and a further red-shift of 1.5 nm was observed upon titration of a 1 mM stock solution of GdQSH complex in methanol (figure 4.20). The final concentrations of complexes added to prepare **EuQS.GdQS.Au** were 5.8 µM EuQSH and 5.8 µM GdQSH. In comparison with fully coated **EuQS.Au** which has an observed red-shift of 6 nm, the effect of coating gold nanoparticles with two different LnQSH complexes is a resulting smaller red-shift in the SPR band of 4.5 nm.
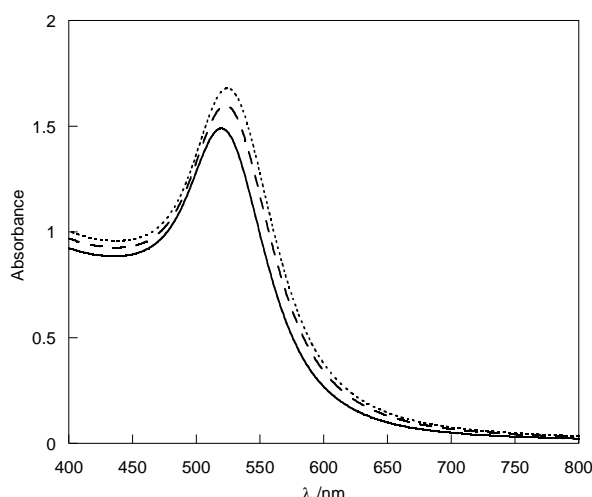
Figure 4.20: UV-Vis spectra of preparation of **EuQS.GdQS.Au. Citrate.Au** (——) with the addition of EuQSH (– – –) and GdQSH (••••••) Final concentrations: [EuQSH] = 5.8 µM, [GdQSH] = 5.8 µM, [AuNPs] = 4.5 nM

Studies of the photophysical properties of **EuQS.GdQS.Au** show the characteristic peak of europium upon excitation of the quinoline. The luminescence lifetime of **EuQS.GdQS.Au** was recorded as 0.53 ms. Figure 4.22A shows the emission spectra of **EuQS.GdQS.Au** as prepared and after purification by size exclusion chromatography. For comparison the same concentration of EuQSH complex used to

prepare **EuQS.GdQS.Au** was added to **Citrate.Au**. The excitation spectra matches the profile of the UV-Vis spectrum of the QSH ligand, which is as to be expected as the quinoline should be responsible for the sensitisation of the europium ions. The europium emission of the **EuQS.GdQS.Au** after purification decreases which is due to the removal of excess complexes and the dilution of the sample due to the purification method. Comparison of the UV-Vis spectra before and after purification by size exclusion chromatography also shows no change in the SPR peak position at 524.5 nm, suggesting that there has been no change to the surface of the nanoparticles as a result of the purification method.
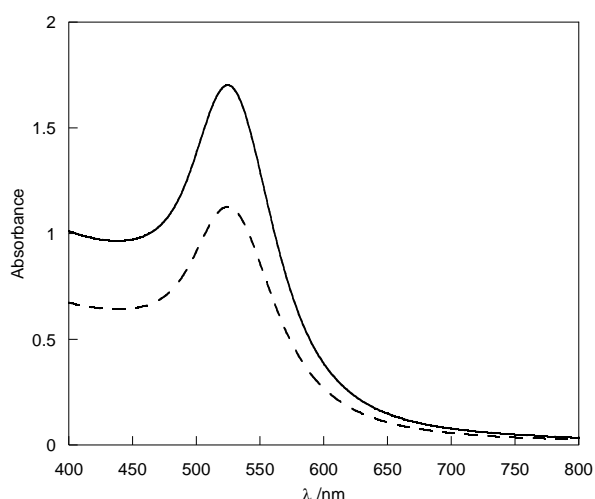
Figure 4.21: UV-Vis spectra of **EuQS.GdQS.Au** before (——) and after (− − −) size exclusion chromatography.

The luminescence studies of **EuQS.GdQS.Au** show a decrease in europium emission intensity upon purification of the nanoparticles (figure 4.22A). The percentage decrease in europium emission intensity calculated by integrating the two spectra shown in figure 4.22A is 44 %. This is quite close to the percentage decrease of 51 % observed by monitoring the dilution of **EuQS.GdQS.Au** by UV-Vis

spectroscopy, which suggests that the emission intensity decrease can be partially attributed to the dilution of the nanoparticles by size exclusion chromatography, as well as the removal of excess unbound complex. A comparison of the europium emission intensity of **EuQS.GdQS.Au** before purification with **EuQS.Au** at the same concentration shows higher europium emission intensity for the sample containing the GdQSH complex. Interestingly, the europium emission from the **EuQS.GdQS.Au** before purification was 2.5 times greater than that of **EuQS.Au** containing the same concentration of EuQSH. The two solutions were isoabsorptive at the excitation wavelength of 310 nm, therefore this suggests that whilst there is the same concentration of EuQSH in both nanoparticle samples, the GdQSH complex appears to be causing an increase in the emission from the europium on the gold nanoparticles.
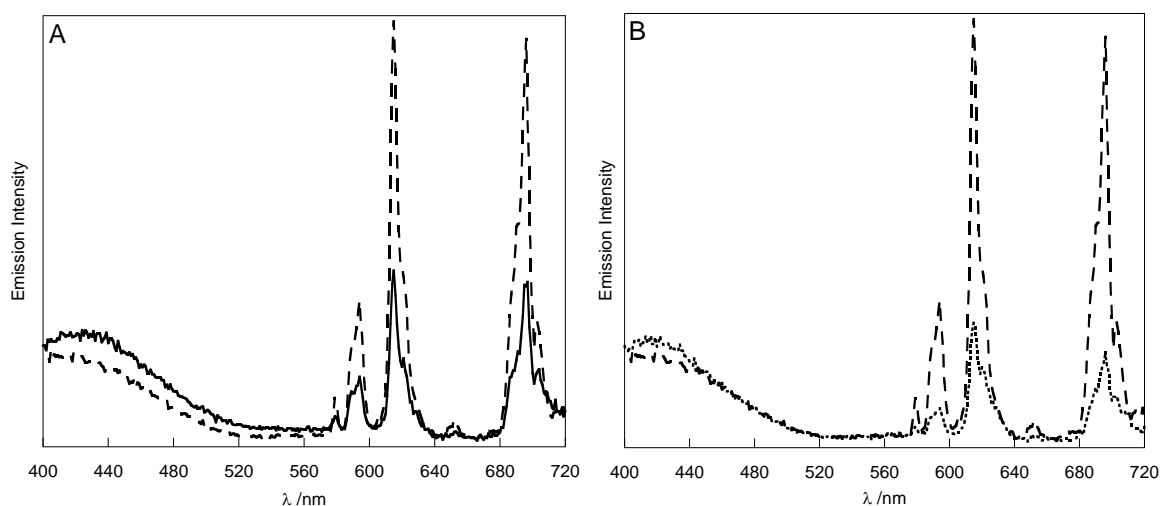
Figure 4.22: **A**: Emission spectra of **EuQS.GdQS.Au** before (– – –) and after purification by size exclusion chromatography (——). **B**: **EuQS.GdQS.Au** before purification and **EuQS.Au** prepared with the same concentration of EuQSH used in **EuQS.GdQS.Au** (••••••).λ_{exc} = 310 nm. Spectra corrected for PMT response. [EuQSH] = 5.8 μM, [GdQSH] = 5.8 μM, [AuNPs] = 4.5 nM

2.5 Preparation and characterisation of *EuQS.GdS.Au*
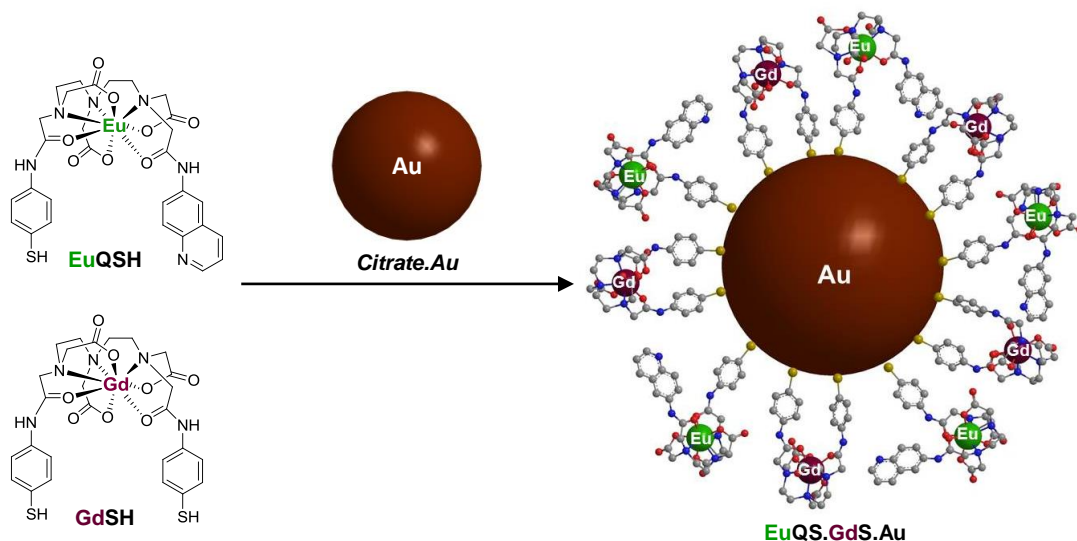
Scheme 4.4: Schematic representation of the preparation of *EuQS.GdS.Au*

EuQS.GdS.Au have been prepare by coating *Citrate.Au* with EuQSH and GdSH complexes. The coating of *Citrate.Au* was monitored by UV-Vis spectroscopy. The coating procedure was similar to that of *EuS.GdQS.Au*. Briefly, a solution of EuQSH in methanol was titrated into *Citrate.Au* to give half the total shift observed upon fully coating the gold nanoparticles. Then GdSH is added to give a further shift in the SPR band. This procedure was repeated in reverse, by adding GdSH first then EuQSH. The titration of µl aliquots of a 1 mM stock solution of EuQSH to *Citrate.Au* gives a 3 nm red-shift and a final concentration of EuQSH of 6.5 µM. To this solution, a stock solution of GdSH was added at a final concentration of 9.8 µM causing a further 0.5 nm red-shift in the SPR band (figure 4.23A). Alternatively addition of GdSH to the gold nanoparticles first gives a 2.5 nm red-shift as expected, with a further 1.5 nm red-shift exhibited upon addition of EuQSH (figure 4.23B).
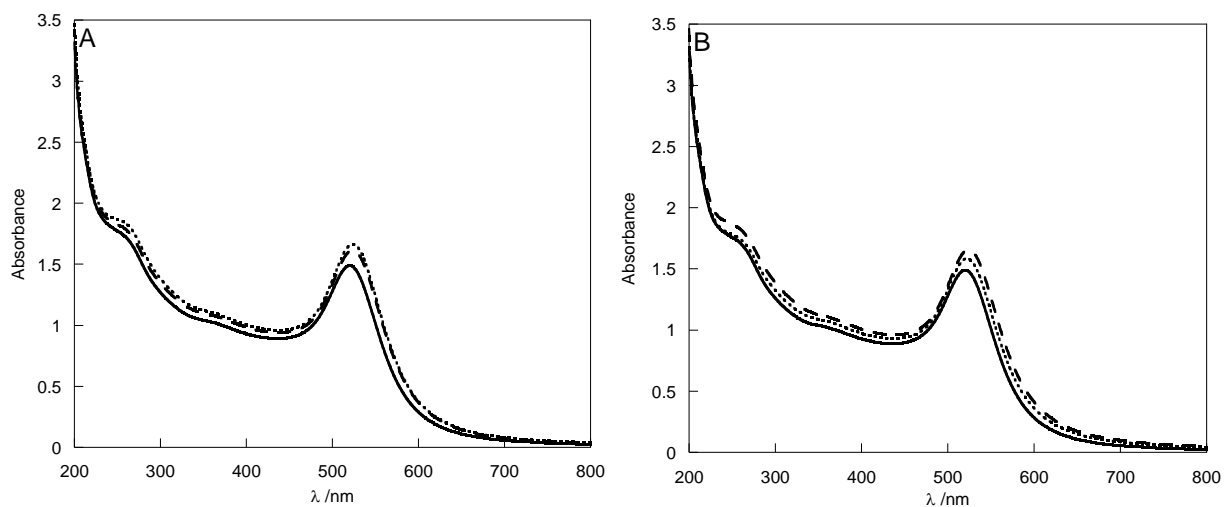
Figure 4.23: UV-Vis spectra of *EuQS.GdS.Au*. **A:** *EuQS.GdS.Au*: *Citrate.Au* (——) with the addition of EuQSH (− − −) and GdSH (••••••). **B:** *GdS.EuQS.Au*: *Citrate.Au* (——) with the addition of GdSH (••••••) and EuQSH (− − −). [EuQSH] = 6.5 µM; [GdSH] = 9.8 µM; [AuNPs] = 4.5 nM.

Despite the difference in shifts in the SPR band of the gold nanoparticles depending on the order in which the complexes are titrated in, the emission profile of the nanoparticles are the same after purification by size exclusion chromatography. This is as expected as the two samples contain the same concentration of EuQSH and GdSH.
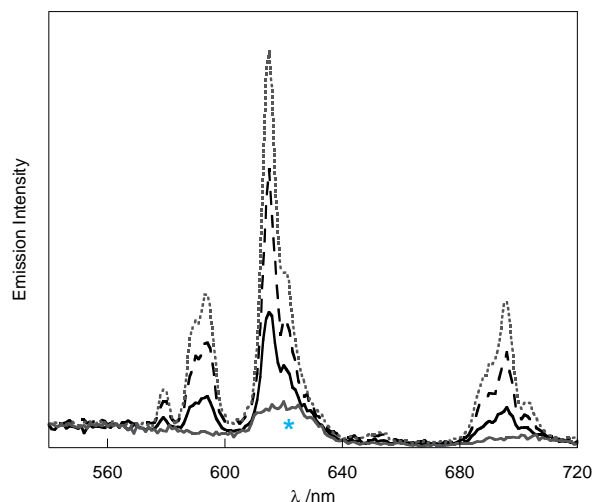
Figure 4.24: Comparison of **EuQS.Au** (——), **EuQS.GdS.Au** (– – –), **GdS.Au** (——) and **GdS.EuQS.Au** (••••••). [EuQSH] = 6.5 µM; [GdSH] = 9.8 µM; [AuNPs] = 4.5 nM. λ_{exc} = 310 nm. Spectra corrected for PMT response. The spectra for **GdS.Au** shows a small second order scattering peak at 620 nm, indicated by *.

Comparison of the luminescence spectra of the two samples before size exclusion chromatography shows an interesting trend (figure 4.24). There is a 35 % increase in europium emission intensity when the GdSH complex is titrated into the **Citrate.Au** first followed by the EuQSH complex rather than titrating in EuQSH first to the **Citrate.Au**. The **EuQS.GdS.Au** co-coated nanoparticles show a 67 % increase in europium emission than the **EuQS.Au** coated with EuQSH at the same concentration. This suggests that the presence of the GdSH improves the europium emission intensity of the EuQSH complex in **EuQS.GdS.Au**. Mixing of the two free complexes in water does not show any enhancement in luminescence intensity of europium, suggesting that the gold nanoparticles contribute to the greater europium emission observed in figure 4.24.

2.6   Conclusion

Gold nanoparticles have been successfully coated in europium complexes and a mixture of europium and gadolinium complexes. The photophysical properties of the two europium complexes EuSH and EuQSH have been compared on gold nanoparticles. Dual coated gold nanoparticles were prepared using the europium and gadolinium complexes of the SH and QSH ligand. Lanthanide complexes based on the two different DTPA bisamide ligands were used for complexing the lanthanide ions, and the combination of different lanthanide complexes appear to effect the photophysical properties of the europium complexes on the gold nanoparticle surface. The table below summarises the effect of co-coating gold nanoparticles with the different lanthanide complexes on the excitation wavelength required to observe europium emission (table 4.2).

	Europium emission observed	
	λ_{exc} = 270 nm	λ_{exc} = 310 nm
EuS.Au	✓	✗
EuS.GdS.Au	✓	✗
EuS.GdQS.Au	✓	✓
EuQS.Au	✓	✓
EuQS.GdS.Au	✓	✓
EuQS.GdQS.Au	✓	✓

Table 4.2: Summary of the europium emission observed at the excitation wavelengths 270 nm and 310 nm.

The most interesting result was obtained from ***EuS.GdQS.Au***. Europium luminescence from the EuSH complex was only observed at the higher excitation wavelength of 310 nm in the presence of the GdQSH. Some energy transfer was observed between the quinoline of the GdQSH complex and the europium ion of

EuSH complex when the two complexes were used to coat gold nanoparticles. The gold nanoparticles appear to provide a suitable platform for this energy transfer to occur, as they provide a large surface area for many of the different probes to bind and interact with one another. All the complexes appear to show some interaction upon mixing, with the emissive properties of the europium complex on nanoparticles improving in the presence of a gadolinium complex.

3 Experimental

3.1 Preparation of lanthanide coated gold nanoparticles

Gold nanoparticles used for these experiments were 13 nm citrate stabilised gold nanoparticles. A 1 mM stock solution of lanthanide complexes were prepared by dissolving the complex in methanol. These solutions were titrated into gold nanoparticles in µl aliquots and the coating of nanoparticles was monitored by UV-Vis spectroscopy.

Time-based emission studies were carried out with stirring with the addition of the two complexes. Hydrazine monohydrate was also added to prevent the formation of disulphide bonds between complexes.

3.2 Isothermal calorimetry

Isothermal calorimetry was carried out on a Microcal VP-ITC isothermal titration calorimeter. Data analysis was performed using Origin 7 Microcal software. In a typical experiment, the europium complex dissolved in water containing 10 % methanol and injected in µl quantities into citrate stabilised gold nanoparticles suspended in water containing 10 % methanol.

4   References

1 C. Kim, P. Ghosh and V. M. Rotello, *Nanoscale,* 2009, **1**, 61-67.

2 X. Wang, Y. Xia, Y. Liu, W. Qi, Q. Sun, Q. Zhao and B. Tang, *Chem- Eur J.,* 2012, **18**, 7189-7195.

3 F. Gao, Q. Ye, P. Cui, X. Chen, M. Li and L. Wang, *Anal. Methods,* 2011, **3**, 1180-1185.

4 X. Huang, T. Lan, B. Zhang and J. Ren, *Analyst,* 2012, **137**, 3659-3666.

5 I. Sun, D. Eun, H. Koo, C. Ko, H. Kim, D. K. Yi, K. Choi, I. C. Kwon, K. Kim and C. Ahn, *Angew. Chem. Int. Ed.,* 2011, **50**, 9348-9351.

6 C. Alric, J. Taleb, G. Duc, C. Mandon, C. Billotey, A. Meur-Herland, T. Brochard, F. Vocanson, M. Janier, P. Perriat, S. Roux and O. Tillement, *J. Am. Chem. Soc.,* 2008, **130**, 5908-5915.

7 Y. Song, X. Xu, K. W. MacRenaris, X. Zhang, C. A. Mirkin and T. J. Meade, *Angew. Chem. Int. Ed.,* 2009, **48**, 9143-9147.

8 M. Song, X. M. Wang, J. Y. Li, R. Y. Zhang, B. A. Chen and D. G. Fu, *J. Biomed. Mat. Res. A,* 2008, **86A**, 942-946.

9 X. Huang, I. El-Sayed, W. Qian and M. El-Sayed, *J. Am. Chem. Soc.,* 2006, **128**, 2115-2120.

10 J. D. Moore and M. J. Allen, *Recent Pat. Nanomed.,* 2011, **1**, 88-100.

11 D. J. Lewis, P. B. Glover, M. C. Solomons and Z. Pikramenou, *J. Am. Chem. Soc.,* 2011, **133**, 1033-1043.

12 C. S. Bonnet, J. Massue, S. J. Quinn and T. Gunnlaugsson, *Org. Biomol. Chem.,* 2009, **7**, 3074-3078.

13 L. K. Truman, S. Comby and T. Gunnlaugsson, *Angew. Chem. Int. Ed.,* 2012, **51**, 9624-9627.

14 R. Nishiyabu, N. Hashimoto, T. Cho, K. Watanabe, T. Yasunaga, A. Endo, K. Kaneko, T. Niidome, M. Murata, C. Adachi, Y. Katayama, M. Hashizume and N. Kimizuka, *J. Am. Chem. Soc.,* 2009, **131**, 2151-2158.

15 D. J. Lewis, T. M. Day, J. V. MacPherson and Z. Pikramenou, *Chem. Commun.,* 2006, **13**, 1433-1435.

16 S. P. Hammond, PhD, University of Birmingham, 2009.

17 S. P. Hammond, *Post-doctoral report*, University of Birmingham, University of Birmingham, 2011.

18 E. Debroye, S. V. Eliseeva, S. Laurent, L. Vander Elst, S. Petoud, R. N. Muller and T. N. Parac-Vogt, *Eur. J. Inorg. Chem.,* 2013, **2013**, 2629-2639.

19 R. Ghai, R. J. Falconer and B. M. Collins, *J. Mol. Recognit.,* 2012, **25**, 32-52.

20 H. Joshi, P. S. Shirude, V. Bansal, K. N. Ganesh and M. Sastry, *J Phys Chem B,* 2004, **108**, 11535-11540.

21 K. Chen, Y. Xu, S. Rana, O. R. Miranda, P. L. Dubin, V. M. Rotello, L. Sun and X. Guo, *Biomacromolecules,* 2011, **12**, 2552-2561.

22 M. De, O. R. Miranda, S. Rana and V. M. Rotello, *Chem. Commun.,* 2009, **16**, 2157-2159.

23 A. Gourishankar, S. Shukla, K. N. Ganesh and M. Sastry, *J. Am. Chem. Soc.,* 2004, **126**, 13186-13187.

New sensitiser for near infrared lanthanides

1   Introduction

Lanthanides that emit in the near-infrared are of interest for imaging of biological systems. There is an interest to develop these probes to improve sensitivity and overcome the challenges faced with imaging probes that emit in the visible region. Tissue and blood can absorb light in the visible region, which can mean that the light emitted from visible probes can be reabsorbed by biological molecules and tissue. Skin and other tissue is transparent to near-infrared light, which makes imaging with near-infrared complexes desirable to improve the detection of the light emitted from the cellular probe. Near-infrared probes also have excited states lower in energy than the visible lanthanides, thus requiring lower energy for excitation. This allows for the use of a chromophore that can be excited in the visible region. Near-infrared complexes have shorter luminescence lifetimes compared with visible lanthanide, but they are still suitable for time-gated experiments. Emission in the near-infrared region is desirable as biological systems do not contain anything that emit in the near-infrared region, and the Stokes shift between the excitation source and the lanthanide emission is significantly large enough to prevent any light from the excitation source being detected.[1]

Developing a sensitiser for near-infrared lanthanides allows for the use of a chromophore that absorbs in the visible region, which is desirable for cellular imaging as excitation above 340 nm is compatible with the optics of the microscope and avoids absorption of the excitation light by some common biomolecules in the cell.[2] There have been various examples of near-infrared lanthanide complexes, with the

primary focus being on developing sensitisers that can be excited in the visible region.[3-5] Pope *et al.* utilised an anthraquinone sensitiser attached to a tetra-alkylated cyclen derivative for chelation of the near-infrared lanthanides neodymium, ytterbium and erbium (figure 5.1).[3] Increasing the pH of this anthraquinone complex was found to induce a bathochromic shift in the absorbance profile, allowing the sensitisation of the near-infrared lanthanides at an excitation wavelength of 575 nm. Xylenol orange has also been investigated as a sensitiser for an ytterbium complex on gold nanoparticles, which was found to exhibit an 'on-off' effect as a result of change in pH.[6] Excitation of this complex at pH greater than 4 was achieved with 580 nm light.
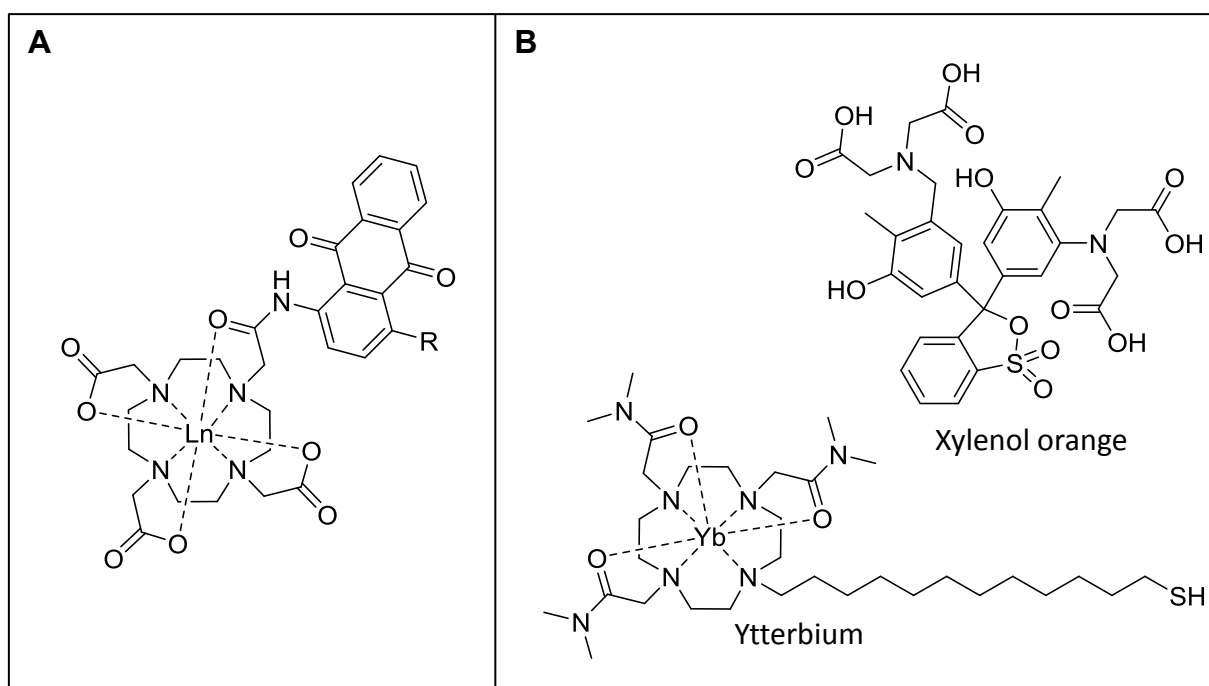

Figure 5.1: **A:** Near-infrared lanthanide complex with anthraquinone sensitiser. Ln = Nd, Yb or Er.[3] **B:** Ytterbium complex for coating gold nanoparticles with xylenol orange sensitiser.[6]

Transition metal complexes have also been used as sensitisers for near-infrared lanthanides. The excitation of near-infrared lanthanides with tethered transition metal complexes is also widely studied.[7-14] The advantages of using transition metal chromophores are that they are strongly absorbing in visible region, and have relatively long-lived triplet excited states which aids energy transfer to the attached lanthanide.[9] One of the first examples of this was the report of neodymium and ytterbium complexes with sensitisation from the transition metal complexes ruthenium (II) tris(bipyridine) or ferrocene (figure 5.2).[10] The ruthenium complex allows for excitation with visible light at 450 nm, whilst the ferrocene sensitiser has much lower absorption in the visible region its triplet state of 13300 cm^{-1} is still close to that of the receiving luminescent states of the near-infrared lanthanides neodymium (11300 cm^{-1}) and ytterbium (10200 cm^{-1}). Both systems were found to give rise to near-infrared emission from neodymium and ytterbium with excitation wavelengths of 450 nm for the ruthenium complex and 320 nm for ferrocene.

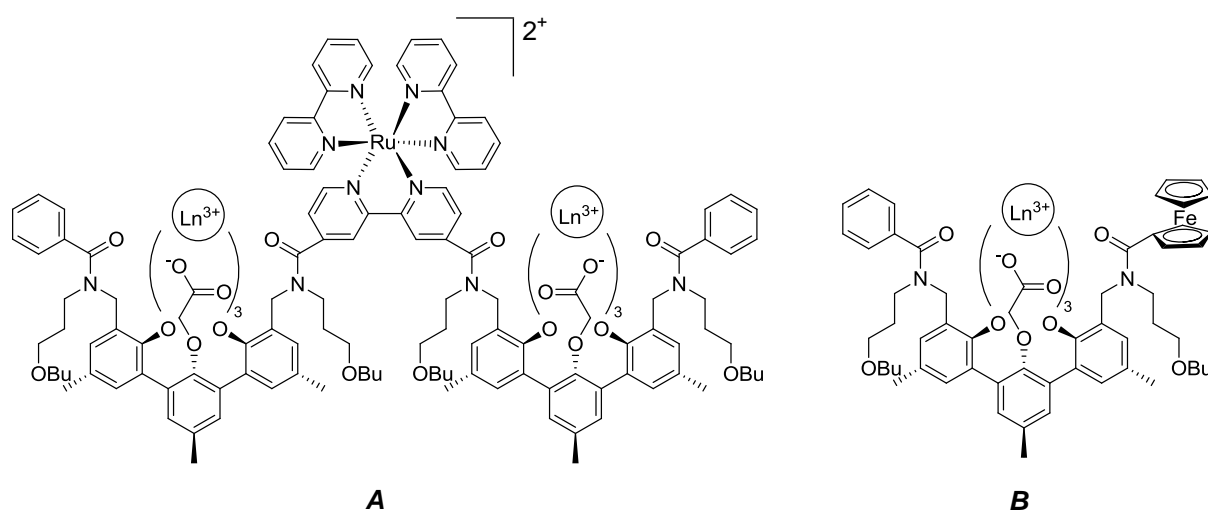Figure 5.2: Structure of near-infrared lanthanide complexes with transition metal sensitisers.[10] **A:** Ruthenium (II) tris(bipyridine) *m*-terphenyl-based lanthanide complex. **B:** Ferrocene *m*-terphenyl-based lanthanide complex. Ln = Nd or Yb

Faulkner *et al.* reported the synthesis of a heterometallic lanthanide complex with an adjoining azo-dye containing neodymium and ytterbium (figure 5.3).[15] The lanthanide ions are complexed within a well-known chelator DO3A. The azo-dye acts as the chromophore for the tethered near-infrared lanthanide complexes which allows for visible light excitation. Monitoring the emission using time-gated emission spectroscopy shows the characteristic emission profile for neodymium and ytterbium upon excitation of the bimetallic complex at 420 nm.

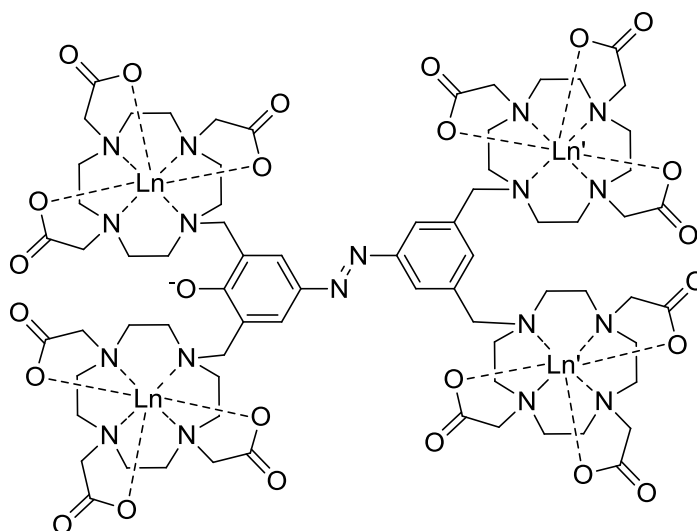Figure 5.3: Structure of polymetallic lanthanide complexes with azo-dye linker.[15] Ln and Ln' = Nd or Yb

The previous chapters have shown that the SH and QSH ligands are suitable for the sensitisation of neodymium. These complexes however are limited by the wavelengths at which the chromophore can be excited, with an excitation wavelength usually lower than 330 nm. We were interested in the study of azo-dyes with

extensive conjugation for higher absorption coefficients in the visible region. Kobrakov *et al.* reported the synthesis and characterisation of an azo-dye which was tested for its ability to be used as a fabric dye.[16] This azo-dye was selected for the studies in this chapter due to its high absorption coefficient, and it was postulated that it would be suitable for use as a near-infrared lanthanides sensitiser. The high absorption in the visible region allows for the possibility of excitation of the azo-dye at wavelengths greater than 400 nm. Whilst the synthesis of these dyes is reported with many steps, each step goes forward in quite high yields which make them quite easy to prepare in large quantities. There have been few examples of azo-dyes being utilised as sensitisers for near-infrared lanthanides.[15] This chapter reports the synthesis of the azo-dye (E)-4-((2-hydroxy-5-nitrophenyl) diazenyl)-1-(2-methoxy-5-nitrophenyl)-3-methyl-1H-pyrazol-5-ol (***compound 5***) and its use as a sensitiser for near-infrared lanthanides (figure 5.4). The azo-dye ***compound 5*** was reacted with the near-infrared lanthanides neodymium and ytterbium and the photophysical properties of the complex formed are investigated.

Azo-dye: **Compound 5**   **Ln(Azo)**
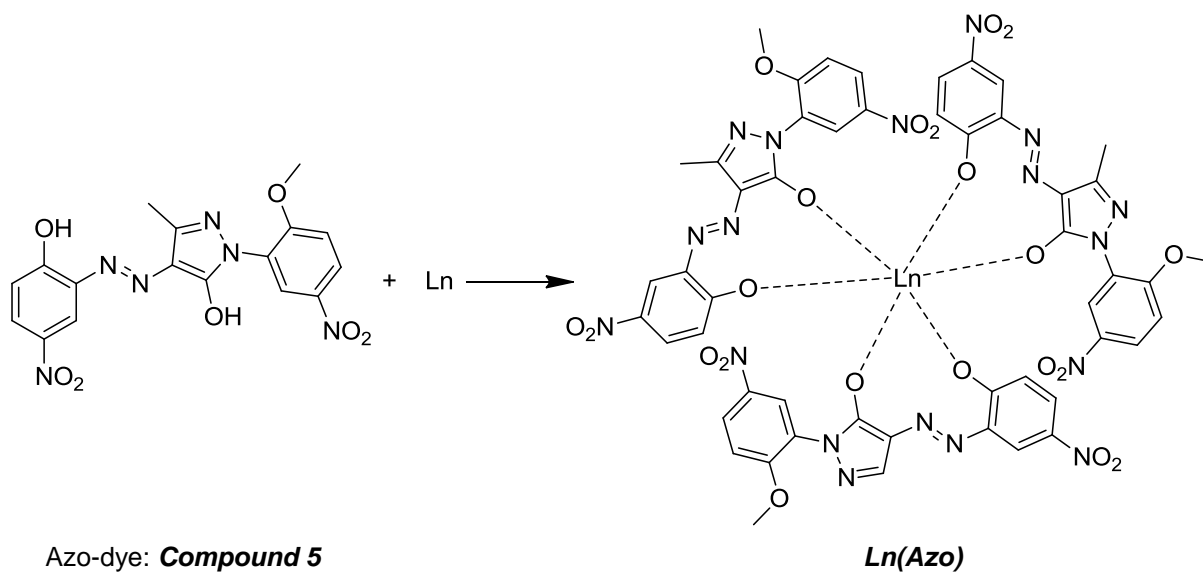
Figure 5.4: Schematic diagram of the reaction of the azo-dye prepared in this chapter with Ln(III) ions and the suggested mode of complexation. Ln = ytterbium and neodymium

2   Results and Discussion

2.1   Synthesis of (E)-4-((2-hydroxy-5-nitrophenyl)diazenyl)-1-(2-methoxy-5-nitrophenyl)-3-methyl-1H-pyrazol-5-ol
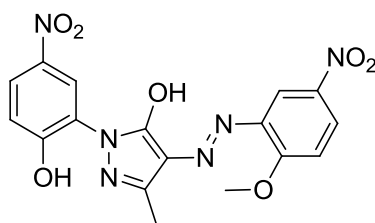
The azopyrazole (E)-4-((2-hydroxy-5-nitrophenyl)diazenyl)-1-(2-methoxy-5-nitrophenyl)-3-methyl-1H-pyrazol-5-ol (**compound 5**) was prepared following the reaction scheme showed in figure 5.5. I was prepared following published procedures.[16, 17]
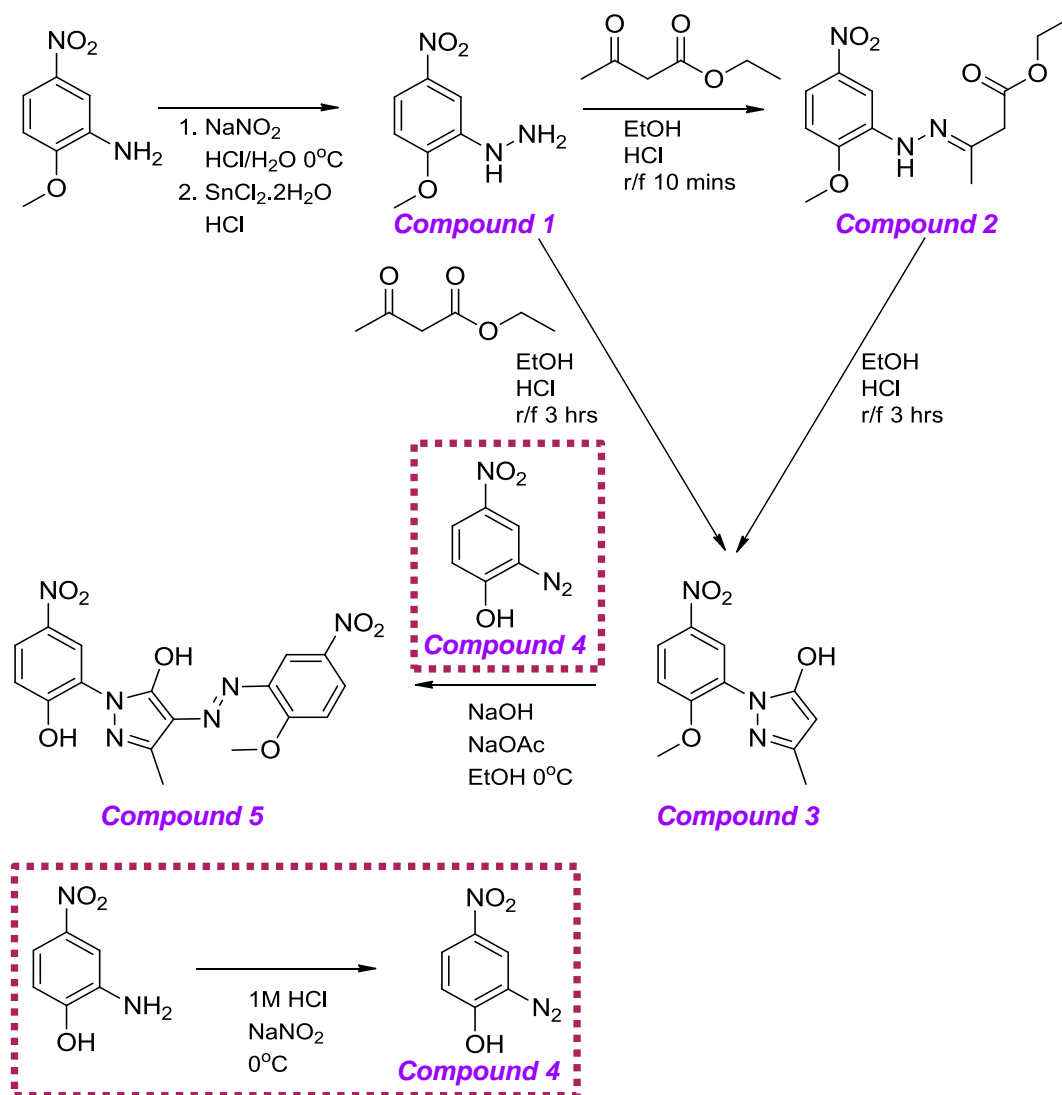
Figure 5.5: Reaction scheme of synthesis of (E)-4-((2-hydroxy-5-nitrophenyl)diazenyl)-1-(2-methoxy-5-nitrophenyl)-3-methyl-1H-pyrazol-5-ol (**Compound 5**).

The synthesis proceeds following the scheme shown in figure 5.5, with the conversion of 2-methoxy-5-nitrophenylaniline to 2-methoxy-5-nitrophenyl hydrazine firstly by the diazotisation of the starting material using sodium nitrite in the presence of HCl. The diazonium salt was then reduced using tin (II) chloride to give the product at a 34 % yield. The ^{1}H NMR spectrum shows peaks at 6.78 and 3.60 ppm corresponding to the protons bound to the NH and NH$_2$ groups. Integration of the

147

peaks gives the appropriate number of protons and agrees with the published procedure.

The next synthetic step is the reaction of the hydrazine **compound 1** with ethylacetoacetate to form the pyrazole. The intermediate product of this reaction (**compound 2**) can be isolated after 10 minutes reflux in ethanol in the presence of HCl. The final product, 1-(2-methoxy-5-nitrophenyl)-3-methyl-1H-pyrazol-5-ol (**compound 3**) was isolated after 3 hours reflux in ethanol in the presence of HCl. Comparisons of the ^{1}H NMR spectra of **compound 2** and **3** (figure 5.6) shows the change in structure as the reaction proceeds, with the loss of the proton bound to the nitrogen and the peak associated with proton H_3 shifting downfield upon the formation of the pyrazole. Also there is the loss of the protons H_8 and H_9 as the ethyl chain is lost upon formation of the pyrazole. Both ^{1}H NMR spectra integrate for the appropriate number of protons expected for each molecule.
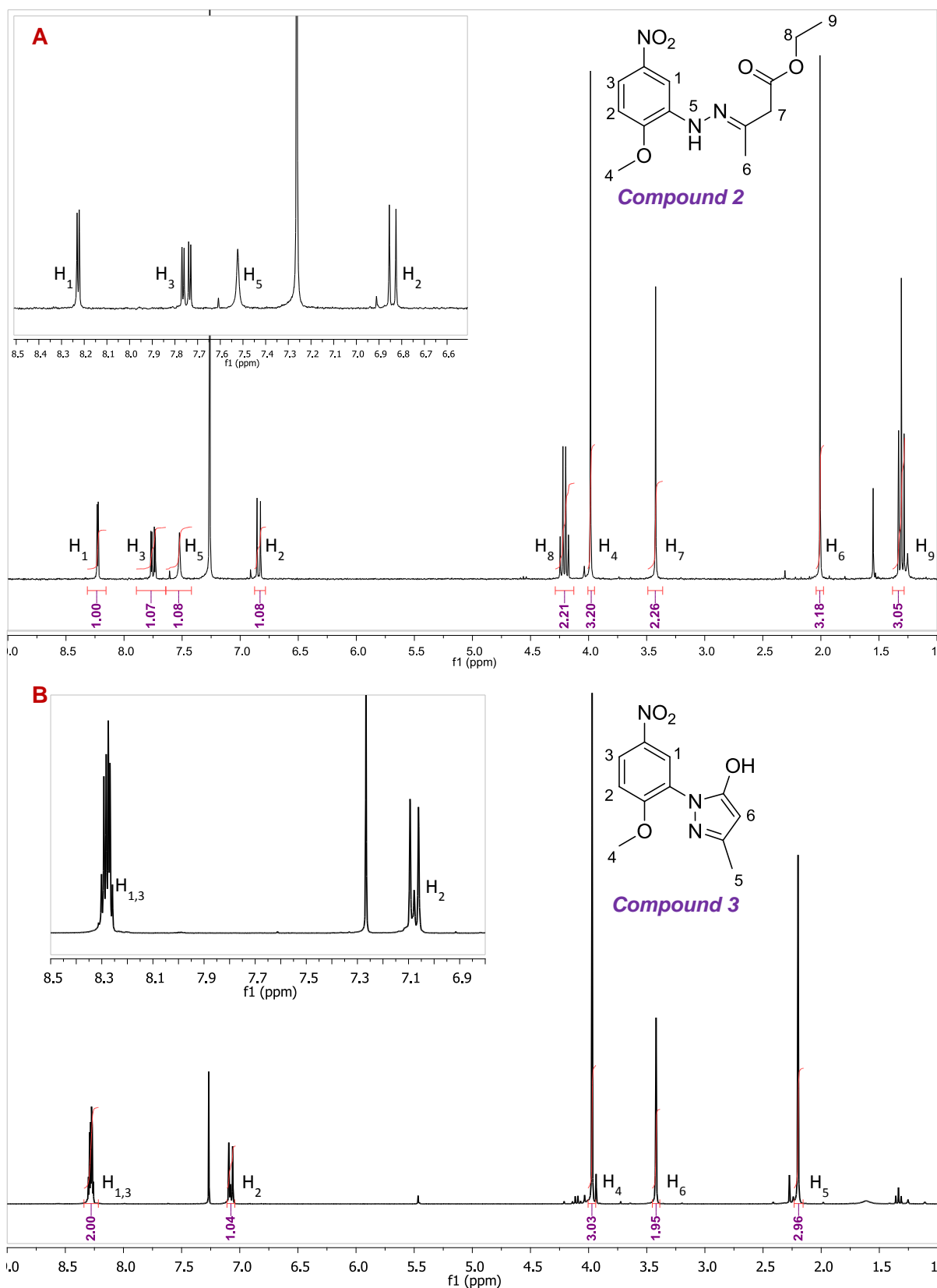
Figure 5.6: ^{1}H NMR spectra of **compounds 2** and **3** in $CDCl_3$. **A:** ^{1}H NMR of **compound 2**. **B:** ^{1}H NMR of **compound 3**.

The reaction for the formation of **compound 4** proceeds with the addition of sodium nitrite to a solution of 2-amino-4-nitrophenol in water. The bright yellow compound was found to be prone to decomposition at room temperature and was used immediately upon preparation for the final step of synthesis of the azo-dye.

The final step in the synthesis of the azo-dye involves the slow addition of the diazonium salt (**compound 4**) into an ethanolic solution of **compound 3**. The complex was characterised by mass spectrometry and NMR spectroscopy. The mass spectrum showed a peak at 413 m/z corresponding to the molecular weight of the product and a peak at 437 m/z corresponding to the sodium adduct. The ^{1}H NMR of the azo-dye with assignment is shown in figure 5.7.
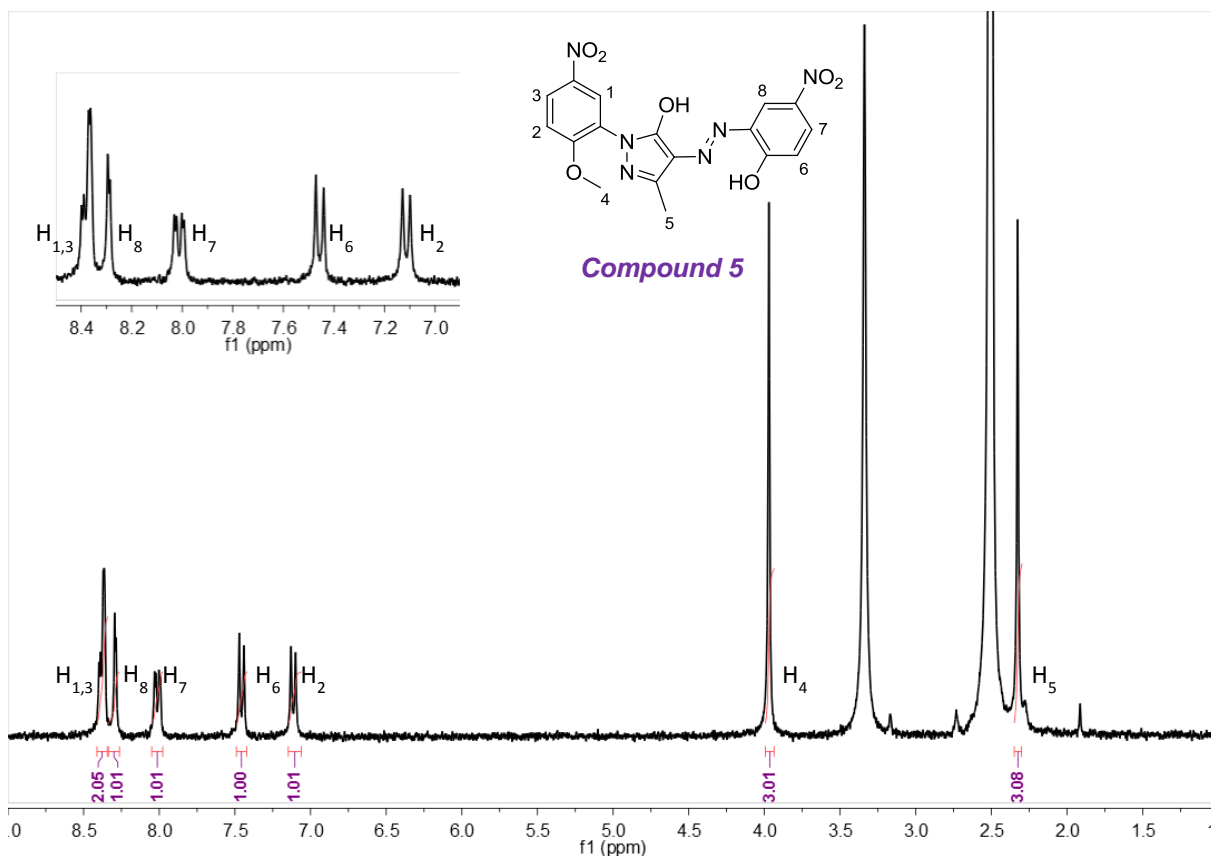
Figure 5.7: ^{1}H NMR spectrum of final azo-dye, **compound 5** in D6-DMSO

The UV-Vis and fluorescence spectra of the azo-dye are presented in figure 5.8. The UV-Vis spectrum shows peaks at 256 nm, 300 nm and 416 nm. Previously observed UV-Vis spectra of azo-derivatives suggests that these peaks can be attributed to $\pi \rightarrow \pi^*$ transitions (256 nm) and n $\rightarrow \pi^*$ transitions (300 nm and 416 nm).[15] Upon excitation at 450 nm, the azo-dye exhibits fluorescence centred around 635 nm.
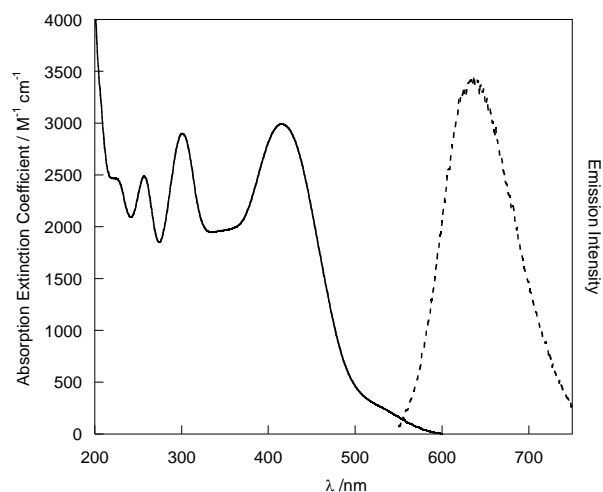
Figure 5.8: UV-Vis and emission spectra of azo-dye in ethanol. [Azo] = 0.417 mM. λ_{exc} = 450 nm

2.2 Preparation and characterisation of neodymium and ytterbium complexes with compound 5: Ln(Azo)

The complexes Ln(Azo) were prepared by addition of $LnCl_3.6H_2O$ (where Ln = Nd or Yb) into a solution of the azo-dye. These complexes give rise to the characteristic lanthanide ion emission when excited at λ_{exc} = 450 nm, shown in figure 5.9. This suggests that the azo-dye sensitises these lanthanides.

Figure 5.9: Luminescence spectra of Nd(Azo) and Yb(Azo) in ethanol. λ_{exc} = 450 nm. [Azo] = 0.3 mM, [LnCl$_3$.6H$_2$O] = 0.1 mM.

By monitoring the titration of lanthanides into a solution of the azo-dye, it should be possible to estimate how many of the azo-dyes are coordinating th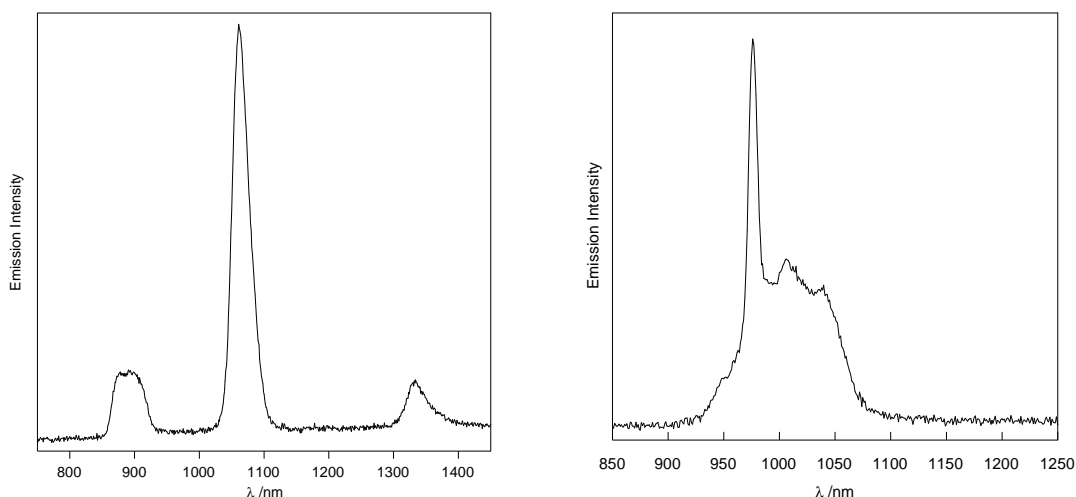e lanthanide. Upon addition of the lanthanide solution to the azo-dye, there is an obvious change in the UV-Vis spectrum (figure 5.10). This is visible by eye, as the solution turns from orange to bright yellow. Titration of Yb^{3+} into the azo-dye solution causes a dramatic change in the UV-Vis spectrum, with the band at 416 nm shifting to 465 nm. A plot of the shift in this band is shown in figure 5.10. This large red-shift in the absorbance profile of the complex allows for the use of excitation wavelengths in the visible region up to 500 nm. The shift in the UV-Vis spectrum appears to stop after the addition of 0.13 mM of YbCl$_3$.6H$_2$O. This stabilisation of the UV-Vis profile suggests that all the azo-dye is bound to Yb^{3+}. The ratio of azo-dye to ytterbium is 3:1 which suggests that three azo-dyes are bound to one Yb^{3+} forming a complex. The profile found by UV-Vis titration is similar to that found upon monitoring the luminescence.

153
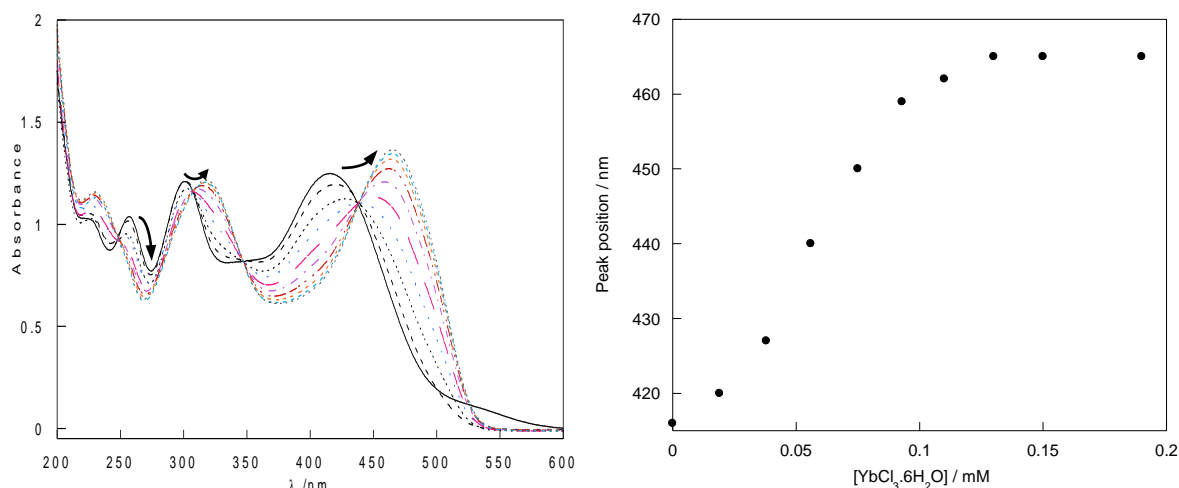
Figure 5.10: UV-Vis titration of Yb^{3+} into the azo-dye. [Azo] = 0.417 mM in ethanol (⎯⎯), [YbCl$_3$.6H$_2$O] = 0.019-0.185 mM. Arrows indicate the direction of shift upon titration of Yb.

The luminescence of the sample should also provide a good indication of the coordination, as the lanthanide itself cannot be directly excited at 450 nm, so once all the azo-dye has been coordinated there should be saturation of the luminescence signal. The titration of Yb^{3+} into the azo-dye is shown in figures 5.10 and 5.11, with both the absorbance and luminescence being monitored during the titration (figure 5.11). Figure 5.11 shows the luminescence spectra of the titration of Yb^{3+} into the azo-dye. The titration curve for the luminescence is slightly different in profile, but they seem to plateau at similar concentrations, agreeing with the 3:1 ratio observed by UV-Vis spectroscopy.
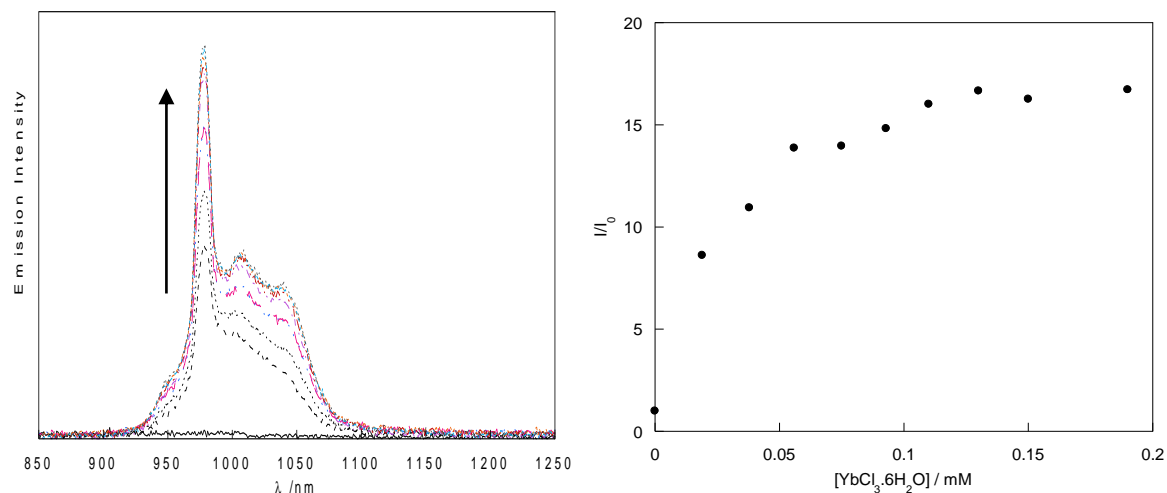
Figure 5.11: Luminescence titration of Yb^{3+}into azo-dye. [Azo] = 0.417 mM. [YbCl$_3$.6H$_2$O] = 0.019-0.185 mM. λ_{exc} = 450 nm

The luminescence titration of Nd^{3+} into the azo-dye gives a similar ratio to that observed with the Yb^{3+} with 3 azo-dyes to 1 Nd^{3+} ion (shown in figure 5.12). This is as expected as all the lanthanides ions have similar coordination. The plot of the relative emission increase was calculated from the growth of the strongest peak at 1056 nm which is associated with the $^4F_{3/2} \rightarrow {}^4I_{11/2}$ transition.
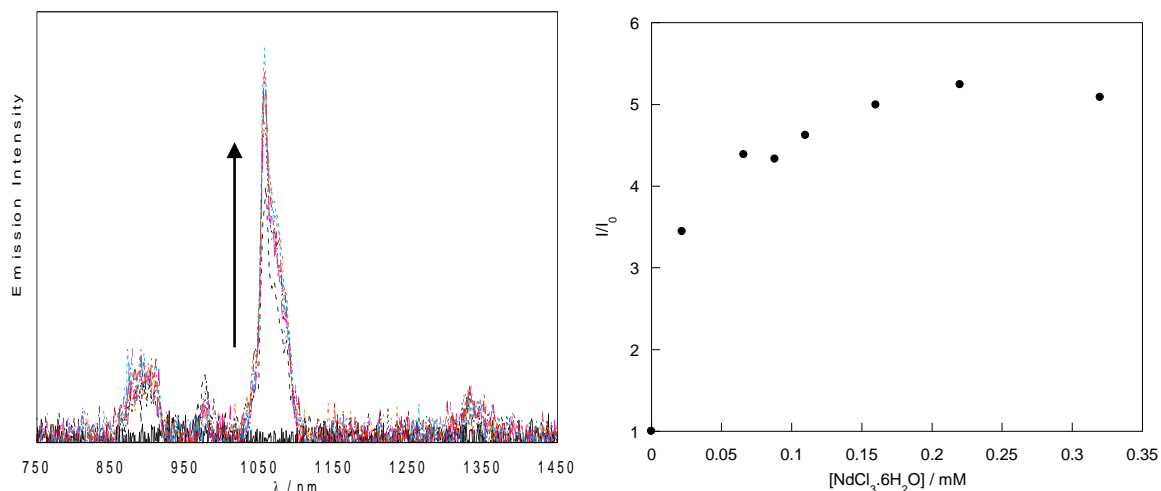
Figure 5.12: Titration of Nd^{3+} into azo-dye in ethanol. [Azo] = 0.3 mM, [$NdCl_3.6H_2O$] = 0.022 – 0.32 mM. λ_{exc} = 450 nm.

The lifetimes of Nd(Azo) and Yb(Azo) in ethanol was found to be 8 µs and 10 µs respectively. The absorbance at higher wavelength upon lanthanide complexation allows for excitation with visible light at wavelengths as high as 500 nm (figure 5.13).
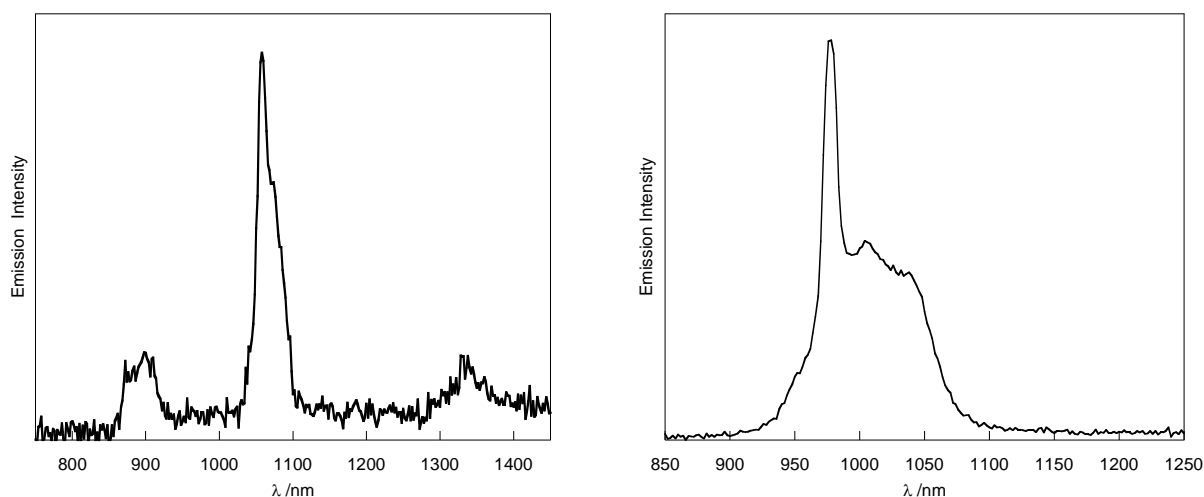
Figure 5.13: Luminescence spectra of azo-dye complexes upon excitation at λ_{exc} = 500 nm. *Left:* Nd(Azo). [Azo] = 0.3 mM, [$NdCl_3.6H_2O$] = 0.022 – 0.32 mM. *Right:* Yb(Azo). [Azo] = 0.417 mM, [$YbCl_3.6H_2O$] = 0.185 mM

156

The azo-dye mixed with lanthanides that emit in the visible region such as europium and terbium did not give rise to emission from the lanthanide ion. This could be due to the triplet state of the azo-dye being too low for excitation of these lanthanides. It is possible if some emission did occur it would be masked by the emission observed from the azo-dye itself, which emits in a similar region to the visible lanthanides with a broad peak. The near-infrared lanthanides have much lower excited states than the visible lanthanide which may make them easier to excite with this azo-dye. Mixing the azo-dye with erbium does not give rise to any erbium emission upon excitation at 450 nm.

2.3   Conclusion

An azo-dye has been synthesised and characterised following a five step synthesis. The azo-dye was found to be suitable for use as a sensitiser for the near-infrared lanthanides neodymium and ytterbium, allowing excitation using visible light up to 500 nm. Titration of lanthanide into a solution of the azo-dye suggests that the azo-dye forms a complex with the lanthanide at a ratio of 3:1 azo-dye to lanthanide. This azo-dye sensitiser can be developed further by modification to allow for attachment to a strongly chelating ligand, such as DTPA. This would allow for the lanthanide to form a more stable complex, whilst still being in close proximity to the azo-dye for sensitisation. Initial attempts to reduce the nitro groups to amines failed to work on the final azo-dye product using mild reducing agents such as Zn, so it is

possible that this reduction could be carried out on one of the starting materials to try and obtain this amine derivative. The development of an assymetric probe with this azo-dye would also allow for the attachment of a surface-active group for attachment to gold nanoparticles.

3 Experimental

3.1 Synthesis of 2-methoxy-5-nitrophenyl hydrazine[16]
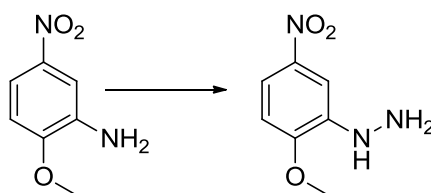
2-methoxy-5-nitrophenylaniline (5 g, 29 mmol) was added to 85 ml 12 M HCl at 0°C. A solution of sodium nitrite (2.3 g, 33 mmol) in 13 ml water was added drop-wise to the reaction mixture to ensure the internal temperature was kept below 10°C. Once the addition was complete, the solution was cooled further using a dry ice/ acetone bath. A solution of $SnCl_2.2H_2O$ (15 g, 66 mmol) in 15 ml HCl was added slowly to the reaction mixture. A further 25 ml HCl was added to the reaction to aid stirring and the solution was stirred for 25 mins. The precipitate formed was filtered and was stirred into 100 ml of a 25 % KOH solution. The orange precipitate formed was collected and stirred in ethyl acetate. The ethyl acetate solution was washed with water (1 x 50 ml), brine (1 x 50 ml) and dried with $MgSO_4$. The ethyl acetate was removed in vacuo and the product recrystallized from 100 ml methanol (1.83 g, 34 %).

^{1}H NMR (300 MHz, CDCl$_3$) δ (ppm) 7.85 (1H, d, Ar$\underline{H}$), 7.71 (1H, dd, Ar$\underline{H}$), 6.78 (1H, d, Ar$\underline{H}$), 5.81 (1H, s, N$\underline{H}$), 3.94 (3H, s, OCH$_3$), 3.60 (2H, s, NH$_2$).

^{13}C NMR (400 MHz, CDCl$_3$) 150.97, 142.49, 141.08, 114.85, 108.33, 105.7, 56.06.

3.2 Synthesis of acetoacetic ester 2-methoxy-5-nitrophenyl hydrazone
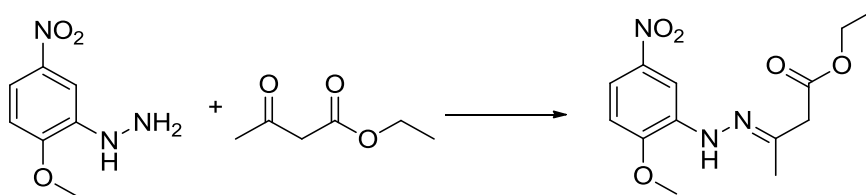
2-methyoxy-5-nitrophenyl hydrazine (0.91 g, 5 mmol) and ethylacetoacetate (0.64 g, 5 mmol) were refluxed for 10 minutes in ethanol (10 ml) with t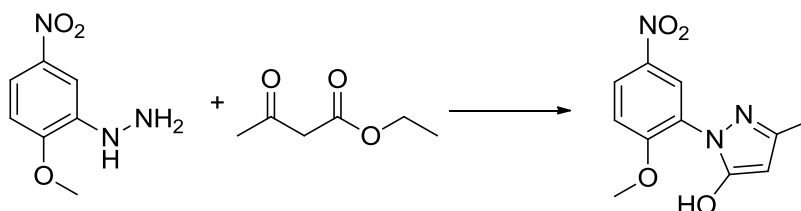he addition of a few drops conc. HCl. The solution was allowed to cool, yielding a yellow precipitate. (0.836 g, 58 %) ^{1}H NMR (300 MHz, CDCl$_3$) δ (ppm) 8.23 (1H, d, Ar$\underline{H}$), 7.75 (1H, dd, Ar$\underline{H}$), 7.52 (1H, s, N$\underline{H}$), 6.84 (1H, d, Ar$\underline{H}$), 4.21 (2H, q, C$\underline{H}_2$CH$_3$), 3.98 (3H, s, C$\underline{H}_3$O), 3.42 (2H, s, CC$\underline{H}_2$C), 2.01 (3H, s, C$\underline{H}_3$C) , 1.31 (3H, t, CH$_2$C$\underline{H}_3$); MS (ES+): m/z 318 [M+Na]$^+$

^{13}C NMR (400 MHz, D6-DMSO) δ (ppm) 115.2, 110.2, 105.9, 60.3, 56.5, 44.0, 15.7, 13.9

3.3 Synthesis of 3-methyl-1-(2-methoxy-5-nitrophenyl)-1H-pyrazol-5-ol

2-methyoxy-5-nitrophenyl hydrazine (0.7 g, 4 mmol) and ethylacetoacetate (0.48 g, 4 mmol) were refluxed for 12 hours in ethanol (50 ml) with the addition of a few drops conc. HCl. Solvent was removed *in vacuo* to give yellow oil which was a mixture of two products. The oil was redissolved in 10 ml water and the pH adjusted to 14. The solution was washed with DCM (2 x 20 ml). The aqueous layer was then acidified and washed with DCM (2 x 20 ml). The organic layer was retained and the solvent removed in vacuo to yield a yellow solid. (0.6600 g, 63 % yield)

^{1}H NMR (300 MHz, CDCl$_3$) δ (ppm) 8.28 (2H, m, Ar$\underline{H}$), 7.08 (1H, d, Ar$\underline{H}$), 3.97 (3H, s, OC$\underline{H}_3$), 3.42 (2H, s, C$\underline{H}_2$), 2.20 (3H, s, C$\underline{H}_3$); ^{13}C NMR (400 MHz, CDCl$_3$) δ (ppm) 125.6, 124.2, 111.7, 56.8, 41.4, 14.6; MS (ES+): m/z 250 [M+H]$^+$

3.4   Synthesis of 2-hydroxy-5-nitrophenyl diazonium
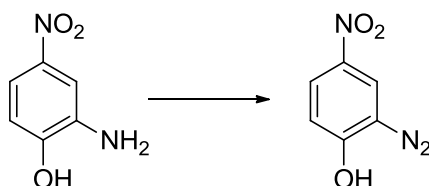
2-amino-4-nitrophenol (0.51 g, 3 mmol) was stirred into 50 ml 1 M HCl at 0°C Sodium nitrite (0.226 g, 3mmol) in 15 ml water was added drop-wise to the reaction mixture. A yellow precipitate formed in the solution which was stirred for 30 minutes. The precipitate was collected by suction filtration and used immediately in the next reaction step. ^{1}H NMR (300 MHz, MeOD) δ (ppm) 8.83 (1H, d), 8.19 (1H, dd), 6.69 (1H, d)

3.5   Synthesis of (E) -4-((2-hydroxy-5-nitrophenyl)diazonyl) -1-(2-methoxy-5-nitrophenyl) -3-methyl-1H-pyrazol-5-ol
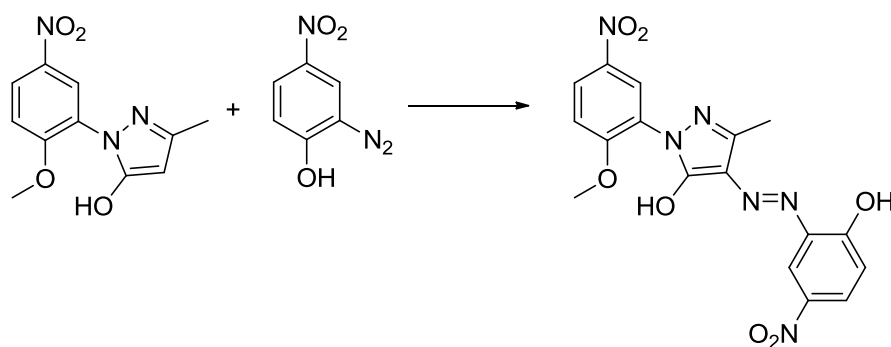
3-methyl-1-(2-methoxy-5-nitrophenyl)-1H-pyrazol-5-ol (0.081g, 0.3 mmol) was dissolved in ethanol and heated to 80°C. Sodium hydroxide (0.013 g, 0.3 mmol) and sodium acetate (0.064 g, 0.8 mmol) were added and the solution was cooled to 0°C. A suspension of 2-hydroxy-5-nitrophenyl diazonium (0.054 g, 0.3 mmol) in 10 ml ethanol was added slowly over 15 minutes. The pH was monitored and kept basic with 10 % NaOH. After the addition was complete, the reaction mixture was stirred for 2 hours. The solution was acidified to pH 5-6 and precipitate was collected by suction filtration. (0.061 g, 45 %). ^{1}H NMR (300 MHz, D$_6$-DMSO) δ (ppm) 8.39 (2H, d), 8.37 (1H, d), 8.01 (1H, dd), 7.46 (1H, d), 7.11 (1H, d), 3.94 (3H, s), 2.33 (3H, s) MS (ES+): m/z 413 [M-H]; 437 [M+Na]$^+$

4   References

1 C. M. Andolina, P. J. Klemm, W. C. Floyd, J. M. J. Frechet and K. N. Raymond, *Macromolecules,* 2012, **45**, 8982-8990.

2 R. A. Poole, G. Bobba, M. J. Cann, J. Frias, D. Parker and R. D. Peacock, *Org. Biomol. Chem.,* 2005, **3**, 1013-1024.

3 J. E. Jones and S. J. A. Pope, *Dalton Trans.,* 2009, **39**, 8421-8425.

4 S. Faulkner, A. Beeby, R. S. Dickins, D. Parker and J. A. G. Williams, *J. Fluoresc.,* 1999, **9**, 45-49.

5 Y. Zhong, L. Si, H. He and A. G. Sykes, *Dalton Trans.,* 2011, **40**, 11389-11395.

6 L. K. Truman, S. Comby and T. Gunnlaugsson, *Angew. Chem. Int. Ed.,* 2012, **51**, 9624-9627.

7 S. Singaravadivel, E. Babu, M. Velayudham, K. Lu and S. Rajagopal, *Polyhedron,* 2013, **60**, 54-58.

8 S. Swavey and R. Swavey, *Coord. Chem. Rev.,* 2009, **253**, 2627-2638.

9 M. D. Ward, *Coord. Chem. Rev.,* 2007, **251**, 1663-1677.

10 S. I. Klink, H. Keizer and F. C. J. M. van Veggel, *Angew. Chem. Int. Ed.,* 2000, **39**, 4319-4321.

11 M. Vázquez López, S. V. Eliseeva, J. M. Blanco, G. Rama, M. R. Bermejo, M. E. Vázquez and J. G. Bünzli, *Eur. J. Inorg. Chem.,* 2010, **2010**, 4532-4545.

12 A. M. Nonat, C. Allain, S. Faulkner and T. Gunnlaugsson, *Inorg. Chem.,* 2010, **49**, 8449-8456.

13 T. Lazarides, N. M. Tart, D. Sykes, S. Faulkner, A. Barbieri and M. D. Ward, *Dalton Trans.,* 2009, , 3971-3979.

14 N. M. Shavaleev, L. P. Moorcraft, S. J. A. Pope, Z. R. Bell, S. Faulkner and M. D. Ward, *Chem- Eur J.,* 2003, **9**, 5283-5291.

15 M. P. Placidi, A. J. L. Villaraza, L. S. Natrajan, D. Sykes, A. M. Kenwright and S. Faulkner, *J. Am. Chem. Soc.,* 2009, **131**, 9916-9917.

16 D. N. Kuznetsov, A. G. Ruchkina and K. I. Kobrakov, *Chem. Heterocycl. Compd. (N. Y , NY, U. S.),* 2011, **47**, 441-447.

17 B. G. Szczepankiewicz and C. H. Heathcock, *Tetrahedron,* 1997, **53**, 8853-8870.

General Experimental

1   Materials and Methods

All chemicals were purchased from Sigma Aldrich or Fisher Scientific and used without further purification unless otherwise stated. Solvents were purchased from Sigma Aldrich and Fisher. HPLC grade solvents were used in photophysical studies. Water was deionised using an Elga Option 3 water purifier.

2   Equipment

2.1   NMR and Mass spectrometry

^1H and ^{13}C NMR were recorded on Brüker AVIII300 and AVIII400 spectrometers. SiMe4 was used for an external reference of the ^1H and ^{13}C shifts. Deuterated solvents were obtained from Goss Scientific and used as supplied.

Matrix assisted laser desorption ionisation – time of flight (MALDI-TOF) mass spectrometry was carried out on a Brüker Biflex IV mass spectrometer, using Gentisic acid in CH_3CN with 0.1% TFA as the matrix. Electrospray mass spectrometry was carried out on a Micromass LC-TOF.

2.2   HPLC

HPLC was carried out on a Dionex summit system, using a Summit P580 quaternary low pressure gradient pump with built-in vacuum degasser. The detector was a Summit UVD 170s UV-VIS multi-channel detector with analytical flow cell for analytical HPLC and a prep flow cell for semi-prep HPLC. The column used for analytical HPLC was the Phenomenex Luna 10 µm particles size C18 analytical

column (250 mm x 4.6 mm). The column used for semi-prep HPLC was the Phenomenex Luna 10 μm particle size C18 semi-prep column (250 mm x 10 mm). All solvents used were HPLC grade solvents, degassed prior to use.

2.3   UV-Vis Spectroscopy

UV-Vis absorption spectra were carried out on Varian Cary 50 or Varian Cary 5000 spectrometers with 300 nm/min UV-vis spectra were taken using 1 cm path length quartz cuvettes.

2.4   Luminescence Spectroscopy

Luminescence studies were carried out on a PTI fluorescence system, using a PTI L-201M with a 75 W xenon arc lamp as the illumination source. The detection system was a Shimadzu R928 PMT in a PTI model 814 analogue/photon counting photomultiplier. The emission monochromator is equipped with two interchangeable blazed gratings at 500 nm and 750 nm. PTI Felix fluorescence analysis software was used to record the data. Luminescence experiments were carried out using 1 x 1cm path length quartz cuvettes with four transparent polished faces.

Luminescence studies for the nanoparticle samples were carried out using an Edinburgh instruments fluorescence system, FLSPM920. The illumination source uses a 450 W xenon arc lamp. The detection system used was a Hamamatsu R928 PMT. The emission monochromator is fitted with two interchangeable gratings blazed at 500 nm and 1200 nm. F900 spectrometer analysis software was used to record the data. Lifetimes were measured using a 100 W μF920H lamp. Lifetime data were

fitted to monoexponential decays using Edinburgh Instruments F900 PC software using the exponential tail fit option.

Lifetimes were alternatively measured using a Continuum Surelite I SSP class 4 pulsed Nd-YAG laser (10 Hz) as the excitation source using the 355 nm harmonic. The signal was collected as a direct output from the PMT to minimise the response time of the apparatus. Data were recorded on a LeCroy 9350AM 500 MHz oscilloscope which was triggered by the laser, with an average of 500 shots. The lifetime data was analysed using Kaleidagraph software (Kaleidagraph 3.51, Synergy Software, 2000) for the PC and fitted using a non-linear least-squares iterative technique (Marquardt-Levenberg algorithm)

2.5   ICP-OES

ICP-OES analysis was run at the University of Warwick using a Perkin-Elmer 5300DV ICP-OES system. PlasmaCal Calibration standards for europium, terbium, gadolinium and gold were purchased from SCP science. Concentrations of europium, terbium, gadolinium and gold in nanoparticle samples were determined using linear calibration curves constructed from purchased standards, with $R_2 > 0.999$ in all cases.

2.6   TEM

TEM samples were imaged using Jeol 1200EX TEM with an operating voltage of 80 keV and Gatan multiscan camera. Samples were air-dried onto 200 mesh formvar coated copper grids supplied by Agar Scientific. Images were acquired using DigitalMicrograph 1.8 (Gatan, CA, USA).

2.7   Luminescence Microscopy

Cell samples were imaged by luminescence microscopy using an Olympus IX71 inverted fluorescent microscope with a LUCPLFLN 40 × 0.60 NA objective coupled to an Edinburgh Instruments FLS920 spectrophotometer. Excitation was achieved with the use of a 450 W Xe lamp and europium emission (>510 nm) was detected by a Hamamatsu EMCCD C9100-13. Excitation and emission wavelengths were controlled using Edinburgh Instruments v6.8 PC software. Images were acquired using CellΛM 3.2 (Olympus Soft Imaging Solutions GmBH) and post-imaging analysis was performed using ImageJ 1.44c. Emission spectra were acquired using Edinburgh Instruments F900 v6.8 PC software.

2.8   Particle Sizing

Particle sizing measurements were made using a Nanosight LM10 system controlled by NTA 2.2 software. Dynamic light scattering measurements were acquired using a Beckman-Coulter DelsaNano C instrument.

2.9   Circular Dichroism

Circular dichroism (CD) spectra were obtained on a JASCO J180 spectropolarimeter using quartz emission cells with 1 cm path length. Spectra were recorded at an internal temperature of $20^{o}C$